



January 2017

Response Of Wind Turbines Subjected To Different Earthquakes

Pradin Suinyal Magar

Follow this and additional works at: <https://commons.und.edu/theses>

Recommended Citation

Suinyal Magar, Pradin, "Response Of Wind Turbines Subjected To Different Earthquakes" (2017). *Theses and Dissertations*. 2146.
<https://commons.und.edu/theses/2146>

This Thesis is brought to you for free and open access by the Theses, Dissertations, and Senior Projects at UND Scholarly Commons. It has been accepted for inclusion in Theses and Dissertations by an authorized administrator of UND Scholarly Commons. For more information, please contact zeinebyousif@library.und.edu.

RESPONSE OF WIND TURBINES SUBJECTED TO DIFFERENT
EARTHQUAKES

by

Pradin Suinyal Magar

Bachelor's Degree, Himalaya College of Engineering, Lalitpur, Nepal, 2014

A Thesis

Submitted to the Graduate Faculty

of the

University of North Dakota

In partial fulfillment of the requirements

for the degree of

Master of Science


Grand Forks, North Dakota

May

2017

Copyright 2017 Pradin Suinyal Magar


This thesis, submitted by Pradin Suinyal Magar in partial fulfillment of the requirements for the Degree of Masters of Science from the University of North Dakota, has been read by the Faculty Advisory Committee under whom the work has been done and is hereby approved.

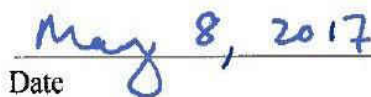

Dr. Sukhvarsh Jerath (Chairperson)


Dr. Iraj H.P. Mamaghani


Dr. Nabil Suleiman

This thesis is being submitted by the appointed advisory committee as having met all of the requirements of the School of Graduate Studies at the University of North Dakota and is hereby approved.


Grant McGimpsey
Dean of the School of Graduate Studies


Date

PERMISSION

Title	Response of Wind Turbines subjected to Different Earthquakes
Department	Civil Engineering
Degree	Masters of Science

In presenting this thesis in partial fulfillment of the requirements for a graduate degree from the University of North Dakota, I agree that the library of this University shall make it freely available for inspection. I further agree that permission for extensive copying for scholarly purposes may be granted by the professor who supervised my thesis work or, in his absence, by the Chairperson of the department or the dean of the School of Graduate Studies. It is understood that any copying or publication or other use of this thesis or part thereof for financial gain shall not be allowed without my written permission. It is also understood that due recognition shall be given to me and to the University of North Dakota in any scholarly use which may be made of any material in my thesis.

Pradin Suinyal Magar

Date: 05/04/2017

TABLE OF CONTENTS

LIST OF FIGURES	VII
LIST OF TABLES.....	XIII
DEDICATION.....	XIV
ABSTRACT.....	XVI
CHAPTER	
I. INTRODUCTION	1
II. BACKGROUND AND LITERATURE REVIEW	18
Standards and Guidelines.....	18
Publications on Earthquake Design and Analysis	20
III. THEORITICAL FORMULATIONS AND METHODOLOGY	27
Equation of Motion and Newmark Method.....	27
Modal Analysis	32
Block Lanczos Method	32
Transient Response (Time-History) Analysis.....	33
Direct Integration Method	34
Modal Superposition Method	34
Damping Calculation.....	35

Earthquake Loads.....	37
Landers Earthquake	39
El Centro Earthquake.....	41
Northridge Earthquake.....	44
Assumptions and Considerations.....	45
IV. TEST AND RESULTS.....	46
Test Description.....	46
Test Results.....	47
V. FINITE ELEMENT ANALYSIS OF WIND TURBINES.....	50
Dimensions of Wind Turbines.....	54
Mass and Stiffness Coefficient	59
Transient Results.....	59
Results from Landers Earthquake.....	61
Results from El Centro Earthquake	64
Results from Northridge Earthquake	67
VI. CONCLUSIONS	71
APPENDICES	74
REFERENCES	93

LIST OF FIGURES

Figure 1. 2016 Installed Wind Power Capacity in U.S. (MW).....	2
Figure 2. 2015 Carbon dioxide savings yearly	3
Figure 3. Growth in size of commercial wind turbines	4
Figure 4. Upwind and Downwind Wind Turbines.....	6
Figure 5. Inland and Coastal Wind Turbines	6
Figure 6. Three different types of Vertical Wind Turbine.....	7
Figure 7. Components of a Wind Turbine	9
Figure 8. Different types of Wind Turbine Towers	11
Figure 9. Parameters of Wind Turbine	12
Figure 10. Large Wind Turbine Height Comparisons	13
Figure 11. Relationship of a Wind Speed to Power Production	14
Figure 12. System of Lumped Masses and Flexible rods used by Ritschel et. al.....	22
Figure 13. Horizontal Acceleration Vs. Time For Landers Earthquake	39
Figure 14. Horizontal Acceleration vs Time for Landers Earthquake.....	39
Figure 15. Horizontal Displacement vs Time for Landers earthquake.....	40
Figure 16. Vertical Displacement vs time for landers earthquake.....	40
Figure 17. Horizontal Acceleration vs Time for El Centro Earthquake	41
Figure 18. Vertical Acceleration vs Time for El Centro Earthquake	41
Figure 19. Horizontal Displacement Vs. Time for El Centro Earthquake.....	42
Figure 20. Vertical Displacement vs Time for El Centro Earthquake.....	42
Figure 21. Horizontal Acceleration vs Time for Northridge Earthquake	43

Figure 22. Vertical Acceleration vs Time for Northridge Earthquake	43
Figure 23. Horizontal Displacement vs Time for Northridge Earthquake.....	44
Figure 24. Vertical Displacement vs time for Northridge Earthquake	44
Figure 25. 65 KW Wind Turbine Shake Table Test	47
Figure 26. Experimentally observed side-to-side modes.....	48
Figure 27. Recorded Acceleration for Landers (100% level Test)	49
Figure 28. Finite Element Model of 65 KW Wind Turbine	50
Figure 29. SHELL 181 and SOLID 186 Elements	53
Figure 30. ANSYS Model of Wind Turbines	56
Figure 31. Mode Shapes of Wind Turbines.....	58
Figure 32. Horizontal Deformation Vs. Time Period (Landers).....	61
Figure 33. Vertical Displacement Vs. Time Period (Landers)	62
Figure 34. Horizontal Acceleration Vs. Time Period (Landers).....	62
Figure 35. Vertical Acceleration Vs. Time Period (Landers).....	63
Figure 36. Horizontal Von Mises Stress Vs. Time Period (Landers)	63
Figure 37. Vertical Von Mises Stress Vs. Time Period (Landers)	64
Figure 38. Horizontal Deformation Vs. Time Period (El Centro).....	64
Figure 39. Vertical Deformation Vs. Time Period (El Centro)	65
Figure 40. Horizontal Acceleration Vs. Time Period (El Centro).....	65
Figure 41. Vertical Acceleration Vs. Time Period (El Centro)	66
Figure 42. Horizontal Von Mises Stress Vs. Time Period (El Centro).....	66
Figure 43. Vertical Von Mises Stress Vs. Time Period (El Centro).....	67
Figure 44. Horizontal Deformation Vs. Time Period (Northridge).....	67
Figure 45. Vertical Deformation Vs. Time Period (Northridge)	68
Figure 46. Horizontal Acceleration Vs. Time Period (Northridge).....	68

Figure 47. Vertical Acceleration Vs. Time Period (Northridge)	69
Figure 48. Horizontal Von Mises Stress Vs. Time Period (Northridge)	69
Figure 49. Vertical Von Mises Stress Vs. Time Period (Northridge).....	70
Figure 50. 0.065S0.5-LX	75
Figure 51. 0.065S1.0-LX	75
Figure 52. 0.065S2.0-LX	75
Figure 53. 0.065S0.5-LX	75
Figure 54. 0.065S1.0-LX	76
Figure 55. 0.065S2.0-LX	76
Figure 56. 0.065S0.5-LX	76
Figure 57. 0.065S1.0-LX	76
Figure 58. 0.065S2.0-LX	76
Figure 59. 0.065S0.5-NX.....	77
Figure 60. 0.065S1.0-NX.....	77
Figure 61. 0.065S2.0-NX.....	77
Figure 62. 0.065S0.5-NX.....	77
Figure 63. 0.065S1.0-NX.....	77
Figure 64. 0.065S2.0-NX.....	78
Figure 65. 0.065S0.5-NX.....	78
Figure 66. 0.065S1.0-NX.....	78
Figure 67. 0.065S2.0-NX.....	78
Figure 68. 0.065S0.5-EX	78
Figure 69. 0.065S1.0-EX	79
Figure 70. 0.065S2.0-EX	79
Figure 71. 0.065S0.50-EX	79

Figure 72. 0.065S1.0-EX	79
Figure 73. 0.065S2.0-EX	79
Figure 74. 0.065S0.5-EX	80
Figure 75. 0.065S1.0-EX	80
Figure 76. 0.065S2.0-EX	80
Figure 77. 1.0S0.5-LY	81
Figure 78. 1.0S1.0-LY	81
Figure 79. 1.0S2.0-LY	81
Figure 80. 1.0S0.5-LY	81
Figure 81. 1.0S1.0-LY	82
Figure 82. 1.0S2.0-LY	82
Figure 83. 1.0S0.5-LY	82
Figure 84. 1.0S1.0-LY	82
Figure 85. 1.0S2.0-LY	82
Figure 86. 1.0S0.5-NY	83
Figure 87. 1.0S1.0-NY	83
Figure 88. 1.0S2.0-NY	83
Figure 89. 1.0S0.5-NY	83
Figure 90. 1.0S1.0-NY	83
Figure 91. 1.0S2.0-NY	84
Figure 92. 1.0S2.0-NY	84
Figure 93. 1.0S2.0-NY	84
Figure 94. 1.0S2.0-NY	83
Figure 95. 1.0S0.5-EY	84
Figure 96. 1.0S1.0-EY	85

Figure 97. 1.0S2.0-EY	85
Figure 98. 1.0S0.5-EY	85
Figure 99. 1.0S1.0-EY	85
Figure 100. 1.0S2.0-EY	85
Figure 101. 1.0S0.5-EY	86
Figure 102. 1.0S1.0-EY	86
Figure 103. 1.0S2.0-EY	86
Figure 104. 5.0S0.5-LZ.....	87
Figure 105. 5.0S1.0-LZ.....	87
Figure 106. 5.0S2.0-LZ.....	87
Figure 107. 5.0S0.5-LZ.....	87
Figure 108. 5.0S1.0-LZ.....	88
Figure 109. 5.0S2.0-LZ.....	88
Figure 110. 5.0S0.5-LZ.....	88
Figure 111. 5.0S1.0-LZ.....	88
Figure 112. 5.0S2.0-LZ.....	88
Figure 113. 5.0S0.5-NZ	89
Figure 114. 5.0S1.0-NZ	89
Figure 115. 5.0S2.0-NZ	89
Figure 116. 5.0S2.0-NZ	89
Figure 117. 5.0S2.0-NZ	89
Figure 118. 5.0S2.0-NZ	90
Figure 119. 5.0S0.5-NZ	90
Figure 120. 5.0S1.0-NZ	90
Figure 121. 5.0S2.0-NZ	90

Figure 122. 5.0S0.5-EZ.....	90
Figure 123. 5.0S1.0-EZ.....	91
Figure 124. 5.0S2.0-EZ.....	91
Figure 125. 5.0S0.5-EZ.....	91
Figure 126. 5.0S1.0-EZ.....	91
Figure 127. 5.0S2.0-EZ.....	91
Figure 128. 5.0S0.5-EZ.....	92
Figure 129. 5.0S1.0-EZ.....	92
Figure 130. 5.0S2.0-EZ.....	92

LIST OF TABLES

Table 1. Peak magnitudes for Landers Earthquake	40
Table 2. Peak Magnitudes for El Centro Earthquakes	42
Table 3. Peak Magnitudes for El Centro Earthquakes	44
Table 4. Material Properties of the Wind Turbine Model	51
Table 5. Element Types	53
Table 6. Dimensions of wind turbines	55
Table 7. Element Types and Meshing.....	56
Table 8. Fundamental modes, frequencies and effective mass to total mass ratio	57
Table 9. Mass and Stiffness Coefficient	59
Table 10. Peak Responses Recorded from ANSYS Workbench.....	60

DEDICATION

To my Grandpa, Late Gore Bahadur Khapangi, who never gave up in his life and taught me the same. I can never achieve what you achieved in your life but I can try to follow your advices.

To my loving parents who sacrificed everything for me, my happiness and my education. I hope that this achievement will complete the dream that you had for me when I first came into this world.

To my family which was the first school of my life.

ACKNOWLEDGEMENTS

The completion of this thesis would not have been possible without the assistance of so many kind people around me whose names may not at all be enumerated. I would like to extend my sincere thanks to all of them.

I am highly indebted to Professor Dr. Sukhvarsh Jerath for his guidance, encouragement, support and patience over the last two years. Thank you so much for having faith in me and imparting your knowledge and expertise in this study. Your support was essential to my success here.

I would also like to thank my committee members Associate Professor Dr. Iraj H.P. Mamaghani and Associate Professor Dr. Nabil Suleiman for reviewing and giving me necessary suggestions to make this work even better.

I am highly indebted to UND and UND Civil Engineering Faculty for providing all the necessary materials and information necessary for the completion of this thesis.

I am very thankful to my fellow classmates, especially, Bahareh Shoghli, Rajib Chandra Shah, Wiriychai Roopkumdee, for sharing their knowledge and ideas in assisting me to complete my thesis. I am grateful to my special friends Debesh Adhikari and Subodh Chandra Subedi for their continuous support throughout my academic career at UND and my dear sister Eju Thapa and brother Shobhakanta Subedi for helping me out during my stay in USA. Lastly, my thanks and appreciation also go to my family and other friends who have willingly helped me out with their abilities.

ABSTRACT

With the rapidly increasing energy crisis in the present world, the demand for the renewable sources of energy is increasing day by day. One of the most efficient source of renewable energy we can depend on is wind energy. Wind turbines are feasible, cost effective and durable source of wind energy which has attracted intensive scientific and societal interest. Research on wind turbine structures has mostly focused on the design and assessment of wind turbines but with the expansion of the wind turbines installation in seismically active areas (e.g, China, USA, India, Southern Europe and East Asia), recent research works are mostly related to the comprehensive seismic design of such structures.

Lack of specific guidelines for the seismic design of wind turbine structures necessitates extensive research work on the seismic behavior of wind turbine structures. In this study, seismic response on three different wind turbines of power capacities 65KW, 1 MW and 5 MW are analyzed considering the effects of different parameters such as geometry, damping and earthquakes with different Peak Ground Acceleration (PGA). For each model of wind turbine a corresponding finite element model was formed in ANSYS Workbench 16.2. All those models were loaded with a series of seismic loads from different earthquakes (Landers, El Centro, and Northridge) and the dynamic responses of those turbines were studied. For all types of wind turbines, the first mode obtained is the fundamental mode of frequency. It was observed that the geometry of the turbines, direction of the load applied, damping ratios and magnitude of applied loads, all played very important role in the study.

CHAPTER I

INTRODUCTION

Energy is the capacity or power to do work. Energy can exist in various forms such as electrical, mechanical, chemical, thermal, nuclear etc, and can be transformed from one form to another. Basically, there are two different sources of energy: renewable sources and nonrenewable sources. Nonrenewable sources are available in limited supplies like coal, nuclear, oil and natural gas. But renewable sources are replenished naturally over a relatively short period of time. The five major renewable energy resources are solar, wind, water, biomass and geothermal.

Day to day developments in the field of scientific research and technological advancement has resulted into more consumption of energy. Fossil fuels make up a large portion of today's energy market, which is available in a finite amount. The forecast of the fossil fuel shortage in the near future combined with the negative environmental impacts of such fuels has led to the exploration of the alternate sources of energy production. Thus the demand of renewable sources seems to be imperative in the current scenario. Wind energy can be considered as one of the fundamental renewable sources of energy as it is a green energy source and does not cause pollution. Ever since man decided to use ships to travel through the sea, wind energy was used to blow sails to drive ships. Also to this day windmills are used for grinding grains. The potential of wind power is at the order of – 20 times more than what the entire human

population needs and there is no way we can run out of it.

Wind turbine is a simple device that converts the wind's kinetic energy into electrical energy which can be used for further purposes. The first known wind turbine used to produce electricity was built in Scotland in 1887 A.D. and in US it was introduced a year later in the U.S (Shahan, 2014). It is expected that by 2030 wind power could reach 2,110 GW in the world, and it can supply up to 20 % of global electricity thus creating new jobs and reducing CO₂ emissions by more than 3.3 billion tonnes per year. This can attract an annual investment of about 200 billion Euros in the world. Global wind energy installations produced 433 GW at the end of 2015 with a prediction that the industry might grow by another 60 GW in 2016 (Global Wind Energy Council, 2017). In 2014, Asia overtook Europe as the region with the most installed wind power capacity and most of the credit goes to China, which installed 23 GW of capacity in 2014 with an estimation that China may have installed 25 GW in 2015 and continued to dominate the world energy market in 2016 (Font, 2016). Similarly, according to some preliminary forecasts United States may be able to meet 10% of its electricity demand via wind power by 2020, 20% by 2030 and 35% by 2050 (Font, 2016).

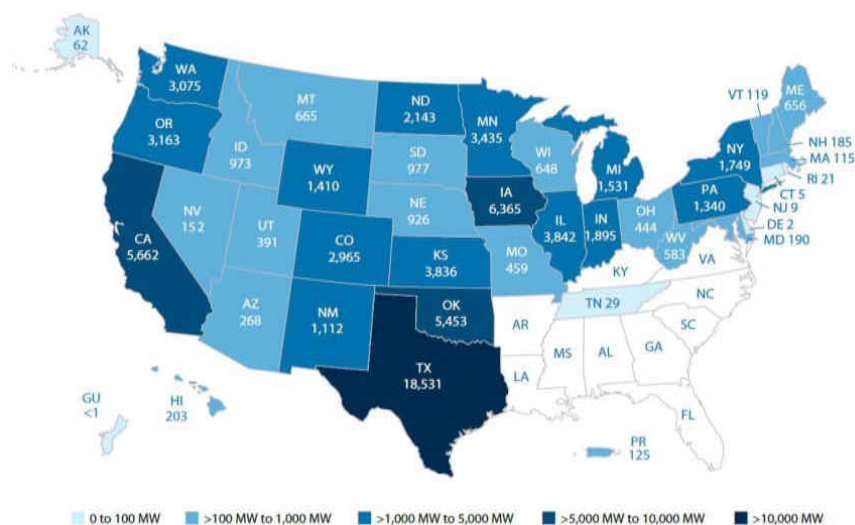
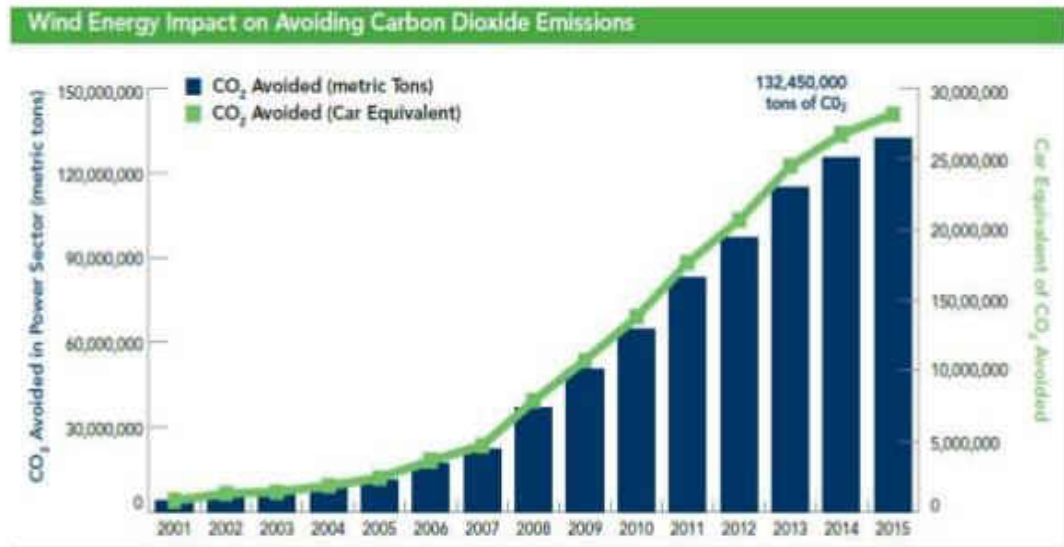


Figure 1. 2016 Installed Wind Power Capacity in U.S. (MW) (American Wind Energy Association, 2016)

Moreover, it has been observed that the rapid development of wind energy in the United States has led to significant reductions in power sector carbon emissions. Wind energy reduced as much CO₂ emissions in 2015 as produced from 28 million cars, which is a great achievement for the air pollution control. (American Wind Energy Association, 2016).



Source: AWEA U.S. Wind Industry Annual Market Report Year Ending 2015

Figure 2. 2015 Carbon dioxide savings yearly (American Wind Energy Association, 2016)

With the significant increase in the wind farms, there is a vast spread of wind turbines installations around several areas worldwide. This has led to a decrease in the number of prime sites with high wind availability, but the demand for wind power is still increasing. So either we need to find more windy sites or increase the height of the towers and blade radius of the rotor. Increased tower height and rotor diameter helps to generate more electricity by utilizing stronger and consistent wind available at the higher altitudes, as the power generated is function of the cube of the wind velocity. This means if the wind speed is doubled the power generated can be increased by a factor of eight. This can be supported by the following equations:

$$\text{Kinetic Energy (KE)} = \frac{1}{2} mv^2$$

Here, 'm' represents the mass of air which can be derived from the product of its density and volume. For a constant wind speed of 'v' and normal section area 'A' we can derive the air mass during a given period of time 't' as

$$m = \rho A v t$$

$$\dot{m} = \rho A v$$

$$\text{Kinetic Energy per unit time (Power)} = \frac{1}{2} \dot{m}v^2$$

$$\text{Thus, Power} = \frac{1}{2} \rho A v^3$$

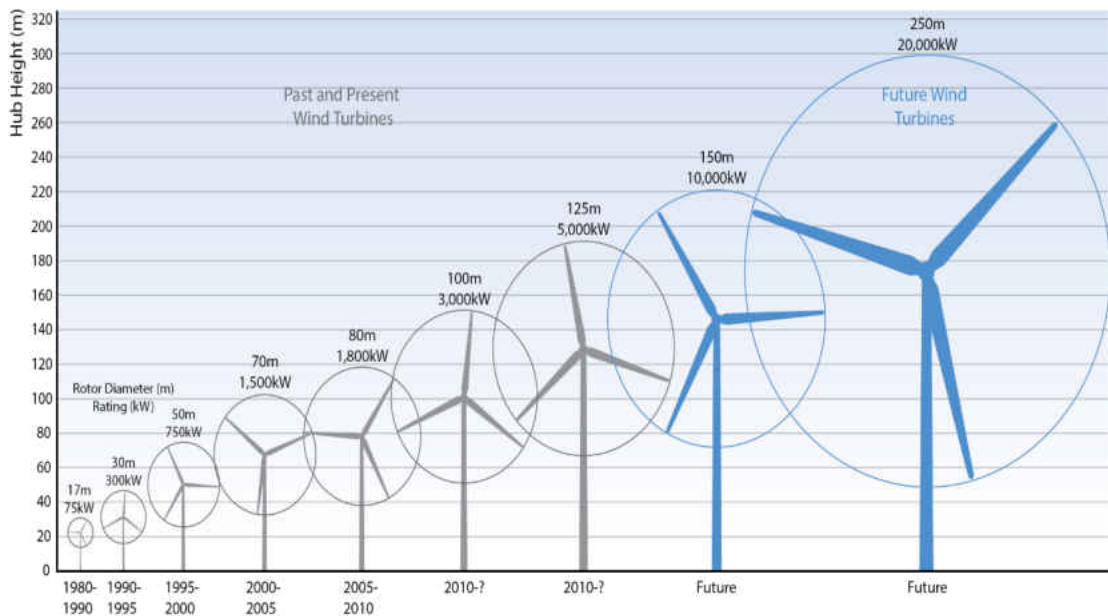


Figure 3. Growth in size of commercial wind turbines (Intergovernmental Panel on Climate Change, 2012)

Increase in the total height of wind turbines means that it is more vulnerable to the lateral loads. The reduction in the more suitable locations for wind turbine installations and the presence of abundant wind resources in high seismic regions, has resulted in an

increase in the number of wind turbine installations in such areas. Wind turbines are also equally prone to earthquake hazards like any other civil structures. Sometimes installing higher wind turbines might result in the seismic forces higher than the wind force. Thus, it is becoming highly necessary to take into account the earthquake forces in the design of sustainable wind turbines.

Although, a wind turbine looks similar to a fan, it works exactly opposite to the working mechanism of a fan. Instead of using electricity to produce wind, wind turbines use the wind energy to produce electricity. The kinetic energy of the wind rotates the blades, which spin the shaft that is connected to a generator to produce electricity. Modern wind turbines fall into two basic groups based on the axis of rotation:

1. Horizontal Axis Wind Turbines
2. Vertical Axis Wind Turbines

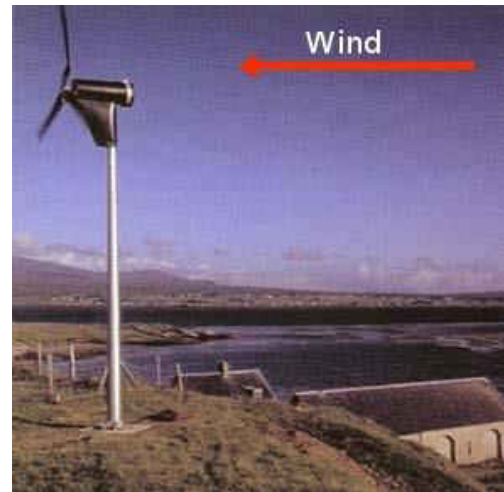
Horizontal Axis Wind Turbines (HAWT) have a design similar to windmill, with the main rotor shaft fixed on top of a tall tower. A HAWT works by capturing the wind that blows at a perpendicular angle to its blades. Therefore, an anemometer is fixed which measures the wind speed and the direction of the wind so that it constantly faces the wind. The blades of these wind turbines help to maintain stability and also collect the maximum amount of wind energy available. But it might have some difficulties when it is operated at low heights. There are basically two types of wind turbines: upwind turbine and downwind turbine, and based on the location there are inland wind turbines and coastal wind turbines.

In upwind type of wind turbine, the rotor faces the wind whereas in case of downwind wind turbine the rotor is on the downside of the tower. Basic advantage of upwind turbine is that it avoids the wind shade behind the tower. On the other hand, there is also some

wind shade in front of the tower which means the air will start to bend away from the tower before it reaches the tower itself. Therefore, there is some loss of power from this type of interference. Similarly, the main advantage of the downwind wind turbine is that the rotor is more flexible, whereas the rotor is rather inflexible in upwind type. (Darling, 2017).



Upwind Wind Turbine



Downwind Wind Turbine

Figure 4. Upwind and Downwind Wind Turbines (POWER-TALK.NET, 2017)



Inland Wind Turbines (Peschel, 2016)



Coastal Wind Turbines
(Web Zone1, 2015)

Figure 5. Inland and Coastal Wind Turbines

Vertical Axis Wind Turbine (VAWT) has the rotor rotating about its vertical axis. Although this type of wind turbine is not as efficient as the HAWT but it can operate even in low wind situations. Unlike HAWT, VAWT does not need to be pointed towards the direction of the wind in order to be effective. This is advantageous in sites where the wind direction is highly variable. Also since VAWT components are placed nearer to the ground, the generator and gearbox are easily accessible for maintenance. This also means that the tower for this wind turbine need not be massive. One of the main drawback of such wind turbine is that it creates a drag when rotating into the wind which decreases their efficiency. Although VAWT are easier and safer to construct but since they are installed nearer to the base on which they rest they can only operate in lower wind speed. Due to this the maximum efficiency is only 30%. Basically there are three types of VAWT: Darrieus Wind Turbine, Giromill Wind Turbine and Savonius Wind Turbine. Figures of different types of vertical axis wind turbines are shown below (Bajaro, 2011).

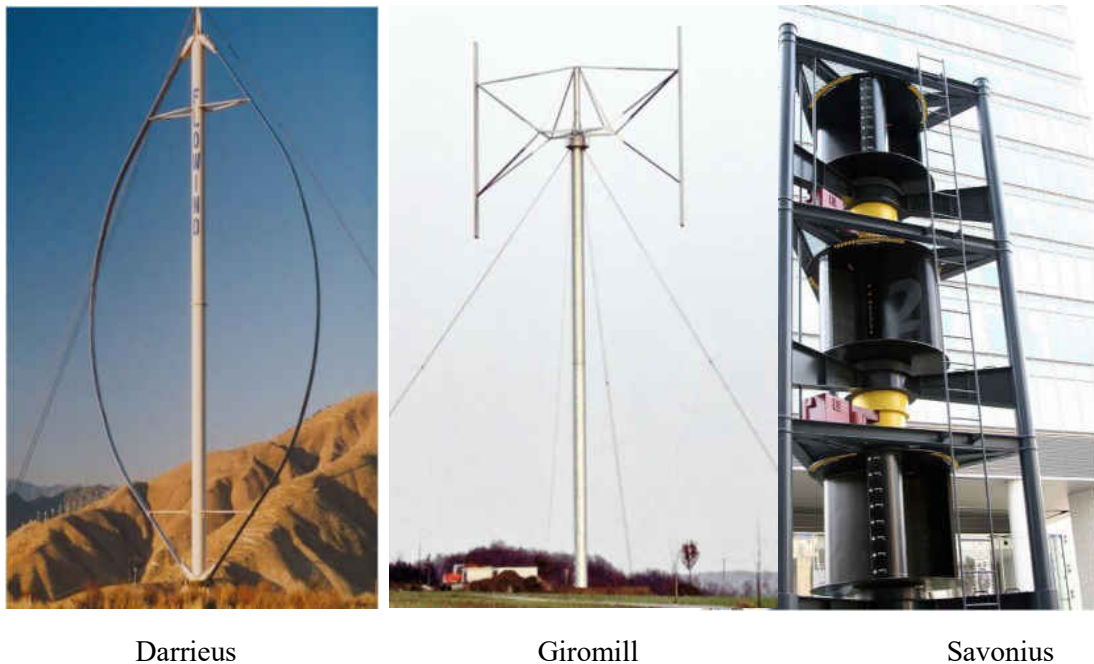


Figure 6. Three different types of Vertical Wind Turbine (Smith, 2007)

Wind turbines can be categorized by the power output into three general classifications: utility (large, over 900 KW), industrial (medium, 50 KW to 250 KW) and residential scale (small, less than 50 KW) (McCaffrey, 2005). A wind turbine consists of a rotor with wing shaped blades attached to a hub which is again connected to a nacelle that houses a gearbox, connecting shafts, brakes, the generators and other machinery, a tower, foundation and ground mounted electrical equipment like transformer (Ancona & McVeigh, 2001). The kinetic energy carried by the wind causes the blades to rotate. The rotor which is connected to the main shaft inside the nacelle which connects to a gearbox that in turn converts the slow motion into a fast motion. The magnetic field produced by this fast motion converts the rotational energy into electrical energy. Finally the electrical energy produced is converted to the appropriate voltage for distribution by a transformer.

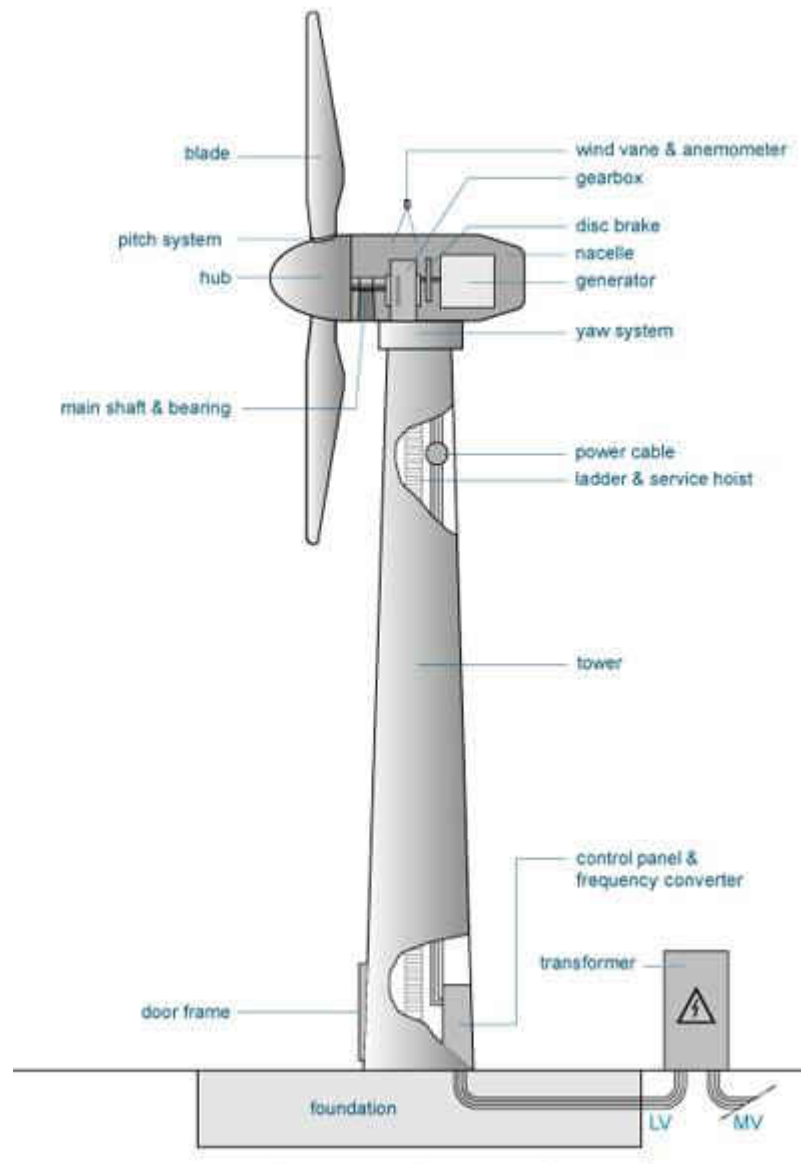


Figure 7. Components of a Wind Turbine (NEWEN, 2017)

Wind Turbine tower carries the nacelle and the rotor. Towers for wind turbines can be tubular, lattice (truss), guyed or hybrid. Most large wind turbines use tubular towers made of steel which are usually conical in shape (diameter decreasing from base to top) in order to increase their strength and save material. Basically, they are manufactured with steel sheets cut, rolled and welded. This type of tower construction is very expensive due to high cost of steel, and also if the size of tower is too big, it is difficult for transportation. Concrete towers can be an alternate solution where the price of steel

is too high. Concrete towers are made of several precast pieces assembled together on site. This results into easy transportation and good control of quality of materials. The only problem for concrete towers is the weight (unless they are designed in a large number of pieces, they can weigh more than the nacelle). Lattice towers also known as truss towers are used to save the cost since they use about half the material required by tubular tower. The main drawback of lattice towers can be their visual appearance. Besides the exposure of the connections of trusses to corrosion can create weak diagonals of the truss which becomes very sensitive during wind excitation. Guyed towers are built with narrow pole towers and supported by guyed wires. Construction of these towers are relatively cheaper. The major disadvantage of this type of tower is that it is hard to get access around the towers for maintenance. Guyed towers are normally used in very small wind turbines. Hybrid towers have combination of any types of towers mentioned above. The installation cost for hybrid tower is too high because it is very complicated process to construct this type of tower. Figure 8 shows various types of wind turbine towers (Miceli, 2012).





Hybrid Tower

Figure 8. Different types of Wind Turbine Towers (Miceli, 2012)

The four important geometric parameters of a wind turbine are rotor diameter, swept area, hub height and maximum height. The maximum height of a wind turbine is the sum of the hub height and rotor radius. The power output of a wind turbine is directly related to the area swept by the blades. Larger is the diameter of its blades the more power it can extract from the wind. The swept area is dependent on the rotor diameter, increase in rotor diameter leads to the increase in the swept area which will ultimately lead to the increase in power output.

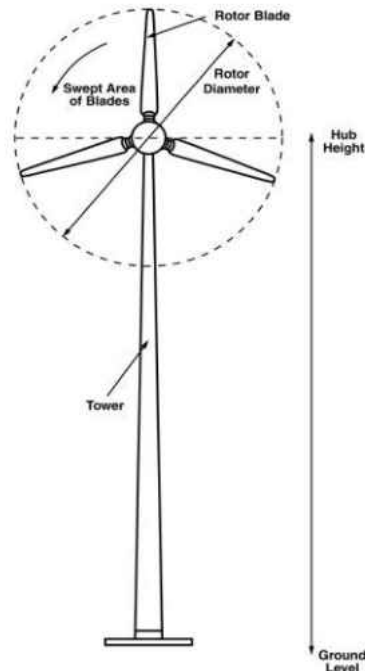


Figure 9. Parameters of Wind Turbine (Clarke, 2003)

The average rotor diameter of a wind turbine installed during 2014 was 99.7 meters for wind turbines 1 MW and larger. The average hub height of a wind turbine installed during 2014 was 82.4 meters (AWEA, 2015).

In 1990s wind turbines were rated below 1 MW with rotor diameters of around 30-50 m and hub heights 40-60 m. Wind turbines rated at 2-5 MW of energy generation had rotor diameters near 100 m and hub heights of 100-120 m (Schwartz & Elliott, 2005). Further development in the power output of wind turbines is being done every day. A 10 MW power capacity wind turbine is being designed by American Energy Technologies Company, AMSC, which will have a rotor diameter of 190 m and a hub height of 125 m (Power-Technology, 2014). As the rotor diameters and hub height of the wind turbine have increased so have the rated capacities of the wind turbine. There is no specific relationship between hub height and a rotor diameter but in general the turbine hub heights are approximately 1 to 1.4 times the rotor diameter (McCaffrey,

2005). Comparison of height of large wind turbines with other tall structures can be shown in the figure.

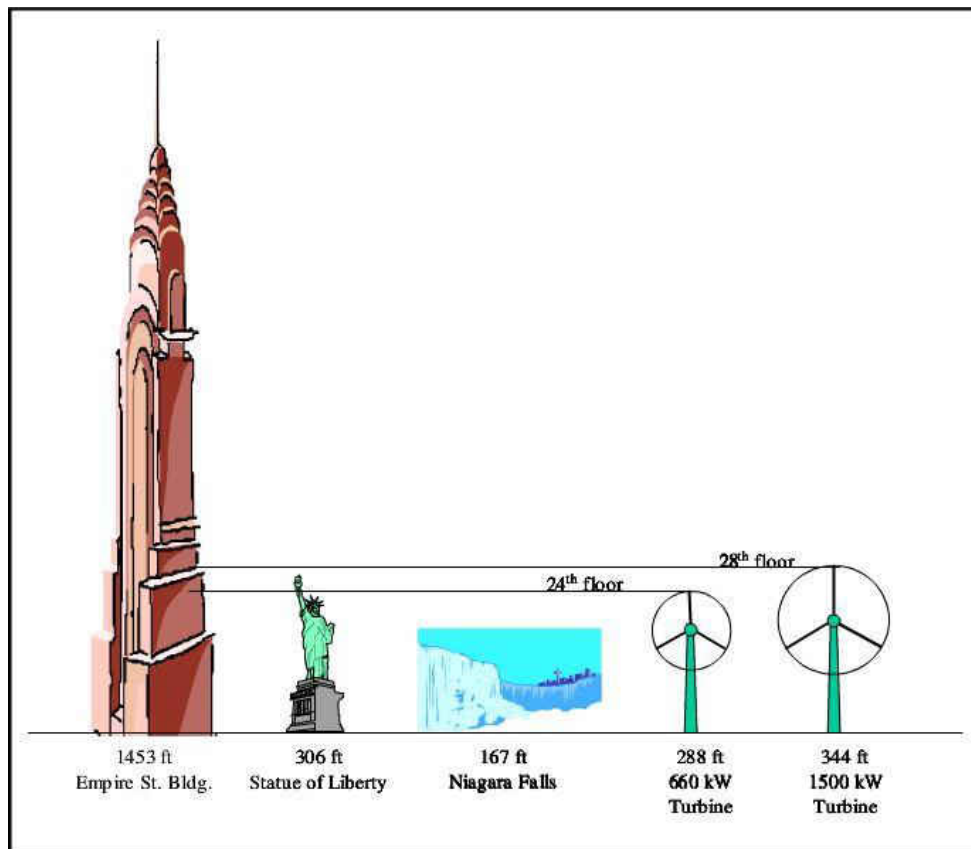


Figure 10. Large Wind Turbine Height Comparisons (McCaffrey, 2005)

Power production by a wind turbine is a function of wind speed. The relationship between wind speed and power can be shown by a power curve. These power curves might vary according to different wind turbine models and sometimes to different site-specific settings. From the curve we can study that at low speed of wind less amount of power is generated. When the wind speed exceeds 3-4 m/s, called as cut-in wind speed, wind turbines get started. At this time the power generated by a wind turbine increases by a 3rd power of the wind speed until the rated wind speed is reached. At wind speeds ranging between 12m/s to about 25 m/s the power is limited to the rated power of the wind turbine with the help of stall-regulation or pitch-control systems. When the wind

speed exceeds 20-25 m/s the wind turbines are normally brought to standstill to avoid high mechanical loads on the turbine elements. This wind speed is called the cut-out wind speed (McCaffrey, 2005).

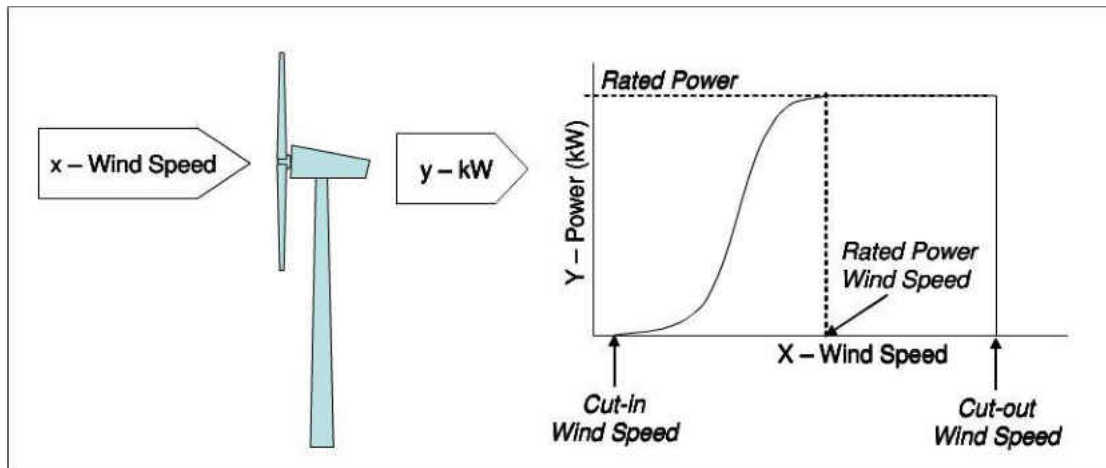


Figure 11. Relationship of Wind Speed to Power Production (McCaffrey, 2005)

As we already know in order to improve the power output by a wind turbine the turbine towers should be taller so that the rotors receive more wind and currents. But at the same time significant challenges are associated with implementing taller wind turbine towers. First of all there is necessity to increase the structural strength and stiffness of the towers so that they can carry the increased turbine weight and also withstand the bending forces created by the wind action on the rotors and the towers. These towers should also be strong enough to resist the damaging resonance from excitation by forcing frequencies associated with the rotor and blades passing the tower. This will result into large cross-sectional area of the towers with large height, which results into difficulty in transportation. Higher towers also require massive and costly foundations. Besides construction time for higher wind turbine towers can be longer. All of these challenges might result into higher costs of the tower because the cost per unit length of tower increases faster than increment energy output (Tricklebank, Halberstadt, & Magee, 2007).

Generally either steel, concrete or composite towers are considered for the construction of wind turbine towers. Steel has the highest strength-to-weight ratio, it is relatively easy to construct and can be recycled. Steel towers are also flexible enough for the cyclic loading. Concrete towers maybe either reinforced (with steel bars or other suitable materials) or prestressed (with pre- or post-tensioned steel bars or strands). Concrete can easily deliver low cost towers with higher performance and low maintenance. Thus concrete towers are popular in off-shore wind turbine farms (Tricklebank, Halberstadt, & Magee, 2007). Some designers use cast-in-place hybrid towers with concrete at the bottom and steel at the top. If designed well, precast concrete-steel towers can offer easy transport, rapid erection, high strength and stiffness, reduced maintenance and life time cost (Zavitz & Kirkley, 2012).

Wind turbine towers are subjected to aerodynamic loads that result from wind (drag and lift force), inertia loads (that result from gravity, rotation, vibration or gyroscopic effects), functional loads (from transient operation conditions of turbine such as braking, yawing, transmitting power to generator) and other loads from environment sources (wave, current, ice, seismic) (Gwon, 2011).

Among all the loads applicable on wind that, the major loads are wind loads and earthquake loads. The wind load consists of direct wind pressure (q_z), gust factor (G) and force coefficient (C_f). Wind loads that act on a wind turbine can be classified as stationary and cyclic. In addition, the rotor is subjected to non-periodic and random loads caused by wind turbulence (Singh, 2007). With a large number of wind turbines installed in seismic regions it is important to study the seismic performance of a wind turbine tower. Sometimes installing tall towers in highly active seismic regions might result into seismic force that is greater than the wind load. In such cases inaccurate estimation of seismic force can either lead to structural failure or uneconomic design.

Traditionally, wind turbines have been analyzed by modal methods which is also used in the design of buildings (Clough & Penzien, 2003). But the behavior of wind turbine is very much different from the behavior of other ordinary structures, thus the modal methods for the analysis of the wind turbine is not enough. Wind turbine consists of a slender tower with a rotating mass on the top and the wind effecting the damping properties (Hodges & Pierce, 2011). Thus we use time history method to analyze the wind turbine structures. Time history analysis also known as linear response history analysis is a numerical technique in which the response of a structural model to a specific ground motion accelerogram is determined through a process of a numerical integration of the equations of motion (Building Seismic Safety Council of the National Institute of Building Sciences, 2003). Compared to traditional method (response spectrum or modal analysis method), time history analysis is not frequently used because of the lack of knowledge and availability of actual ground motion data. However this method is the most accurate method. In this method, structure's response history is evaluated by subjecting it to a designed earthquake. The main advantage of time history analysis is that it provides a time dependent history of the response of the structure to a specific ground motion (Mehta & Gandhi, 2008).

Until now the wind turbine design codes have relatively simple procedures to calculate the seismic forces. There are a series of assumptions and simplifications involved in considering seismic characteristics of the structure including the mass distribution, damping ratio and frequency with these codes. Thus it is very difficult for an engineer to compare the variances seen in the small wind turbine and large wind turbine. There are also other uncertainties involving the effect of different structural parameters including height and weight on the significance of seismic force directionality and frequency of the structure which is important from the design perspective because

engineers should adjust frequency to avoid resonance created by seismic forces and also avoid frequencies that affect mechanical functions.

The main objective of this project is to study the behavior of wind turbines of different sizes under different types of earthquakes. Three wind turbines of power capacities 65 KW, 1 MW and 5 MW are used for the study and the earthquakes used are Landers, Northridge and El Centro. A finite element software ANSYS Workbench 16.2 is used to model and run the analysis. The wind turbine parameters under study are turbine size, damping ratio (0.5%, 1% and 2%), base acceleration direction and earthquake types. The responses studied are peak displacement and peak acceleration at the top of the nacelle and the maximum Von Mises Stress at the tower near the base. Finally a spectrum with the time period of the wind turbines and the obtained responses are plotted for different earthquake loads applied under different damping ratios

CHAPTER II

BACKGROUND AND LITERATURE REVIEW

Like other civil engineering structures, it is necessary to design wind turbines accurately for the various types of loadings that could be experienced during a wind turbine's lifetime. In early years much literature had been devoted to the analysis of wind turbine structures under wind loading but the growth of wind turbines in the seismic regions has led to an interest in addressing seismic loads as well. Only after 2000, some experimental and analytical studies were done to study the behavior of wind turbines under the seismic loading. Most analysis are done in a finite element software and very less data are available from the experiments. Due to this reason it is very difficult to investigate the damping behaviors in a wind turbine. A recent real size shake table test was performed on a small wind turbine which is still considered as the basic data to be compared with the obtained results from finite element software. This chapter contains the review of the past studies done. The first part is the overview of the available standards and guidelines for the design of wind turbines and the second part includes the results of the research publications and their conclusions.

Standards and Guidelines

There are three main wind turbine standards that consist of the design requirements and technologies along with components and technologies which have significant impact on the function of wind turbines. The three main guidelines that provide direct guidance for seismic loading and design of wind turbines are:

1. Guidelines for Design of Wind Turbines (Risø, 2001)
2. Guideline for the Certification of Wind Turbines (GL, 2003)
3. IEC 61400-1 Ed 3: Wind Turbines – Part 1: Design Requirements (IEC, 2005)

GL and Risø guidelines are coordinated with the International Electrotechnical Commission (IEC) standards (Claxton, 2014).

The Risø standard is a combined effort between Det Norske Veritas (DNV) and Risø National Laboratory. The Risø guideline provides the most general methodology for seismic loading based on SDOF (Single Degree of Freedom). A simple SDOF model is considered with a tower, nacelle, rotor and on top one-fourth of the mass of the tower is lumped. Then analysis of the responses of the model after the application of the selected spectral response acceleration from a design response spectrum (Claxton, 2014). There is no recommendations for the appropriate level of damping in Risø guideline thus an assumed level of damping, i.e 5% is implied (ICC, 2006) . There is also no any specific guidance provided in translating the resulting spectral response acceleration into design loads, thus an appropriate building code procedure will be used (DNV, Risø, 2001) .

The Germanischer Lloyd (GL) (Germanischer Lloyd, 2010) guidelines suggest that either local building codes should be applied or in the absence of specific provisions, the American Petroleum Institute (API) (DNV, Risø, 2001) recommendations are to be applied (Asareh, Dynamic Behavior of operational wind turbines considering aerodynamic and seismic load interaction, 2015). GL standard provides guidelines which are prescriptive with detailed guidance on particular aspect of seismic risk, which is the main difference from Risø standard. GL standard prescribes a return period of 475 year as the design level earthquake and a safety factor of 1.0 for the earthquake load.

To estimate the seismic demand this code implies the use of both frequency and time methods, with at least 3 natural modes for the frequency domain and 6 simulations for the time domain. There is no guidance provided regarding the level of viscous damping similar to the RisØ guideline (DNV, RisØ, 2001).

International Electro-technical Commission (IEC) guidelines (International Electrotechnical Commission, 2005) provide International Standards for all electrical, electronic and related technologies. IEC 61400 has a series of guidelines for the design requirements of wind turbines. This guideline also considers a return period of 475 years and the resulting loads must be superimposed with the maximum of operating loads or emergency shutdown loads with a unit safety factor. IEC suggests the use of a design response spectrum from local building code to find the design response acceleration using the first natural frequency of the tower with 1% damping ratio (Agbayani, 2014).

Publications on Earthquake Design and Analysis

Bazeos et al. (Bazeos, Hatzigeorgiou, Hondros, Karamaneas, & Karabalis, 2002) studied the load bearing capacity and the behavior of a prototype steel tower for a 450 KW wind turbine with a tower height of almost 38 meters. Two models: refined and simplified models were developed for the static and seismic analysis respectively and both these models were in close agreement. The refined finite element model was necessary for the static and buckling analysis whereas simplified analytical models are recommended by building codes to predict the critical loads related to local buckling. Even approximate numerical models can produce accurate results for seismic analysis with the use of appropriate boundary conditions (Bazeos, Hatzigeorgiou, Hondros, Karamaneas, & Karabalis, 2002).

Osamu Kiyomya et al. (Kiyomiya, Rikiji, & Van Gelder, 2002) studied the occurrence probability of the mean wind velocities and large-scale earthquake events from Weibull Distributions. The probability of the simultaneous occurrence of storms and large-scale earthquake was very small. When large-scale earthquake was adopted for structural seismic design the mean wind speed was the reasonable value to combine with the earthquake events, inversely, when the wind speed during storm conditions was considered the earthquake forces could be ignored (Kiyomiya, Rikiji, & Van Gelder, 2002).

Ritschel et al. (Ritschel, Warnke, & Kirchner, 2003) did simulation on a wind turbine having hub height 60 m in order to study its seismic behavior under PGA of 0.3g. Two approaches were used: modal approach and time-domain approach. In the modal approach, four oscillation modes of the four fundamental modes were considered and the mass of the nacelle and rotor were considered as the point load at the top of the tower. This approach showed that the results were relatively conservative at the base of the tower. In time-domain approach a full scale mechanical model was considered for the seismic analysis with the application of acceleration time series. Results for time-domain approach were relatively conservative at the tower top. They concluded that an envelope of both approaches was a reliable measure in estimating the design load for tower (Ritschel, Warnke, & Kirchner, 2003).

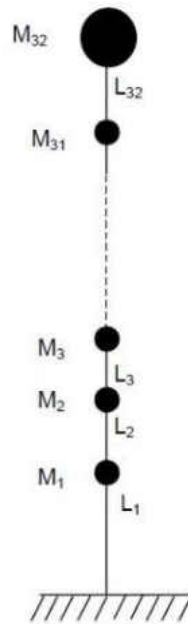


Figure 12. System of Lumped Masses and Flexible rods used by Ritschel et. al. (Ritschel, Warnke, & Kirchner, 2003)

Lavassas et al. (Lavassas, et al., 2003) performed finite element analysis of the prototype of a steel 1 MW wind turbine which was 44.075 meters high and had a tubular shape with a variable cross section and thickness along the height. The seismic loading in this investigation was based on Eurocode 3 with seismic zone II and rocky soil. According to the results a linear static model was sufficient to accurately estimate the response to a gravity and seismic load but not accurate enough for the ultimate limit state (ULS) design because it neglects the local stress concentrations. The dominant load for a wind turbine is the extreme wind; seismic load can be severe than wind only if the wind turbine is constructed in a seismically hazardous area (Lavassas, et al., 2003).

Witcher et al (Witcher, 2005) introduced the GH Bladed wind turbine simulation package. By considering the seismic analysis in the time domain, the correct aeroelastic interaction of the dynamic motion of the wind turbine structure with the wind load

acting on the blades and the response of the turbine controller can be modelled (Witcher, 2005).

X. Zhao et al. (Zhao & Maisser, 2006) used a multi-body model of a wind turbine as well as the soil-structure interaction (SSI) to study the seismic response properties in time domain. It was observed that the SSI had influence on the dynamic characteristics of a wind turbine tower. The earthquake loads should also be considered in the design of a wind turbine but since severe earthquake is very rare event it is neither economical nor practical to design wind turbine structures to survive such events (Zhao & Maisser, 2006).

M. Hänler et al. (Hänler, U., & I., 2006) presents results on ongoing development of a simulation program (SIWEC) for the dynamic analysis of horizontal axis wind turbine. The main objective of this program is to effectively and accurately perform all the load calculations and virtual prototyping at high speed. The wind turbine consisted of a multi-body system with flexible parts described by a variable number of modes as desired by the user. The study with the earthquake loads on the turbine showed that higher tower modes are much more important in earthquake analysis than in normal operation conditions. Work on the aerodynamic model is still on progress (Hänler, U., & I., 2006).

X. Zhao et al. (Zhao, MaiXer, & Wu, 2007) introduced a new multibody modelling methodology for wind turbine structures based on the hybrid multibody system composed of rigid, flexible bodies, force elements and joints. This helped to capture almost all the relevant dynamic characteristics of the wind turbine with very low degree of freedom. It is more reliable for the analysis of global vibrations, dynamic loads and time-domain approach (Zhao, MaiXer, & Wu, 2007).

Gunjit Bir et al. (Bir & Jonkman, 2007) studied the aerostatic stability of 5 MW, both onshore and offshore, wind turbines under certain parked conditions. The instabilities seen on the wind turbine were sensitive to the rotor azimuth and nacelle yaw position. These instabilities could be mitigated by using several strategies such as feathering the blades at non-90⁰ angles and applying generator brakes (Bir & Jonkman, 2007).

Prowell et al. (Prowell & Veers, 2009) summarized the existing design methods and the research works about the seismic risk on wind turbine. This study suggested that it is more efficient to use the full system models in analyzing seismic demand for wind turbines than just analyzing the tower. It also showed that the soil structure interaction when incorporated into these full system models had strong influence on higher nodes. The research concluded that a good progress has been made in the systematic consideration of different kind of loads in the wind turbine especially the seismic load and the consistent consideration of these loads will definitely enhance the reliability and economic viability of wind turbines (Prowell & Veers, 2009).

Prowell et al. (Prowell I. , Veletzos, Elgamal, & Restrepo, 2009) performed a full-scale shake table test and a finite element model of 65 KW wind turbine with a hub height of 23 m to study the seismic response characteristics. The wind turbine was loaded with five historical earthquakes of California both uni-axially and bi-directionally and both in parked situation. First mode damping was estimated to be below 1% for the tested parked-turbine configuration. For small scale wind turbines, first mode of response spectrum provided a reasonable approximation but in case of larger turbines higher modes may play a prominent role in the overall seismic response (Prowell I. , Veletzos, Elgamal, & Restrepo, 2009).

Prowell et al. (Prowell, Elgamal, Uang, & Jonkman, 2010) compared the results of three earthquake loads applied on a 5 MW wind turbine while idling, continuously operating and in emergency shutdown scenarios combined with the wind load using the FAST code. In each case the structure was subjected to 11.4 m/s wind field and 22 sets of earthquakes were used. The results obtained will be used to validate the experimental outputs and refine the capability to the FAST code to accurately incorporate base shaking as a load source for wind turbines (Prowell, Elgamal, Uang, & Jonkman, 2010).

Nuta et al. (Nuta, Christopoulos, & Packer, 2011) performed finite element analysis of a 1.65 MW wind turbine tower under increment dynamic loads in three locations: Los Angeles, Eastern Canada and Western Canada. The analysis in either location in Canada showed that the seismic risk was very low but in Los Angeles area was very high but still not significant at the intensity level of the design earthquake. This is due to the long fundamental period of the tower and the short predominant period of most earthquakes (Nuta, Christopoulos, & Packer, 2011).

Remi André Kjølraug et al. (Kjølraug, 2013) conducted research on 65 KW wind turbine and a hypothetical 5 MW wind turbine using finite element software SAP2000. Responses obtained from 65 KW wind turbine compared well with the experimental values obtained from the shake table test so it assured the validity of finite element model of 5 MW. The wind turbine was excited uni-axially by vertical and horizontal components of the 1985 Nahanni, Canada earthquake. Also the wind load was applied as a static load, dynamic load and not applied at all. The responses were severe at the upper part of wind turbine tower when vertical acceleration was applied. In case of the horizontal acceleration applied the responses were maximum in the middle parts of the tower. Finally in case of wind loads, dynamic wind-induced load produced large displacements than most of the displacement from the earthquake load and also it

induced larger response than the statically applied wind. Soil-structure interaction was extremely important in case of application of both components of earthquake loads but had less effect with wind-induced load alone (Kjørlaug, 2013).

CHAPTER III

THEORITICAL FORMULATIONS AND METHODOLOGY

Equation of Motion and Newmark Method

In obtaining a solution to a time dependent (dynamic) problem, a finite difference procedure is utilized by discretization of time over the history of dynamic action and reaction in order to obtain a solution of time dependent (dynamic) problem. For single degree of freedom (SDOF) system with linear damping and stiffness, dynamic equation governing the motion of spring-damper-mass system is:

$$M \ddot{u}(t) + C \dot{u}(t) + K u(t) = F^a \quad (1)$$

Where, M is the mass

C is the damping

K is the stiffness

$\ddot{u}(t)$ is the acceleration

$\dot{u}(t)$ is the velocity and

$u(t)$ is the displacement

F^a is the applied force

Similarly for a multi-degree of freedom (MDOF), dynamic equation can be represented as

$$[M]\{\ddot{u}(t)\} + [C]\{\dot{u}(t)\} + [K] \{u(t)\} = \{F^a\} \quad (2)$$

Where, [M], [C] and [K] are mass, damping and stiffness matrices respectively.

$\{\ddot{u}(t)\}, \{\dot{u}(t)\}, \{u(t)\}$ are nodal acceleration, velocity and displacement respectively.

$\{F^a\}$ is the applied force vector.

The most general approach for the solution of the dynamic response of structural systems is the direct numerical integration of the dynamic equilibrium equations. There are large number of accurate, higher order, multi-step methods that have been developed in order to solve the differential equations. In order to calculate the response using the above equations over the duration of an earthquake load or earthquake time history, solution of these equations has to be calculated over a series of time steps that start from the beginning of the earthquake load. Ending time depends on the damping properties of the system and whether the free vibration phase should be studied or not.

The solutions obtained from these methods are assumed to be a smooth function with continuous higher derivatives but the exact solution of non-linear structures requires the acceleration and the second derivative of the displacement not to be smooth functions. Therefore for the solution of this kind of discontinuity in acceleration only single-step methods is implemented.

Newmark developed a family of single-step integration methods for the solution of structural dynamic problems for both blast and seismic loading known as Newmark time integration method. This method is a popular method used by ANSYS in order to solve the above stated equation (2). This method uses finite difference expansions in the time interval Δt , in which it is assumed that

$$\{\dot{u}_{n+1}\} = \{\dot{u}_n\} + [(1 - \delta) \{\ddot{u}_n\} + \delta \{\ddot{u}_{n+1}\}] \Delta t \quad (3)$$

$$\{u_{n+1}\} = \{u_n\} + \{\dot{u}_n\} \Delta t + \left[\left(\frac{1}{2} - \alpha \right) \{\ddot{u}_n\} + \alpha \{\ddot{u}_{n+1}\} \right] \Delta t^2 \quad (4)$$

where,

α and δ are the Newmark integration parameters

$\{u_n\}, \{\dot{u}_n\}, \{\ddot{u}_n\}$ are nodal displacement, velocity and acceleration vectors respectively at time t_n

$\{u_{n+1}\}, \{\dot{u}_{n+1}\}, \{\ddot{u}_{n+1}\}$ are the nodal displacement, velocity and acceleration vector respectively at time t_{n+1}

Here in this equation $\Delta t = t_{n+1} - t_n$

The governing equation (1) can be written at time t_{n+1} to calculate $\{u_{n+1}\}$ as follows:

$$[M] \{\ddot{u}_{n+1}\} + [C] \{\dot{u}_{n+1}\} + [K] \{u_{n+1}\} = \{F_{n+1}^a\} \quad (5)$$

Rearranging equations (4) and (5) as follows to find the value of $\{u_{n+1}\}$:

$$\{\ddot{u}_{n+1}\} = a_0 (\{u_{n+1}\} - \{u_n\}) - a_2 \{\dot{u}_n\} - a_3 \{\ddot{u}_n\} \quad (6)$$

$$\{\dot{u}_{n+1}\} = a_5 \{\dot{u}_n\} - a_6 \{\ddot{u}_n\} - a_7 \{\dot{u}_{n+1}\} \quad (7)$$

$$\text{where, } a_0 = \frac{1}{\alpha \Delta t^2}, \quad a_1 = \frac{\delta}{\alpha \Delta t}, \quad a_2 = \frac{1}{\alpha \Delta t}, \quad a_3 = \frac{1}{2\alpha} - 1$$

$$a_4 = \frac{\delta}{\alpha} - 1, \quad a_5 = \frac{\Delta t}{2} \left(\frac{\delta}{\alpha} - 2 \right), \quad a_6 = \Delta t (1 - \delta) \quad \text{and} \quad a_7 = \delta \Delta t$$

$\{\ddot{u}_{n+1}\}$ in equation (3) can be substituted in equation (4), the equations for $\{\ddot{u}_{n+1}\}$ and $\{\dot{u}_{n+1}\}$ are thus expressed in terms of unknown displacements $\{u_{n+1}\}$ and the known displacements $\{u_n\}$, velocities $\{\dot{u}_n\}$ and accelerations $\{\ddot{u}_n\}$ at the time t_n . The equations for $\{\ddot{u}_{n+1}\}$ and $\{\dot{u}_{n+1}\}$ are then substituted in equation (5) to get,

$$(a_0 [M] + a_1 [C] + [K]) \{u_{n+1}\} = \{F_{n+1}^a\} + [M] (a_0 \{u_n\} + a_2 \{\dot{u}_n\} + a_3 \{\ddot{u}_n\}) + [C] (a_4 \{u_n\} + a_5 \{\dot{u}_n\} + a_6 \{\ddot{u}_n\}) \quad (8)$$

First the unknown displacements $\{u_{n+1}\}$ are obtained from equation (8), equation (6) and equation (7) are used to update the velocities and accelerations. The Newmark parameters are related to the input as follows:

$$\alpha \geq \frac{1}{4} \left(\frac{1}{2} + \delta^2 \right)^2 \quad \text{and} \quad \delta \geq \frac{1}{2} \quad (9)$$

γ is the amplitude decay factor. If $\gamma \geq 0$, the solutions of equation (5) are stable (Zienkiewicz, Taylor, & Taylor, 1977). The above conditions can be written as:

$$\alpha = \frac{1}{4} (1 + \gamma)^2, \quad \text{and} \quad \delta = \frac{1}{2} + \gamma \quad (10)$$

The amount of numerical dissipation can be controlled by one parameter δ in Eq. (9). However, at lower frequency modes the Newmark method fails to retain the second-order accuracy since $\delta > \frac{1}{2}$. Note that the Newmark implicit method (constant average method, namely $\delta = \frac{1}{2}$ and $\alpha = \frac{1}{4}$), which is unconditionally stable and second-order accurate, has no numerical damping. If other sources of numerical damping are not introduced, the lack of numerical damping can be undesirable so that the higher frequencies of the structure can produce unacceptable levels of numerical noise (Hughes, 1987). To circumvent the drawbacks of the Newmark family of methods, the ANSYS program implements the generalized HHT- α method which sufficiently damps out spurious high-frequency response via introducing controllable numerical dissipation in higher frequency modes, while maintaining the second-order accuracy. It should be noted that the generalized HHT- α method incorporated in the program is capable of recovering the WBZ- α method (Wood, Bossak, & Zienkiewicz, 1980) and the HHT- α method (Hilber, Hughes, & Taylor, 1977) as well as the Newmark family of time integration algorithms, depending upon the user's input.

To solve for the three unknowns $\{u_{n+1}\}$, $\{\dot{u}_{n+1}\}$ and $\{\ddot{u}_{n+1}\}$ along with equation (3) and equation (4) the generalized HHT- α method uses the algebraic equation:

$$[M] \{\ddot{u}_{n+1-\alpha_m}\} + [C] \{\dot{u}_{n+1-\alpha_f}\} + [K] \{u_{n+1-\alpha_f}\} = \{F_{n+1-\alpha_f}^a\} \quad (11)$$

where,

$$\{\ddot{u}_{n+1-\alpha_m}\} = (1 - \alpha_m) \{\ddot{u}_{n+1}\} + \alpha_m \{\ddot{u}_n\},$$

$$\{\dot{u}_{n+1-\alpha_f}\} = (1 - \alpha_f) \{\dot{u}_{n+1}\} + \alpha_f \{\dot{u}_n\},$$

$$\{u_{n+1-\alpha_f}\} = (1 - \alpha_f) \{F_{n+1}^a\} + \alpha_f F_n^a \text{ and}$$

$$\{F_{n+1-\alpha_f}^a\} = (1 - \alpha_f) \{F_{n+1}^a\} + \alpha_f \{F_n^a\}$$

The generalized- α method uses the Newmark difference approximation equations which contain two parameters, γ and β . The quantities $\{u_{n+1}\}$, $\{\dot{u}_{n+1}\}$ and $\{\ddot{u}_{n+1}\}$ are linearly interpolated between two time stations t_n and t_{n+1} . These interpolations introduce two more parameters α_m and α_f , which is used to control the amplification of high frequency numerical modes.

Equation (11) give the finite difference form:

$$\begin{aligned} (a_0 [M] + a_1 [C] + (1 - \alpha_f)[K]) \{u_{n+1}\} = & (1 - \alpha_f) \{F_{n+1}^a\} + \alpha_f \{F_n^a\} - \\ & \alpha_f [K] \{u_n\} + [M](a_0 \{u_n\} + a_2 \{\dot{u}_n\} + a_3 \{\ddot{u}_n\}) + [C](a_1 \{u_n\} + a_4 \{\dot{u}_n\} + \\ & a_5 \{\ddot{u}_n\}) \end{aligned} \quad (12)$$

where,

$$\begin{aligned} a_0 = \frac{1-\alpha_m}{\alpha \Delta t^2}, \quad a_1 = \frac{(1-\alpha_f)\delta}{\alpha \Delta t}, \quad a_2 = a_0 \Delta t, \quad a_3 = \frac{1-\alpha_m}{2\alpha} - 1, \quad a_4 = \frac{(1-\alpha_f)}{\alpha} - 1, \\ a_5 = (1 - \alpha_f) \left(\frac{\delta}{2\alpha} - 1 \right) \Delta t \end{aligned}$$

HHT- α method uses equation (12) to calculate the value of $\{u_{n+1}\}$ at time t_{n+1} . Similarly, equation (6) and equation (7) can be used to find other two unknowns $\{\dot{u}_{n+1}\}$ and $\{\ddot{u}_{n+1}\}$. The generalized HHT- α method is an implicit time scheme so the structural stiffness matrix must be factorized to solve for $\{u_{n+1}\}$ at time t_{n+1} . This method is unconditionally stable and second order accurate if the parameter meet the following conditions (Prowell, Veletzos, & Elgamal, Full Scale Testing for Investigation of Wind Turbine Seismic Response, 2008):

$$\delta = \frac{1}{2} - \alpha_m + \alpha_f, \quad \alpha \geq \frac{1}{2} \delta \quad \text{and} \quad \alpha_m \leq \alpha_f \leq \frac{1}{2} \quad (13)$$

where $\alpha_m \leq 0$ (Wood, Bossak, & Zienkiewicz, 1980) [47] and $\alpha \leq \beta \leq \frac{1}{2}$ (Hilber, Hughes, & Taylor, 1977). The user can also control the amount of numerical damping by introducing the amplitude decay factor $\gamma \geq 0$. In HHT- α method the amplitude decay factor is recommended to be $\gamma = 0.05$ (Hughes, 1987), with which any spurious

participation of the higher modes can be damped out and the lower modes remain unaffected. Although it is not recommended but a significant amount of damping can be introduced by setting $\gamma = \frac{1}{3}$.

Modal Analysis

Mode Analysis is the most fundamental analysis type which is used to determine a structure's vibration characteristics such as:

- Natural Frequencies
- Mode Shapes
- Mode participation factors (how much mode participates in a given direction)

Thus it is important to perform a modal analysis first before trying any other dynamic analysis. Mode extraction is the term used to describe the calculation of eigen values and eigen vectors. There are several methods of modal analysis in ANSYS workbench (Block Lanczos, Subspace, Reduced, Damped (full), QR Damped etc.). Block Lanczos method is a fast and robust method used for most applications as the default solver.

Block Lanczos Method

Block Lanczos method is a frequency domain procedure used to analyze the modal properties of the structures. The great number of Eigen pairs is needed often for seismic analysis, the Block Lanczos method is recognized as a most powerful tool for extraction of large number of Eigen pairs in large-scale problems of structural mechanics. This method uses the Lanczos algorithm to solve the Eigen vectors. Fundamental features of the Block Lanczos method can be listed as follows:

- Efficient extraction of large number of modes in most models

- Typically used in complex models with mixture of solids/shells/beams etc.
- Efficient extraction of modes in a frequency range
- Handles rigid-body modes as well.

For accurate results using Block Lanczos method, number of modes are selected in a way to include at least 90% of the effective mass. The effective mass for the i^{th} mode is

$$M_{ei} = \frac{\gamma_i^2}{\{\emptyset\}_i^T [M]_i \{\emptyset\}_i} \quad (14)$$

where, $\gamma_i, \{\emptyset\}_i, [M]_i$ are shape factor, mode shape and mass matrix for the i^{th} mode respectively.

Note that $\{\emptyset\}_i^T [M]_i \{\emptyset\}_i = 1$ so that the effective mass reduces to γ_i^2 .

The cumulative mass fraction for the i^{th} mode is

$$\widehat{M}_{ei} = \frac{\sum_{j=1}^i M_{ej}}{\sum_{j=1}^N M_{ej}} \quad (15)$$

where, N is the number of modes

Transient Response (Time-History) Analysis

In ANSYS Workbench, we use transient analysis to calculate the response of a structure under an action of arbitrary time-dependent loading. Two methods are available to perform transient analysis: Direct Integration Method and Modal Superposition Method.

Direct Integration Method

This method is a step by step integration method, where the integration of the equations of motion of a structure is solved for a given time interval using solutions of a previous time step as an initial value. There is no need for the calculation of the natural mode

shapes and natural frequencies in this method. Direct integration method can be used for both linear and non-linear analyses. It is used for systems that have non-symmetric stiffness and complex damping (i.e damping dependent on frequency, etc). However the main drawback of this method is that it requires more computational resources compared to modal superposition method. This method produces large number of output, which requires a large-processing effort to perform all the necessary design checks as a function of time.

Modal Superposition Method

Modal equations of motions which are a reduced form of the equations of motion by expressing the displacement of the physical system in terms of vibration modes. For linear response analysis, the mode superposition method is used to uncouple the system's equation of motion so that the dynamic response can be obtained separately for each mode of vibration and then these responses can be superimposed for all significant modes to obtain the total response. The main advantage of mode superposition method over the direct step method is that it is faster and requires less computational resources. Thus this method is more reliable method for performing linear or mildly non-linear dynamic analysis. This method is not as reliable as direct step method for non-linear analysis.

Damping Calculation

Damping can be defined as the measure of energy dissipation in a vibrating structure that results in bringing it to rest. Damping causes the amplitude of a vibrating body to decay with time. Critical damping C_c is defined as the amount of damping that will produce an equilibrium state with no oscillation. There is another term called “damping

ratio”, denoted by ξ , which is a dimensionless quantity and is defined as the ratio of actual damping to the critical damping.

$$\xi = \frac{\text{Actual Damping}}{\text{Critical Damping}} = \frac{c}{c_c} \quad (16)$$

Depending on the characteristics of damping, a structure can be categorized as undamped, under-damped, over-damped and critically damped structure. If $\xi = 0$, $\xi < 1$, $\xi = 1$ and $\xi > 1$ then it is called undamped, under-damped, critically damped and over-damped respectively.

Determining the damping values is a complicated and tricky process. There are many factors and design details that affect damping. The material and friction force (the internal friction existing in the materials and Coulomb friction existing in connections of the structure) can be the major source of damping. However, the exact sources of damping are very complex and also it is a complicated process to represent damping mathematically. Moreover, damping is often not linear, thus, it is very difficult to calculate the actual value of damping. One can find the actual damping ratio of a structure by test measurement which is the most accurate method.

For a direct integration method, a physical damping mechanism such as dashpot (uses viscous friction) is often used to introduce damping. But for other structures which do not have such an option, general mechanism of damping such as Rayleigh Damping Model is used. Rayleigh Damping is also known as proportional damping. Although the model may not be physically correct (infinite damping at $\omega = 0$), but it is accepted for general use of damping (Gwon, 2011). ANSYS workbench permits the application of Rayleigh Damping method in which we first consider mass-proportional damping and stiffness-proportional damping:

$$[C] = \alpha [M] \text{ and } [C] = \beta [K] \quad (17)$$

Where the constants α and β have units s^{-1} and s , known as mass and stiffness damping coefficients respectively.

In order to construct a classical damping matrix somewhat consistent with the experimental value, damping is assumed to be a linear combination of damping associated with the mass and stiffness matrix:

$$[C] = \alpha [M] + \beta [K] \quad (18)$$

The damping ratio for the n^{th} mode of such a system is

$$\xi_n = \frac{\alpha}{2\omega_n} + \frac{\beta}{2} \omega_n \quad (19)$$

The coefficients α and β can be determined from specific damping ratios ξ_i and ξ_j for the i^{th} and j^{th} modes, respectively.

Solving the above matrix considering the same damping ratio ξ , which is reasonable based on experimental data we obtain

$$\alpha = \frac{2\omega_i\omega_j}{\omega_i^2 - \omega_j^2} (\omega_i - \omega_j) \xi \quad (20)$$

$$\beta = \frac{2}{\omega_i^2 - \omega_j^2} (\omega_i - \omega_j) \xi \quad (21)$$

Where,

ω_i and ω_j represent the natural circular frequency of the i^{th} and j^{th} modes respectively.

α is mass coefficient

β is stiffness coefficient

Earthquake Loads

The expansion of wind turbine in the seismically active regions have all of a sudden spurred the interest in the consideration of earthquake loads on wind turbines (Riso 2001, Agbayani, 2002, Bazeos et al 2002, Lavassas et al 2003, Witcher 2005, Zhao and Maisser 2006, Zhao et al 2007). The main concerns for such kind of loading are (Prowell, Veletzos, & Elgamal, Full Scale Testing for Investigation of Wind Turbine Seismic Response, 2008) :

1. Seismic Risk
 - a. Anticipated Level of Shaking
 - b. Recurrence of shaking
2. Local Soil Properties
3. Structural Properties
 - a. Structural Frequency
 - b. Structural Ductility
 - c. Structural Damping

Earthquake loads are included as both vertical and horizontal accelerations applied as uni-axial excitations input in the form of time history accelerations at the tower base. The responses that can be studied from the applied accelerations can be displacement and acceleration at the top of the nacelle and stress near the base of the tower.

In order to study the effects of resonance in the earthquake loading, selected earthquake loads should have frequencies close to the frequency of turbines so that they can excite natural modes of the turbine. Thus we selected three different earthquakes as follows:

1. Horizontal and Vertical Components of Landers Earthquake (June 28th, 1992) with Peak Ground Acceleration (PGA) = 0.154g and 0.1667g respectively (DHS station). Moment magnitude of Landers Earthquake was 7.3 M_w .
2. Horizontal and Vertical Components of Imperial Valley Earthquake (May 18th, 1940) with PGA = 0.348g and 0.21g respectively (USGS station 117). Moment magnitude of Imperial Valley earthquake was 6.9 M_w .
3. Horizontal and Vertical Components of Northridge Earthquake (January 17th, 1994) with PGA = 0.344g and 0.552g respectively (Arleta-Nordhoff Ave Fire Station station 24087). Moment magnitude of Northridge earthquake was 6.7 M_w .

Each of the three horizontal load components were simulated twice for each model in two horizontal directions.

All the datas for these earthquakes were collected from “Center for Engineering Strong Motion Data (CESMD)”.

Landers Earthquake

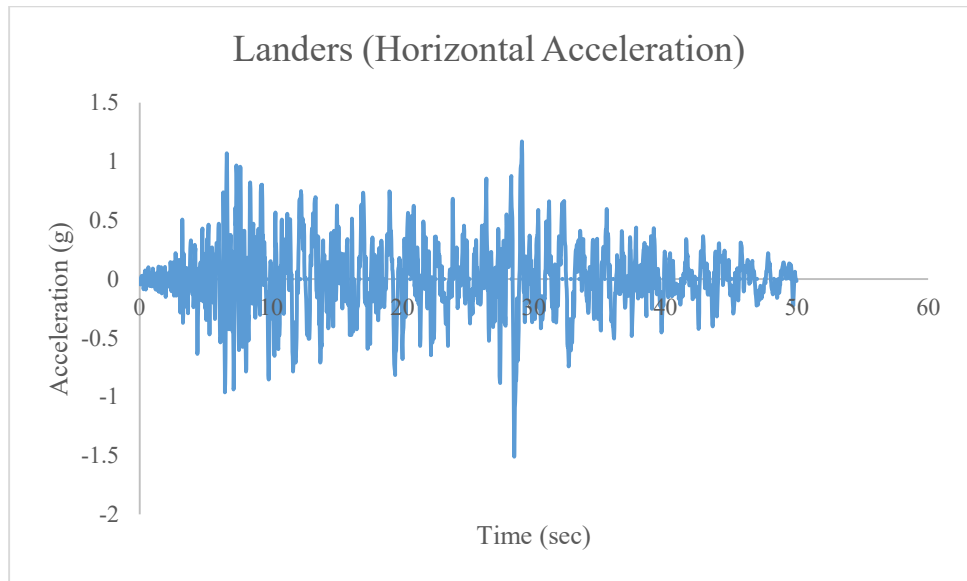


Figure 13. Horizontal Acceleration Vs. Time For Landers Earthquake

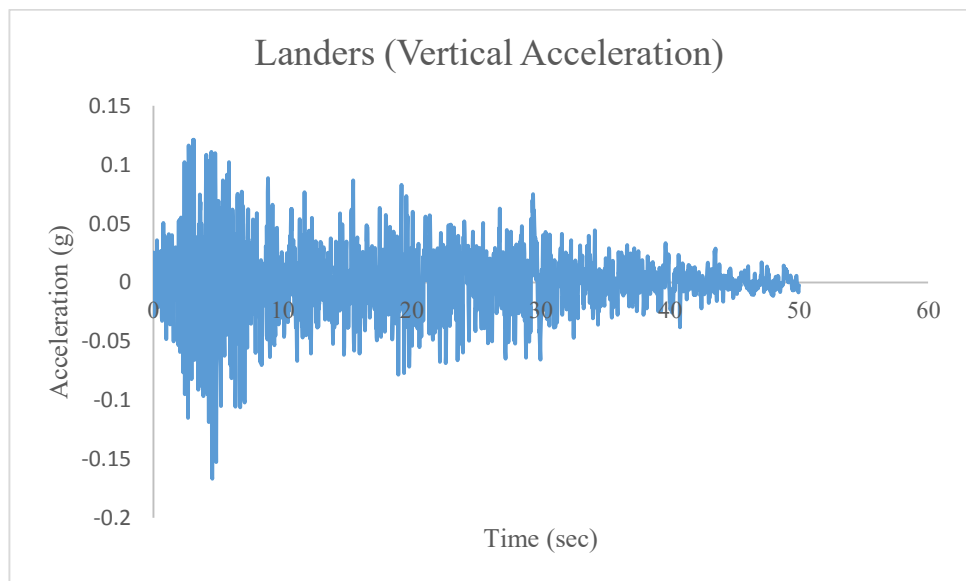


Figure 14. Horizontal Acceleration vs Time for Landers Earthquake

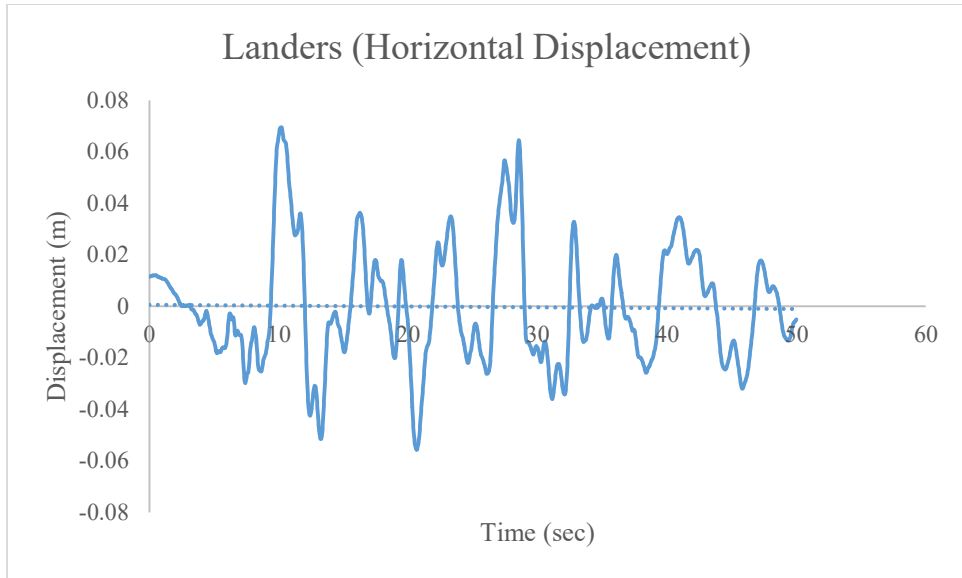


Figure 15. Horizontal Displacement vs Time for Landers earthquake

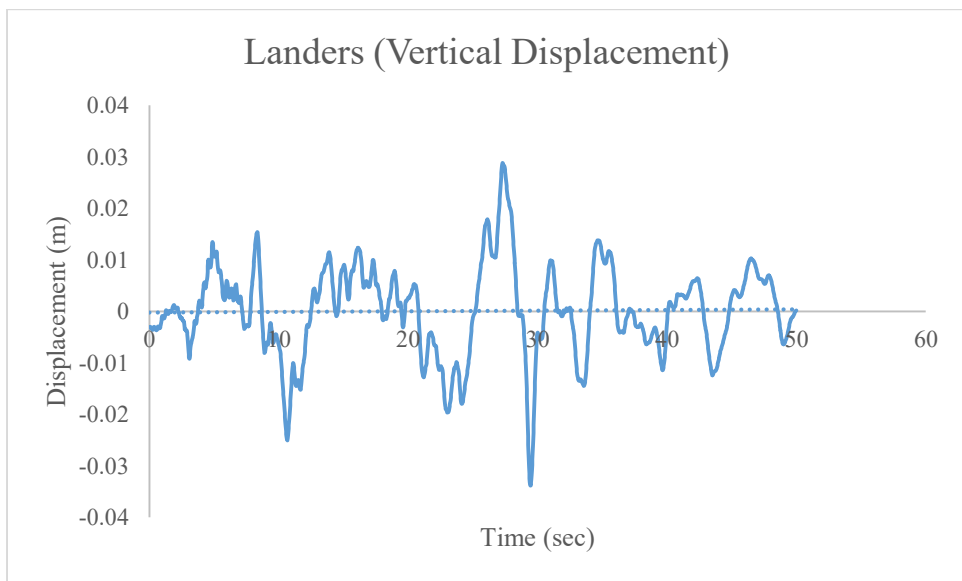


Figure 16. Vertical Displacement vs time for landers earthquake

Table 1. Peak magnitudes for Landers Earthquake

Landers Earthquake	Horizontal	Vertical
Acceleration (g)	0.154	0.166
Velocity (m/s)	0.208	0.098
Displacement (m)	0.069	0.033

El Centro Earthquake

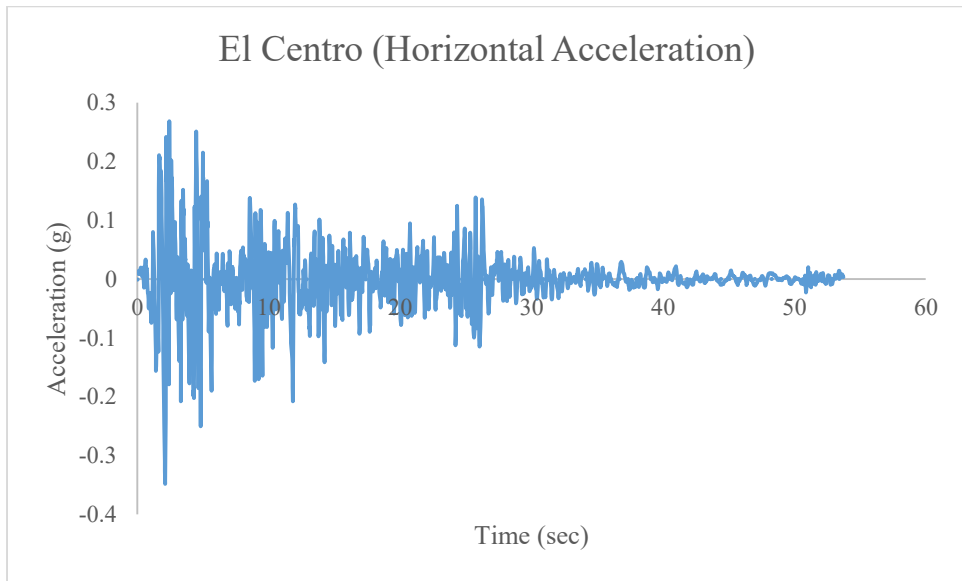


Figure 17. Horizontal Acceleration vs Time for El Centro Earthquake

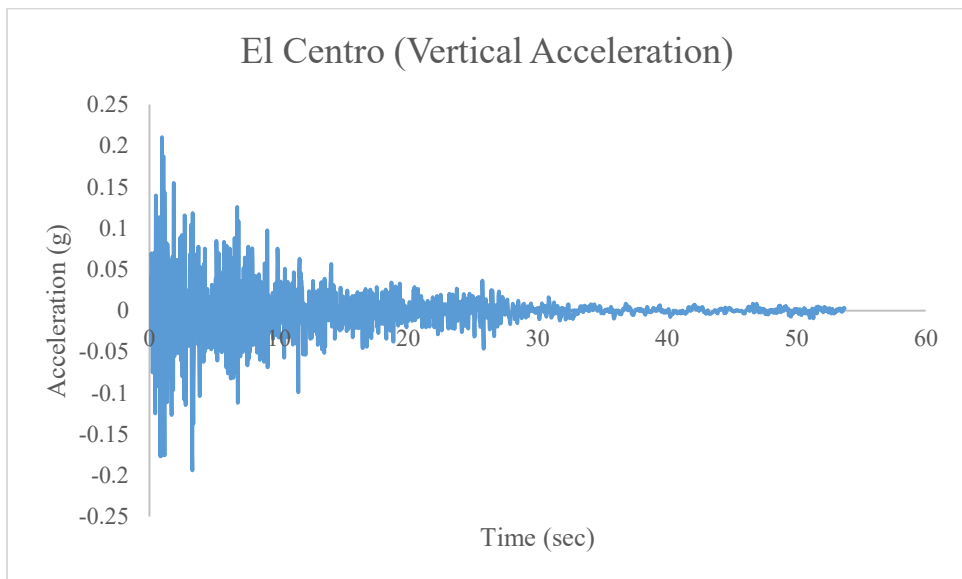


Figure 18. Vertical Acceleration vs Time for El Centro Earthquake

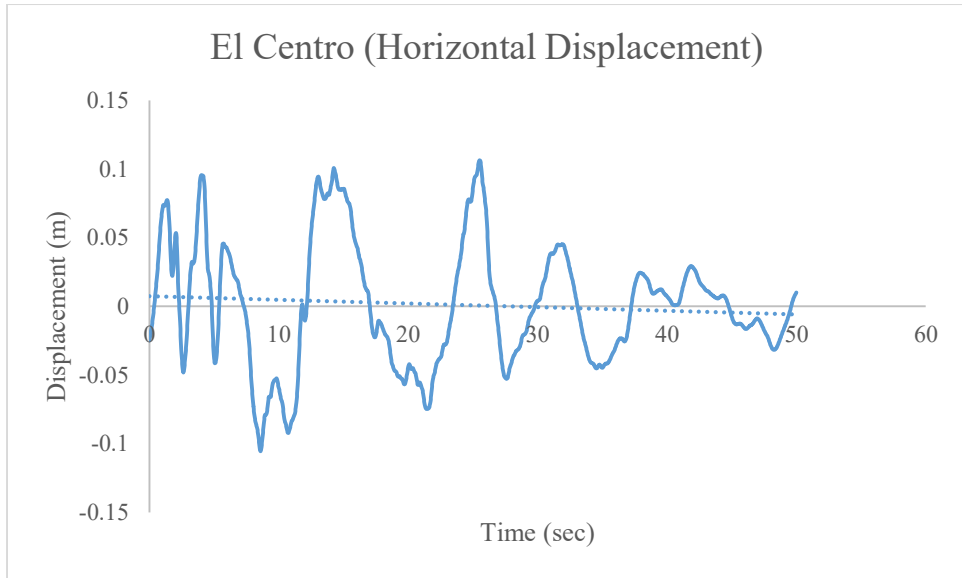


Figure 19. Horizontal Displacement Vs. Time for El Centro Earthquake

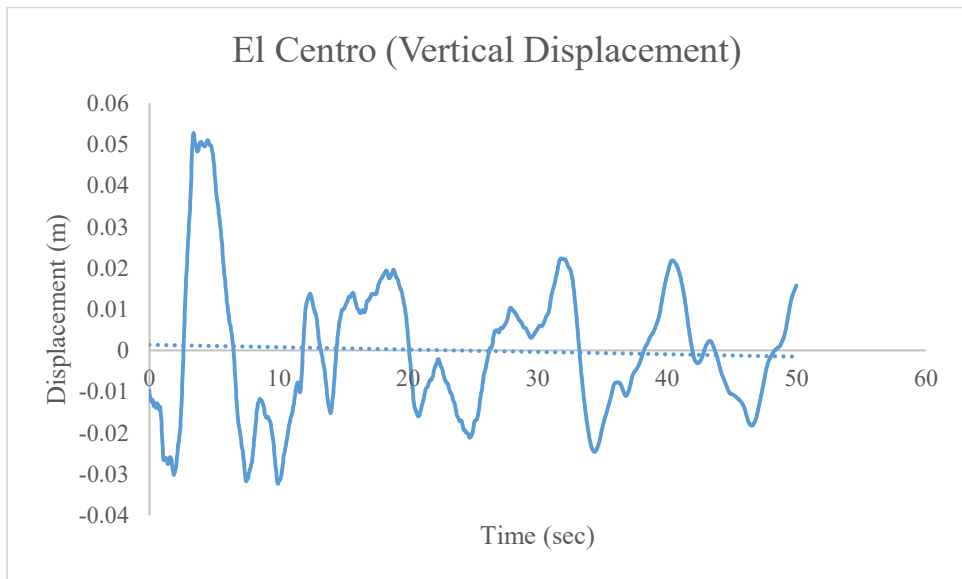


Figure 20. Vertical Displacement vs Time for El Centro Earthquake

Table 2. Peak Magnitudes for El Centro Earthquakes

El Centro	Horizontal	Vertical
Acceleration (g)	0.348	0.21
Velocity (m/s)	0.331	0.11
Displacement (m)	0.106	0.052

Northridge Earthquake

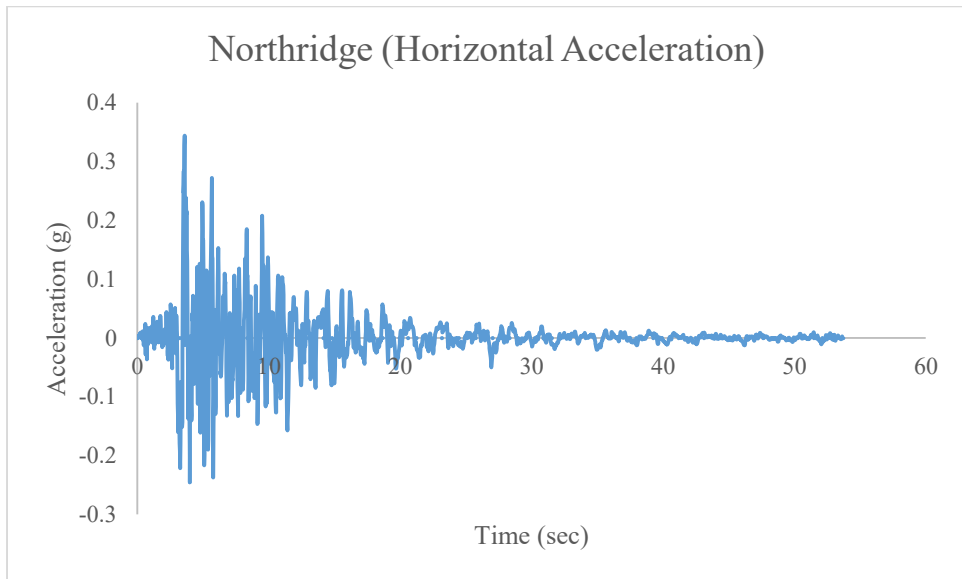


Figure 21. Horizontal Acceleration vs Time for Northridge Earthquake

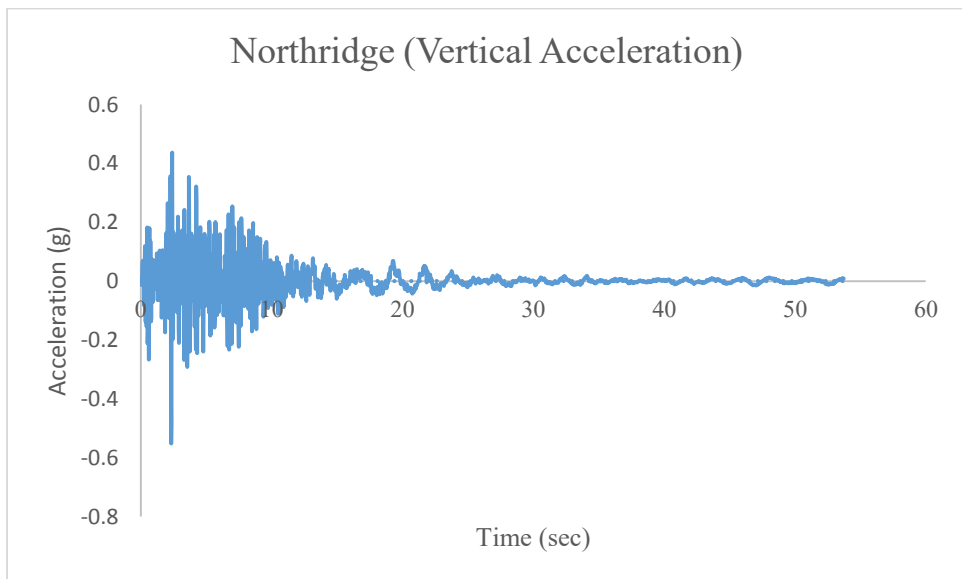


Figure 22. Vertical Acceleration vs Time for Northridge Earthquake

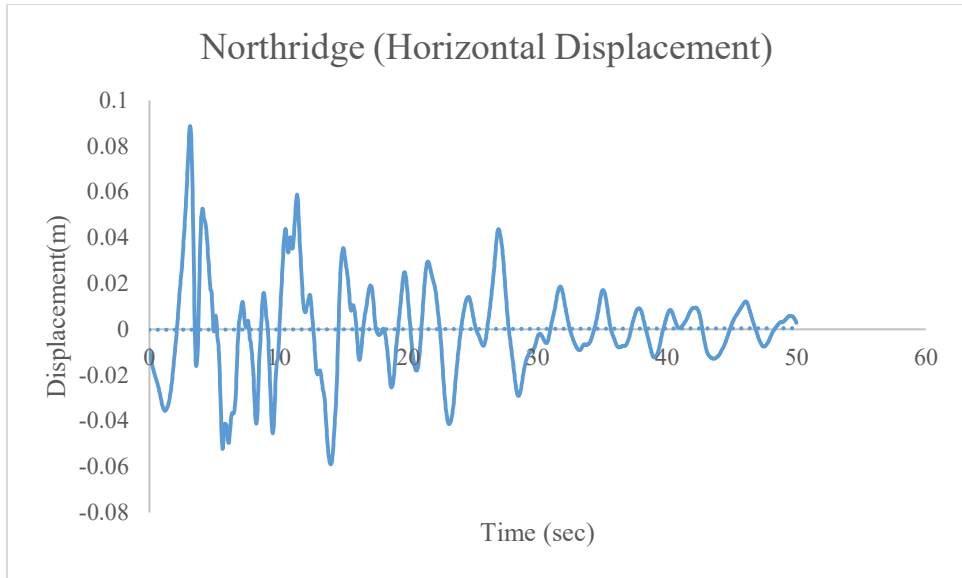


Figure 23. Horizontal Displacement vs Time for Northridge Earthquake

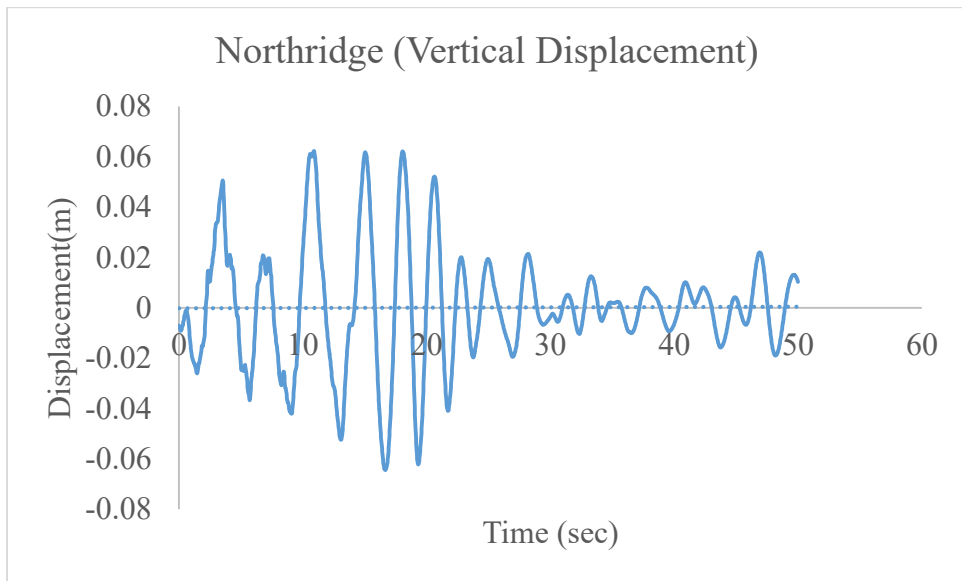


Figure 24. Vertical Displacement vs time for Northridge Earthquake

Table 3. Peak Magnitudes for Northridge Earthquakes

Northridge Earthquake	Horizontal	Vertical
Acceleration (g)	0.344	0.552
Velocity (m/s)	0.403	0.175
Displacement (m)	0.088	0.064

Assumptions and Considerations

All the models of wind turbine consist of a flexible tower, a nacelle attached to a tower and a rotor attached to a nacelle via hub. The shell element of a tower is considered to withstand buckling thus the local buckling is neglected. Usually, stiffeners are used in order to prevent local buckling but in computer model we do not consider modelling stiffeners because it reduces the number of nodes and elements which means the time required for the analysis reduces drastically. The base of the tower has fixed support so all the translational degree of freedom at the base is restricted to zero. Similarly the connection between the nacelle and tower is fixed. The rotor blades are considered to be locked and they are in parked condition with one of the rotor blade facing vertically downwards. The locking of the blades helps to prevent excessive force on the mechanical parts. The effect of soil-foundation-structure interaction and also air-structure interaction is neglected so that these factors have no effect in the damping. The total analysis time for each simulation depends on the duration of the earthquake load applied and the number of nodes and elements in each component of the wind turbine. Material, geometrical and other nonlinearities are ignored since all turbines are assumed to perform linearly elastic under the design loads.

CHAPTER IV

TEST AND RESULTS

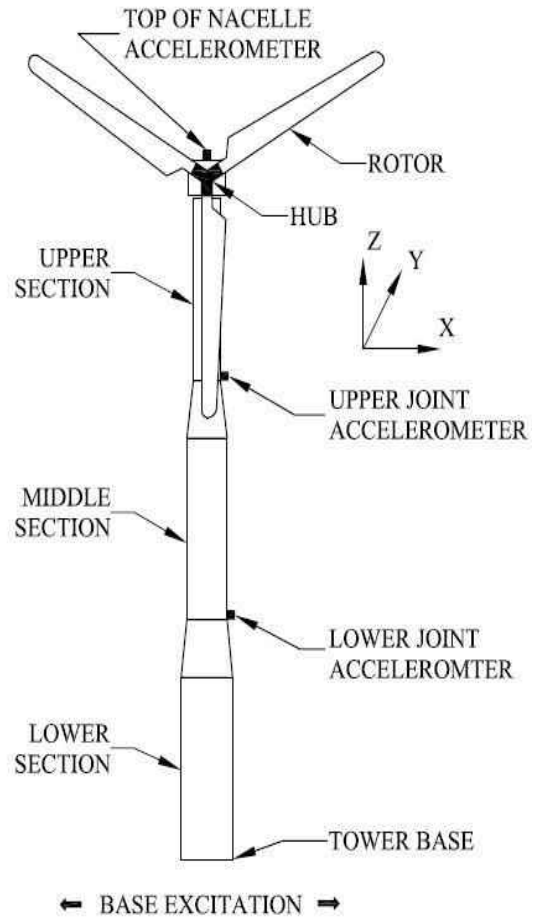
Test Description

Researchers at the University of San Diego (UCSD) performed a full scale test of a 65 KW Wind Turbine, provided by Oak-Creek Energy Systems of Mojave, CA. The wind turbine was mounted on the Network for Earthquake Engineering Simulation (NEEC) shake table located at UCSD and subjected to base shaking that simulated an actual earthquake. The responses to the applied earthquakes were recorded by instruments attached to the turbine (Prowell, Veletzos, & Elgamal, Full Scale Testing for Investigation of Wind Turbine Seismic Response, 2008) [49].

In November 2004, the wind turbine was mounted on a shake table and subjected to the earthquake excitation. The tower of the turbine was made of three tubular steel sections with two frustum transitional regions and is similar to the modern conical towers. The experiment was performed with the rotor having one of its blade oriented vertically downwards, parallel to the main tower. The acceleration data was derived from Desert Hot Spring (DHS) station; East-West component (0.15g PGA) of Landers Earthquake (June 28th, 1992 with moment magnitude $M_w = 7.3$). Earthquake load was applied uni-axially in the horizontal direction, applied to the basement of the tower through a 7.6 x 12.2 m² shaking table perpendicular to the rotor's axis.



(a) Shake Table Setup



(b) Accelerometer Locations

Figure 25. 65 KW Wind Turbine Shake Table Test (Prowell I. , An experimental and numerical study of wind turbine seismic behavior, 2011)

To remove the unnecessary DC offset (mean amplitude displacement from zero) as well as high frequency noise, the original earthquake record was filtered with a pass band of 0.05 to 25 Hz. The record was then scaled to approximately 100%, 150% and 200% of the original amplitude for the tests (Prowell I. , An experimental and numerical study of wind turbine seismic behavior, 2011) [50].

Test Results

The natural frequencies and the corresponding mode shapes of the wind turbine were derived from the experimentally observed data, obtained from different accelerometers

placed at different heights of the tower. Observed first and second natural frequencies are 1.7 Hz and 11.7-12.3 Hz respectively. Mode shapes at each accelerometer location are obtained using an average of the amplitude and phase of the estimate of the frequency response of the transfer function. These mode shapes seem to resemble the bending modes of a cantilever beam with a point mass (Laura, Pombo, & Susemihl, 1974) [51]. Equivalent viscous damping at the first natural frequency was estimated using the recorded time histories by log decrement method and is found to be 0.86%.

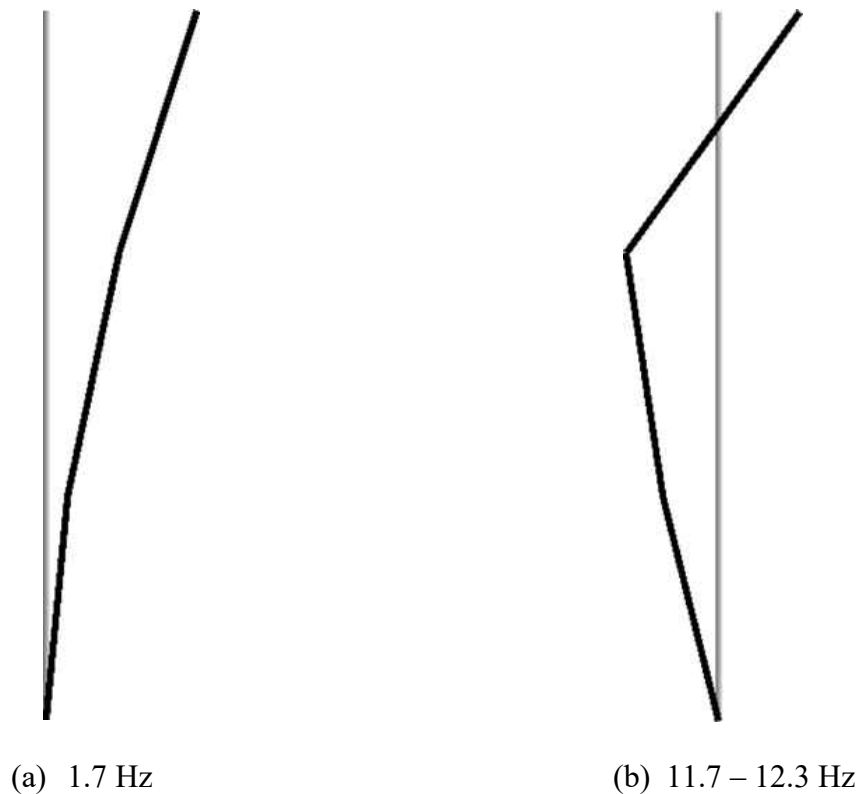


Figure 26. Experimentally observed side-to-side modes (Prowell, Veletzos, & Elgamal, Full Scale Testing for Investigation of Wind Turbine Seismic Response, 2008)

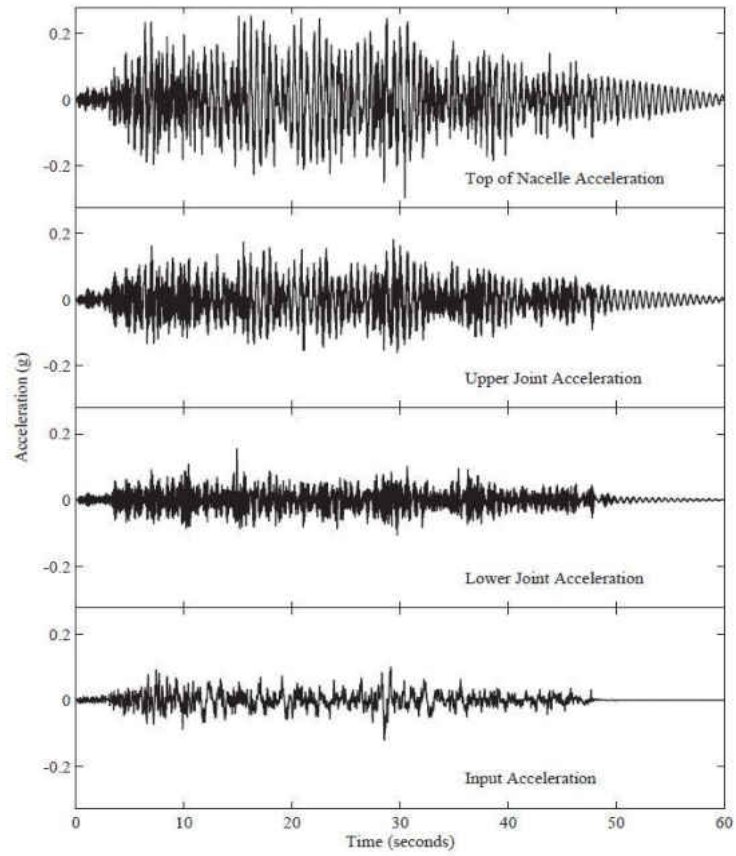


Figure 27. Recorded Acceleration for Landers (100% level Test) (Prowell, Veletzos, & Elgamal, Full Scale Testing for Investigation of Wind Turbine Seismic Response, 2008)

CHAPTER V

FINITE ELEMENT ANALYSIS OF WIND TURBINES

ANSYS workbench is a common platform for solving engineering problems. You can either import a model or draw a model in ANSYS workbench, perform FEA analysis and obtain the results in various formats depending on the type of simulation. The modelling and simulation of the wind turbine models are done by a finite element software ANSYS 16.2.

A three dimensional FE model of the wind turbine is modelled with each model comprising of a long slender tower, a nacelle, a hub and a rotor. Tower and rotor blades are meshed using shell elements and nacelle and hub are meshed with solid elements. The base of the tower is constrained in all directions.

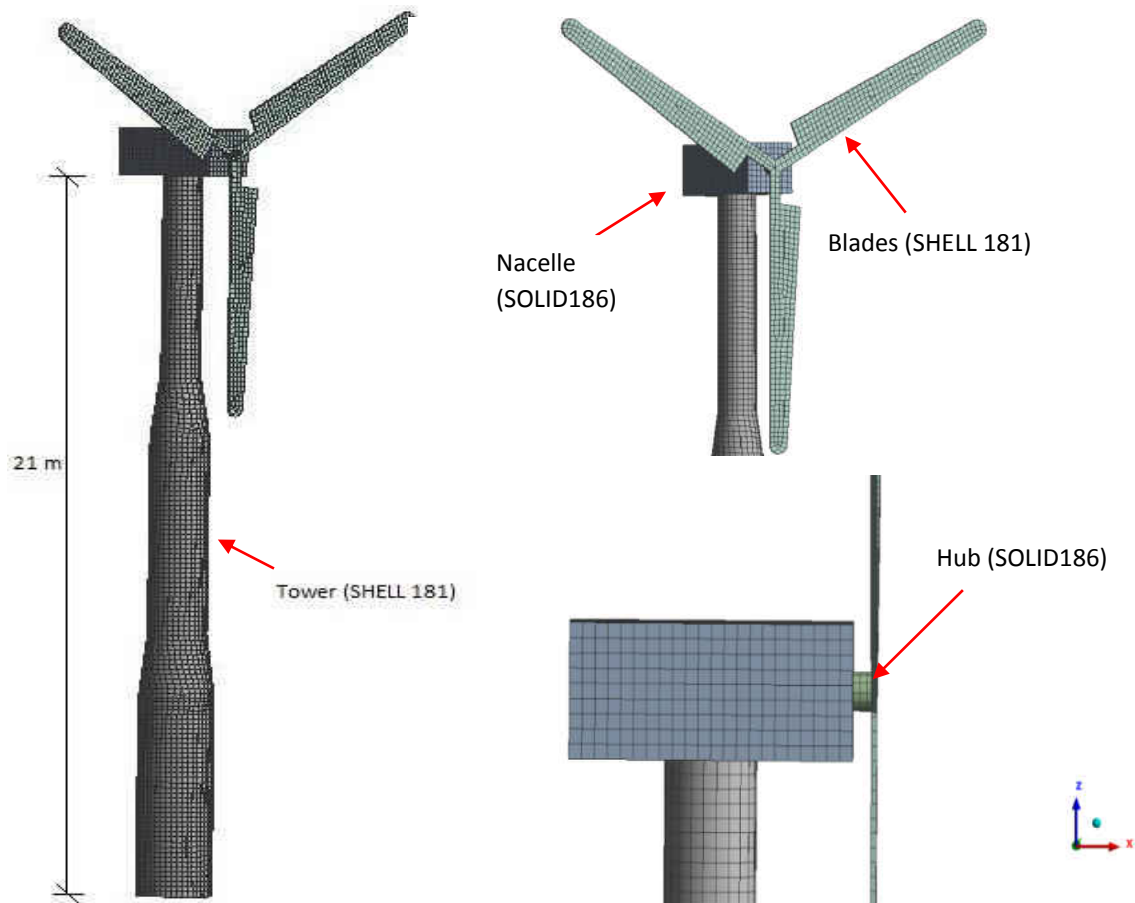


Figure 28. Finite Element Model of 65 KW Wind Turbine

In our case we perform the dynamic analysis of the wind turbines that we model in ANSYS Workbench. Dynamic analysis, basically consists of a modal analysis, response spectrum analysis and transient dynamic (time-history) analysis. In modal analysis, a set of undamped natural frequencies and the mode shapes of the model are calculated. The results obtained from the modal analysis were used as a basis for further step, the transient response analysis. These analysis were performed in order to obtain the responses of the wind turbine model after the application of time-varying transient load: earthquake.

Wind Turbines come in many sizes and configurations and are built from wide range of materials. In our case, two different materials are used while modelling the wind turbine. A carbon fiber composite material (epoxy reinforced with carbon fibers) is used for the rotor blades. Similarly, structural steel is used for the tower, nacelle and hub. Since the nacelle is a hollow steel box that contains rotor, magnets, electric wiring and other parts for generating electric power, its weight is much less than the steel box with the same volume. Hence we consider an equivalent low density for the nacelle in the FE model. Additional parts of the tower (flanges, bolts etc) are 1929 kg and modelled as distributed mass.

Table 4. Material Properties of the Wind Turbine Model

Property	Steel	Composite 1	Composite 2	Composite 3
Density	7,860 kg/m ³ (40 lbm/ft ³)	1,760 kg/m ³ (109.87 lbm/ft ³)	648 kg/m ³ (40 lbm/ft ³)	992 kg/m ³ (62 lbm/ft ³)
Young's Modulus	200,000 MPa (29,000 ksi)	235,000 MPa (34,084 ksi)	235,000 MPa (34,084 ksi)	235,000 MPa (34,084 ksi)
Poisson's Ratio	0.3	0.3	0.3	0.3
Tensile Yield Strength	250 MPa (36,000 psi)	3,920 MPa (569 ksi)	3,920 MPa (569 ksi)	3,920 MPa (569 ksi)
Tensile Ultimate Strength	460 MPa (66,700 psi)	3,920 MPa (569 ksi)	3,920 MPa (569 ksi)	3,920 MPa (569 ksi)

Composite 1, Composite 2 and Composite 3 are the material used for the blades of wind turbines 65 KW, 1 MW and 5 MW respectively.

SHELL elements are used to model structural elements in which two dimensions are much greater than the third one (thin structures) and when the change of the analyzed feature across this third direction can be neglected, however, if the change of the analyzed feature is on a comparable level in all the directions of the analyzed element SOLID elements should be used.

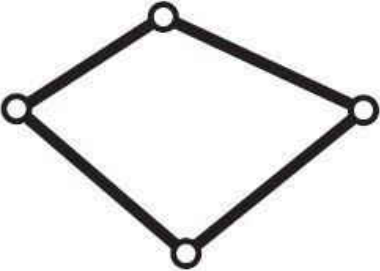
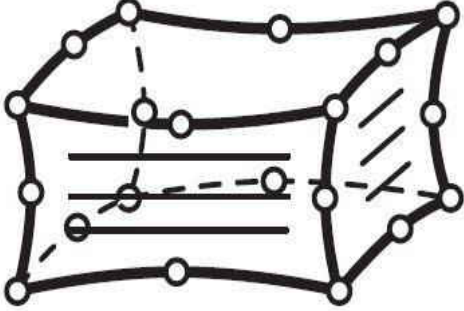
SHELL 181 is suitable for analyzing thin to moderately thick shell structures. SOLID 186 is well suited for modelling irregular meshes, linear, large rotation and/or large strain nonlinear applications. It is a 4-node element with 6 degree of freedom at each node: translations and rotation in x, y and z directions. If we use the membrane option in the SHELL element then it has translational degrees of freedom only. The degenerate triangular option should only be used as filler elements in mesh generation.

SOLID 186 is a higher order three dimensional solid element with 20 nodes and each node having three degree of freedom: translations in the nodal x, y, and z directions. SOLID 186 exhibits quadratic displacement behavior. The element supports plasticity, hyperplasticity, creep, stress stiffening, large deflection and large strain capabilities. SOLID 186 can mix any of the capabilities when running the simulations for nearly incompressible elastoplastic materials and fully incompressible hyperelastic materials. SOLID 186 is basically available in two forms:

- i. Homogenous Structural Solid: This element is suited to model irregular meshes. The element may have any spatial variations.
- ii. Layered Structural Solid: This element is used to model layered thick shells of solids.

Following table shows the comparison between SHELL181 and SOLID186 (ANSYS, 2013) [51].

Table 5. Element Types

Elements	Pictures
<p><u>SHELL 181</u></p> <p>4 – Node Structural Shell</p> <p>4 nodes 3 – D space</p> <p>DOF : $U_x, U_y, U_z, ROT_x, ROT_y, ROT_z$</p>	
<p><u>SOLID 186</u></p> <p>3-D 20-Node Structural Solid</p> <p>20 nodes 3 – D space</p> <p>DOF : U_x, U_y, U_z</p>	

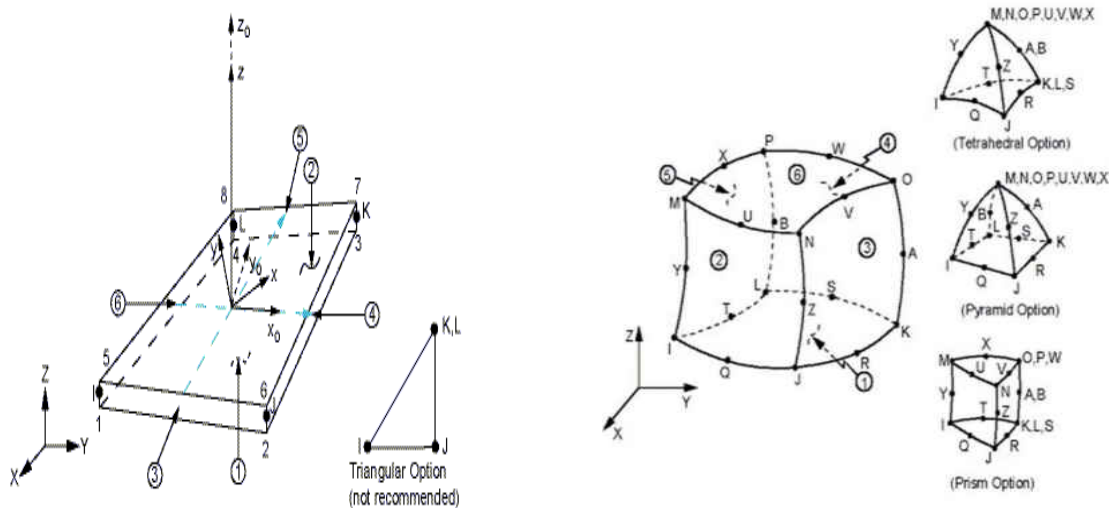


Figure 29. SHELL 181 and SOLID 186 Elements (ANSYS, 2013)[51]

Dimensions of Wind Turbines

The dimensions of wind turbines of power capacity 65 KW, 1 MW and 5 MW are based on the geometry of those turbines currently being used in the industry. The height of the vertical tower made of steel ranges from 21.9 m (71.8 ft) to 88.5 m (290.3 ft). Towers are conical in shape with constant thickness throughout the height for each wind turbine, ranging from 5.3 mm (0.21 in) to 27 mm (1.06 in) for smallest to largest wind turbine respectively. The tower for 65 KW wind turbine has two transition regions such that the whole tower is divided into three intermediate regions. But for the tower of 1 MW and 5 MW wind turbines they are purely conical in shape with relatively larger diameter at the base than at the top. The mass of the nacelle varies from 2400 kg (164 slugs) to 240,000 kg (16,445 slugs) for 65 KW, 1 MW and 5 MW turbines respectively. The mass of the hub varies from 246.93 kg (16.92 slugs) to 37334.8 kg (255.915 slugs) for 65 KW, 1 MW and 5 MW turbines respectively. The rotor of all three wind turbines consists of three blades made of composite material (epoxy carbon). Table 3 shows the geometrical properties of the wind turbine used in the study.

Table 6. Dimensions of wind turbines

Parts	65 KW	1 MW	5 MW
Blade Radius	8 m (26.25 ft)	30.31 m (99.44 ft)	63 m (206.693 ft)
Outer Diameter at the bottom of tower	2.02 m (6.63 ft)	3.88 m (12.73 ft)	6 m (19.685 ft)
Diameter at the top of tower	1.06 m (3.478 ft)	2.45 m (8.038 ft)	3.87 m (12.697 ft)
Diameter of middle tower section	1.58 m (5.18 ft)	**	**
Length of lower tower section	2.02 m (6.63 ft)	**	**
Length of middle tower section	7.94 m (26.05 ft)	**	**
Length of upper tower section	6.05 m (19.849 ft)	**	**
Length of transition regions (vertical)	1.91 m (6.27 ft)	**	**
Hub Height	22.6 m (74.1 ft)	61.14 m (200.6 ft)	90 m (295.3 ft)
Tower total height	21.9 m (71.85 ft)	57.19 m (187.63 ft)	88.5 m (290.35 ft)
Tower thickness	5.3 mm (0.21 in)	18 mm (0.71 in)	27 mm (1.06 in)
Nacelle mass	2,400 kg (164 slug)	53,700 kg (3680 slug)	240,000 kg (16,445 slug)
Rotor Mass	1,653.07 kg (113.27 slug)	34,098.27 kg (2336.474 slug)	106,265.2 kg (7281.479 slug)
Hub Mass	246.93 kg (16.92 slug)	7,901.73 kg (541.44 slug)	3,734.8 kg (255.915 slug)
Tower mass	6,400 kg (439 slug)	78,600 kg (5,386 slug)	347,460 kg (23,809 slug)
Thickness of Blades	60 mm (2.362 in)	480 mm (18.89 in)	590 mm (23.228 in)

1 slug = 32.174 lbm

** Towers are uniformly conical with decreasing diameter from base to top.

The components of the wind turbine are assembled together, assigned with the appropriate ANSYS elements, then, meshing is done. Meshing helps to solve the equations at cell/node locations. Following Table 4 shows the types of elements used for each components of the wind turbine along with the number of nodes and number of elements in each components after meshing.

Table 7. Element Types and Meshing

Parts	65 KW Turbine		1 MW Turbine		5 MW Turbine		Element Type
	Elements	Nodes	Elements	Nodes	Elements	Nodes	
Tower	4738	4766	15378	15426	4819	4847	Shell 181
Nacelle	1980	9527	1280	6345	960	4893	Solid 186
Hub	78	452	72	465	42	284	Solid 186
Blades	742	907	459	619	787	1133	Shell 181
Total	7538	15652	17189	22855	6608	11157	

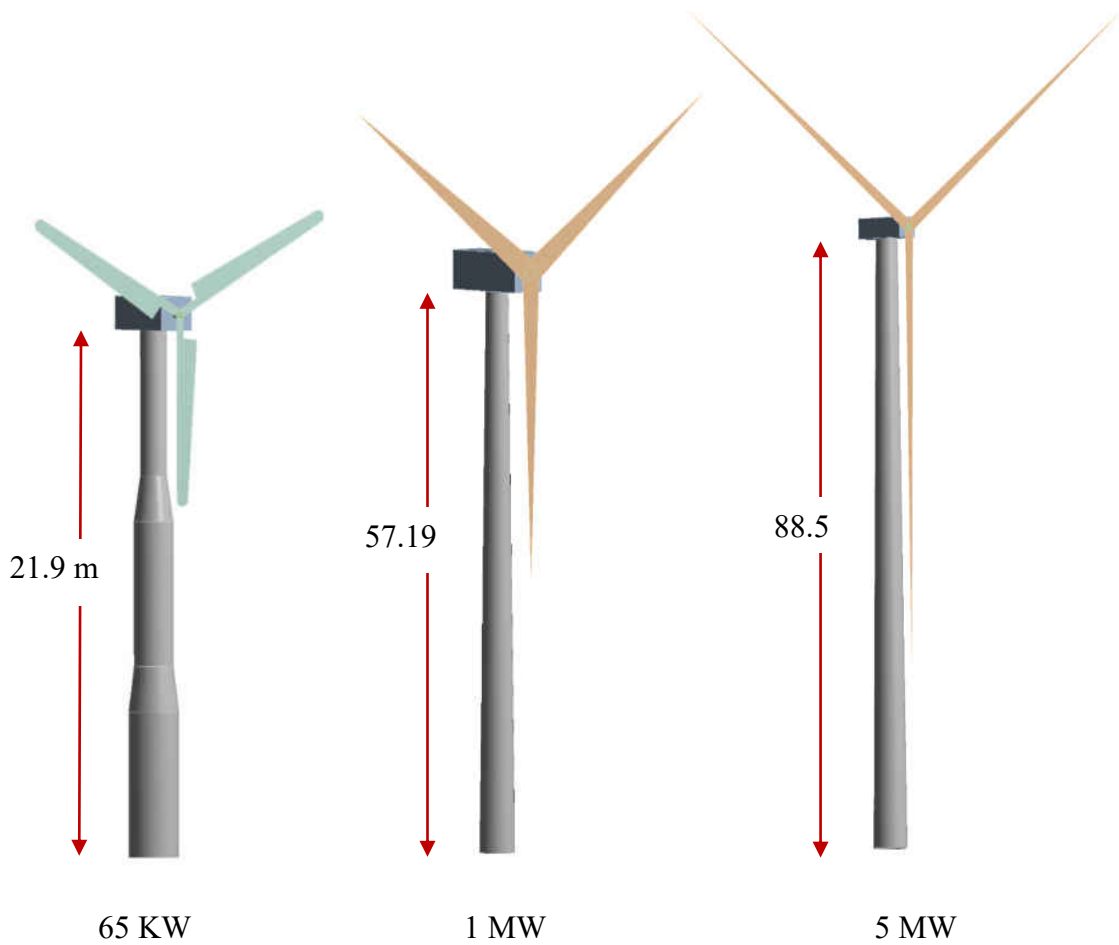


Figure 30. ANSYS Model of Wind Turbines

The towers in ANSYS are analyzed in ANSYS workbench software with linear elastic material and geometry. Analysis of detailed model of wind turbines is done with tower and blades as shell elements and nacelle and hub as solid elements. Creating and analyzing detailed model helps to increase the accuracy of the simulation and output

result by accurately distributing the mass across the body. This helps to take into account the effect of stress concentration in the connections and also stress distribution in the tapered section.

In detailed model of all wind turbines, X direction is parallel to the rotor's axis and Z direction is parallel to the vertical tower. Though the wind turbine is rotationally symmetric it is important to consider tower bending modes in all directions because of the presence of nacelle and rotor which produce different mode shapes and natural frequencies for each direction. For each wind turbine model (65 KW, 1 MW, and 5 MW) first 50 modes were obtained using ANSYS that included 90% of the effective mass. The modal analysis is performed using Block Lanczos method as explained in the previous chapter. From the mass ratio obtained it is seen that first three modes have the fundamental effects on the wind turbine's dynamic behavior in the corresponding direction whereas the other modes have much smaller effect. The base of the tower is fixed. Following table 5 gives the first three fundamental natural frequencies of each wind turbine model in each direction and also the ratio of effective mass ratios.

Table 8. Fundamental modes, frequencies and effective mass to total mass ratio

Tower	Mode	X- Direction		Y-Direction		Z-Direction	
		Frequency (Hz)	Ratio of Effective Mass to Total Mass	Frequency (Hz)	Ratio of Effective Mass to Total Mass	Frequency (Hz)	Ratio of Effective Mass to Total Mass
65 KW	1	1.618	0.605	1.602	0.595	31.457	0.685
	2	8.18	0.142	7.412	0.136	19.132	0.031
	3	19.132	0.089	17.664	0.097	8.18	0.028
1 MW	1	0.447	0.717	0.444	0.711	12.255	0.737
	2	2.903	0.107	2.750	0.108	2.903	0.046
	3	7.254	0.063	7.121	0.067	7.254	0.043
5 MW	1	0.286	0.722	0.282	0.701	7.281	0.782
	2	1.769	0.094	1.373	0.099	7.300	0.012
	3	4.102	0.067	3.741	0.081	9.335	0.018



1st X Mode



2nd X Mode



3rd X Mode



1st Y Mode



2nd Y Mode



3rd Y Mode



1st Z Mode

Figure 31. Mode Shapes of Wind Turbines

Mass and Stiffness Coefficient

As mentioned earlier the mass coefficient and stiffness coefficient for each wind turbine in different directions and at different damping ratios (0.5%, 1.0% and 2.0%) are calculated using Block Lanczos Method. Mass stiffness is represented by ' α ' which is also known as viscous damping component and stiffness coefficient by ' β ' also known as hysteresis or solid damping component. The most dominant response frequency is selected to calculate the values of ' α ' and ' β '. The following table 6 shows the values of mass coefficient and stiffness coefficient according to the fundamental modal frequencies obtained from ANSYS.

Table 9. Mass and Stiffness Coefficient

Wind Turbines		65 KW		1 MW		5 MW	
Axes	Damping Ratios	α	β	α	β	α	β
X	0.50%	0.084	0.0001624	0.024	0.000475	0.015	0.000774
	1.00%	0.169	0.0003248	0.048	0.00095	0.030	0.001548
	2.00%	0.339	0.0006497	0.097	0.0018999	0.061	0.0030962
Y	0.50%	0.082	0.000176	0.024	0.000498	0.014	0.000961
	1.00%	0.165	0.000353	0.048	0.000996	0.029	0.001922
	2.00%	0.331	0.0007059	0.096	0.0019929	0.058	0.003844
Z	0.50%	0.747	0.0000314	0.147	0.000105	0.229	0.0001091
	1.00%	1.495	0.0000629	0.294	0.0002099	0.458	0.0002183
	2.00%	2.989	0.000126	0.589	0.0004199	0.916	0.0004366

Transient Results

The Table below shows the absolute maximum values of displacement and acceleration simulated at the top of the nacelle and also the maximum Von Mises stress obtained at the base of the tower for three different earthquake loads applied under three different damping conditions. For simplicity a naming convention is assigned for each wind turbines under different conditions for the responses obtained. The first number is the

power capacity of the wind turbine (i.e. 0.065 MW, 1 MW, 5 MW), the second alphabet represents the type of material used (S for steel), the third number represents the damping ratio (0.5%, 1% and 2%) and the last alphabet represents the earthquake (L, N and E for Landers, Northridge and El-Centro respectively). In all cases, the direction of the response recorded is the direction of the application of the earthquake applied.

Table 10. Peak Responses Recorded from ANSYS Workbench

Model	Max Acceleration (g)			Max Deformation (mm)			Max Von Mises Stress (MPa)		
	X	Y	Z	X	Y	Z	X	Y	Z
0.065S0.5-L	0.413	0.455	0.219	50.953	53.083	2.4918	52.121	54.358	13.98
0.065S1-L	0.365	0.399	0.217	47.87	46.552	2.4112	49.395	48.206	13.516
0.065S2-L	0.309	0.325	0.213	42.846	37.867	2.2685	44.446	40.049	12.714
0.065S0.5-N	1.087	1.117	0.2187	109.73	114.63	2.4275	113.7	113.92	14.199
0.065S1-N	1.011	1.045	0.2167	103.69	107.13	2.3469	106.51	107.06	13.647
0.065S2-N	0.878	0.918	0.2126	96.763	93.999	2.2042	97.709	96.326	12.856
0.065S0.5-E	0.979	1.044	0.2197	108.89	113.08	2.5199	109.57	112.52	14.621
0.065S1-E	0.834	0.888	0.2176	92.841	96.086	2.4014	93.569	97.077	13.773
0.065S2-E	0.639	0.6797	0.214	73.734	75.404	2.2567	74.73	77.89	12.968
1S0.5-L	0.193	0.1725	0.7258	238.19	166.49	31.806	60.361	50.516	43.527
1S1-L	0.177	0.1635	0.7185	226.05	154.41	30.794	56.693	48.071	41.974
1S2-L	0.162	0.1539	0.7042	208.91	139.1	28.973	52.407	44.12	39.114
1S0.5-N	0.3221	0.3693	0.72	396.75	361.21	33.542	101.4	101.45	46.227
1S1-N	0.3235	0.369	0.7132	387.47	345.91	32.498	98.641	97.31	44.416
1S2-N	0.326	0.3684	0.6989	369.53	317.7	30.617	93.47	89.714	41.479
1S0.5-E	0.433	0.384	0.7282	534.03	421.86	34.104	130.02	118.33	45.62
1S1-E	0.4215	0.375	0.721	507.74	406.97	33.076	124.59	113.72	43.83
1S2-E	0.3995	0.357	0.706	477.43	379.24	31.225	119.35	105.55	40.64
5S0.5-L	0.135	0.128	0.652	311.75	233.66	25.895	61.622	54.939	37.863
5S1-L	0.131	0.122	0.644	303.69	221.82	24.428	59.575	52.05	35.17
5S2-L	0.124	0.118	0.628	288.7	206.53	22.072	56.31	47.53	31.44
5S0.5-N	0.225	0.215	0.6416	447.95	372.93	26.618	88.974	85.78	39.8
5S1-N	0.222	0.212	0.634	438.46	361.47	25.114	86.969	83.077	37.383
5S2-N	0.214	0.208	0.6182	420.7	350.07	23.122	83.057	78.282	34.908
5S0.5-E	0.261	0.25	0.684	488.6	294.16	25.966	93.571	72.41	40.521
5S1-E	0.258	0.25	0.65	479.3	289.88	24.433	90.528	69.579	37.496
5S2-E	0.252	0.241	0.66	462.37	294.441	21.836	84.952	67.863	30.856

From the above results, we construct graphs so that it would be easier to study the behavior of wind turbines considered under the earthquakes of different magnitude. In order to construct a graph, the time period (T_n), is plotted in the X-direction, which is

derived from the natural frequency of the wind turbines. Since the first mode of frequency is the fundamental natural frequency in each direction, we calculate the natural time period for each wind turbine using the first natural frequency. Similarly, in Y- direction we plot the responses obtained (deformation, acceleration and stress) for the corresponding time period.

In our case we observe the responses seen in the X-direction and Y-direction are comparable, so we take the average of the responses obtained in X and Y-direction as well as the natural time period and plot them in the same graph. For, Z-direction the responses seen is not comparable to the responses observed in X and Y direction so a different graph is plotted.

Results from Landers Earthquake

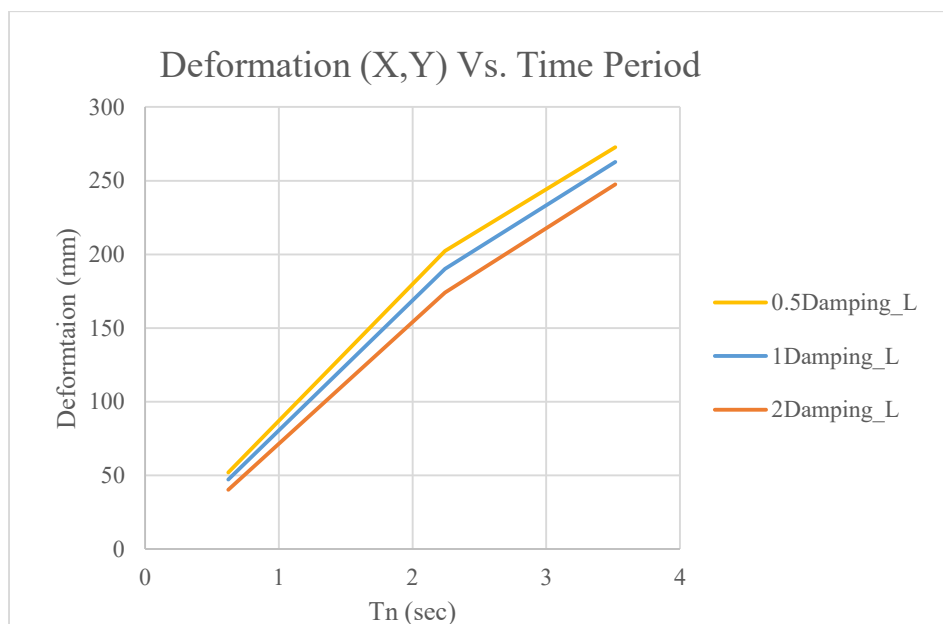


Figure 32. Horizontal Deformation Vs. Time Period (Landers)

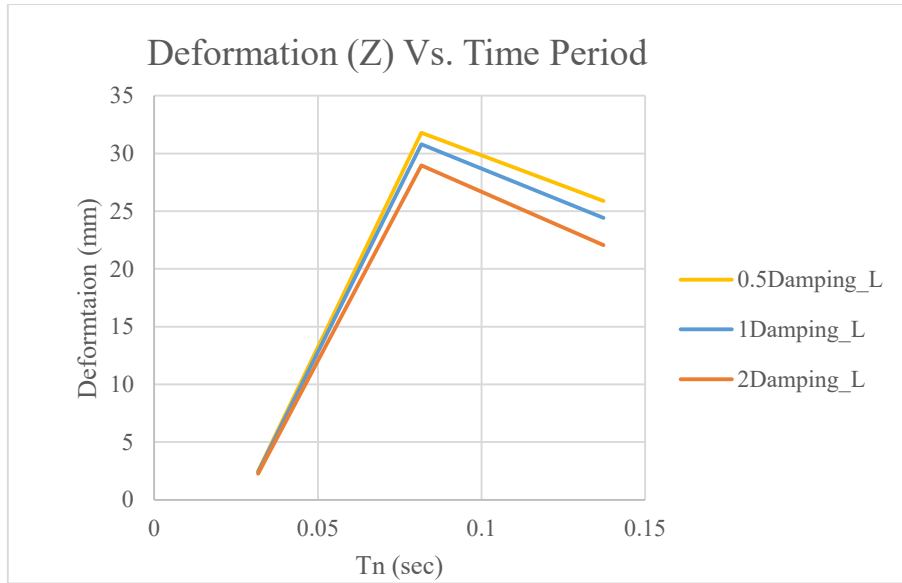


Figure 33. Vertical Displacement Vs. Time Period (Landers)

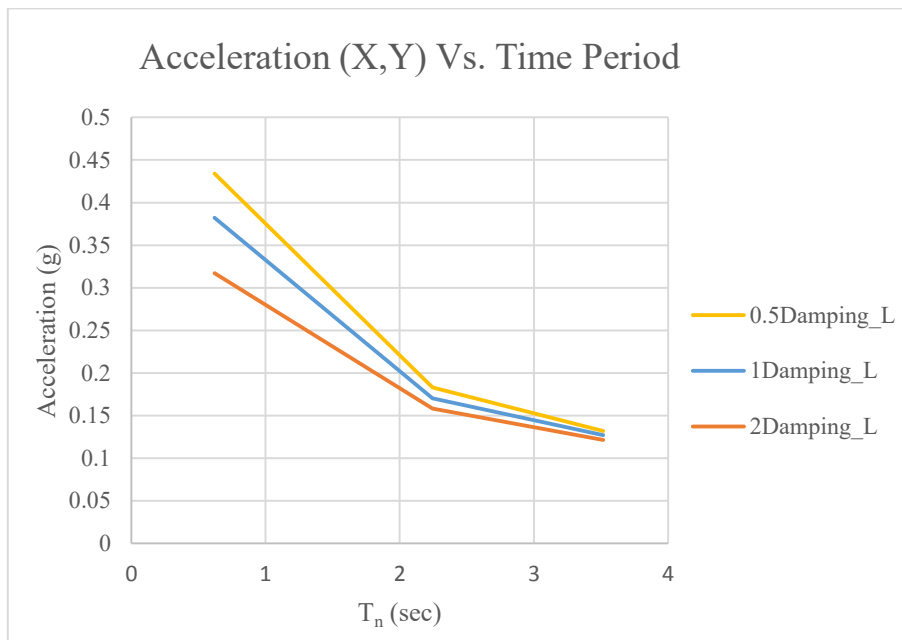


Figure 34. Horizontal Acceleration Vs. Time Period (Landers)

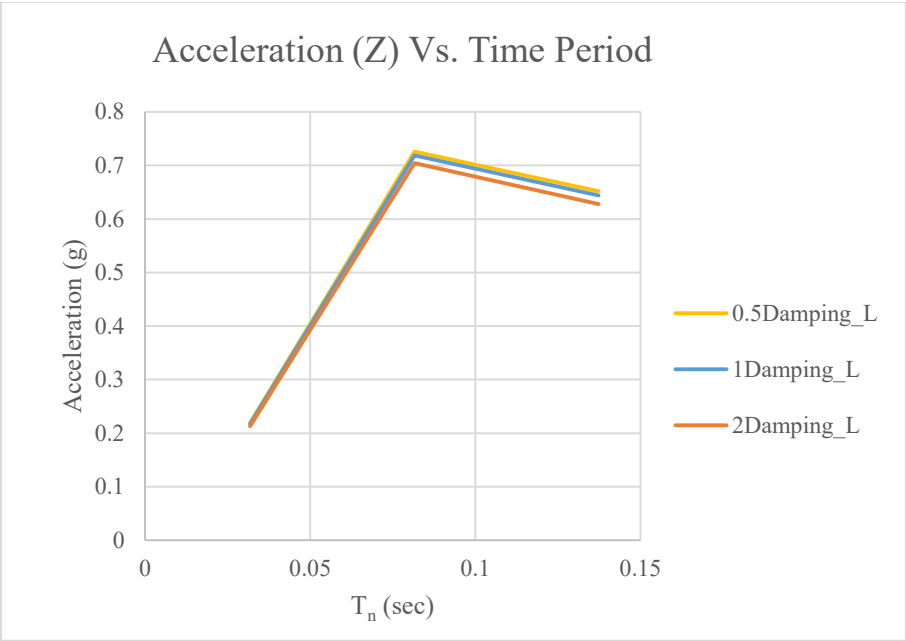


Figure 35. Vertical Acceleration Vs. Time Period (Landers)

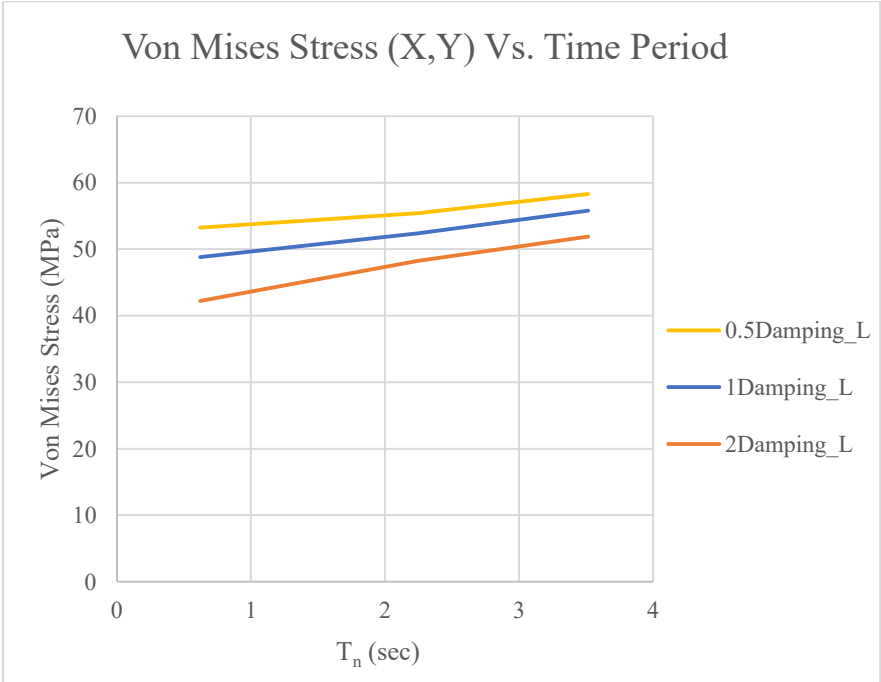


Figure 36. Horizontal Von Mises Stress Vs. Time Period (Landers)

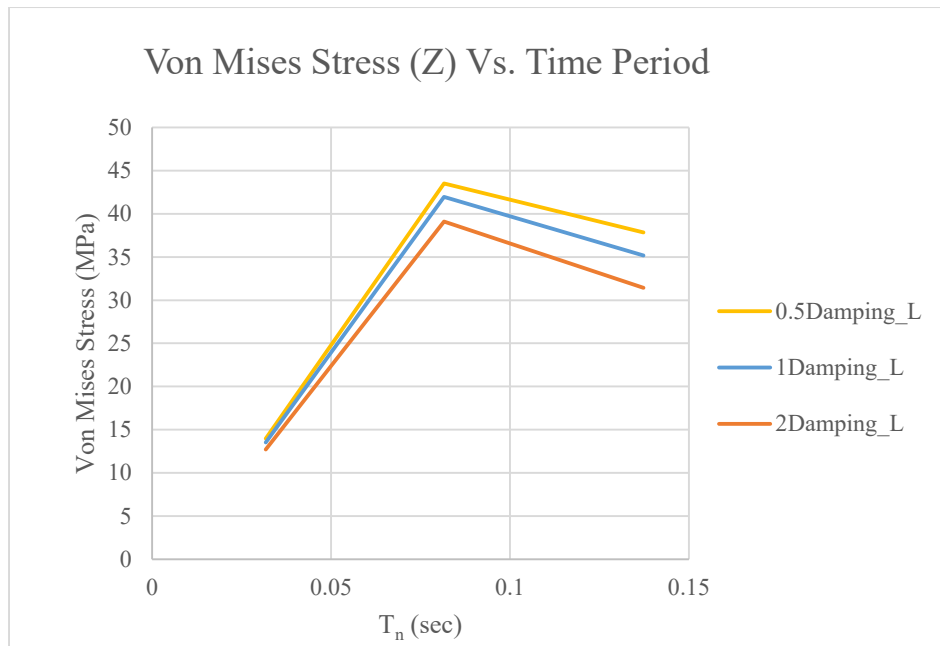


Figure 37. Vertical Von Mises Stress Vs. Time Period (Landers)

Results from El Centro Earthquake

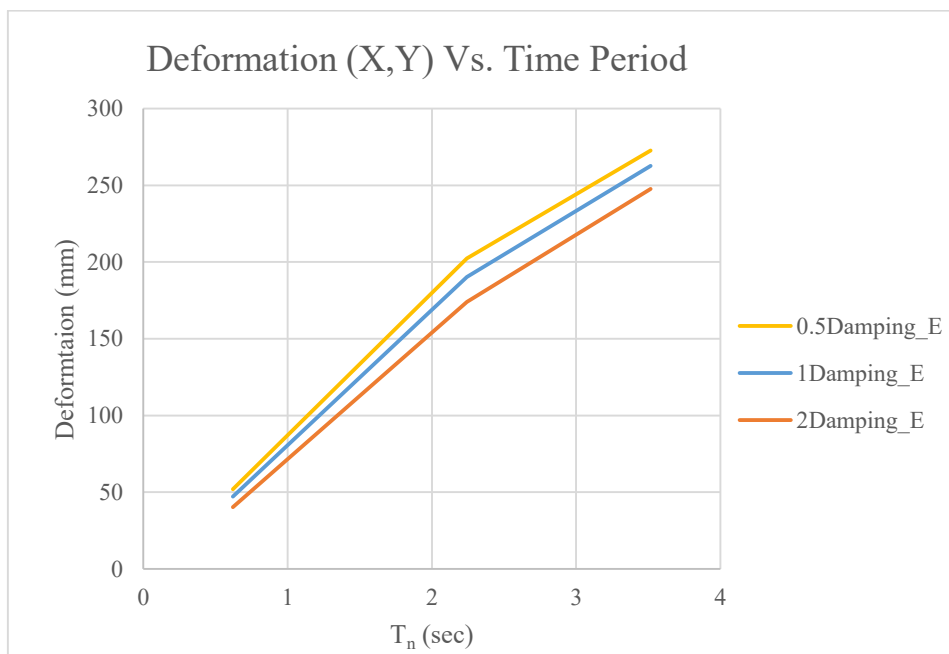


Figure 38. Horizontal Deformation Vs. Time Period (El Centro)

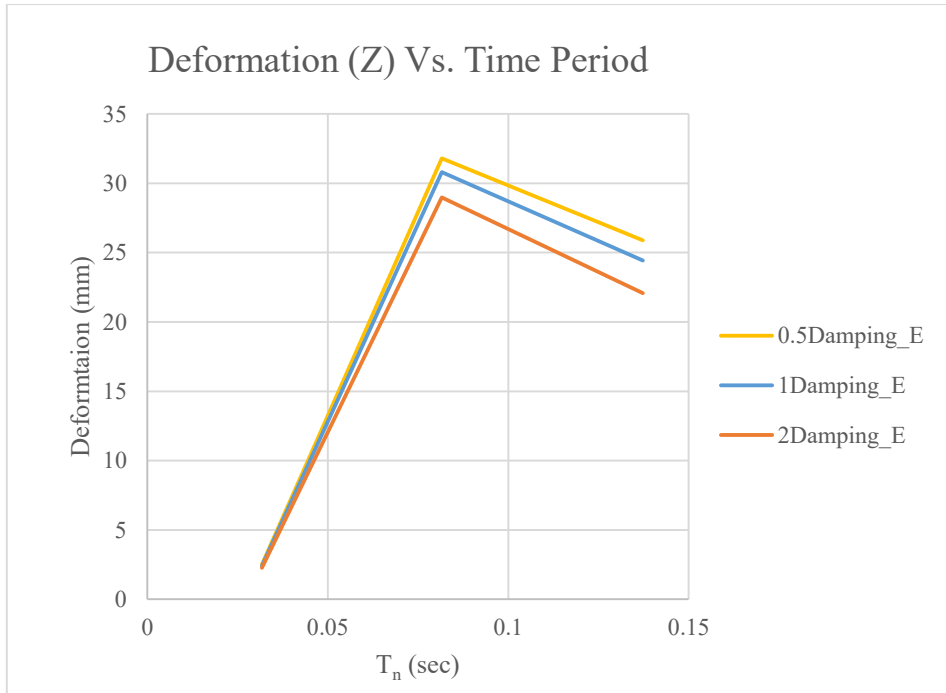


Figure 39. Vertical Deformation Vs. Time Period (El Centro)

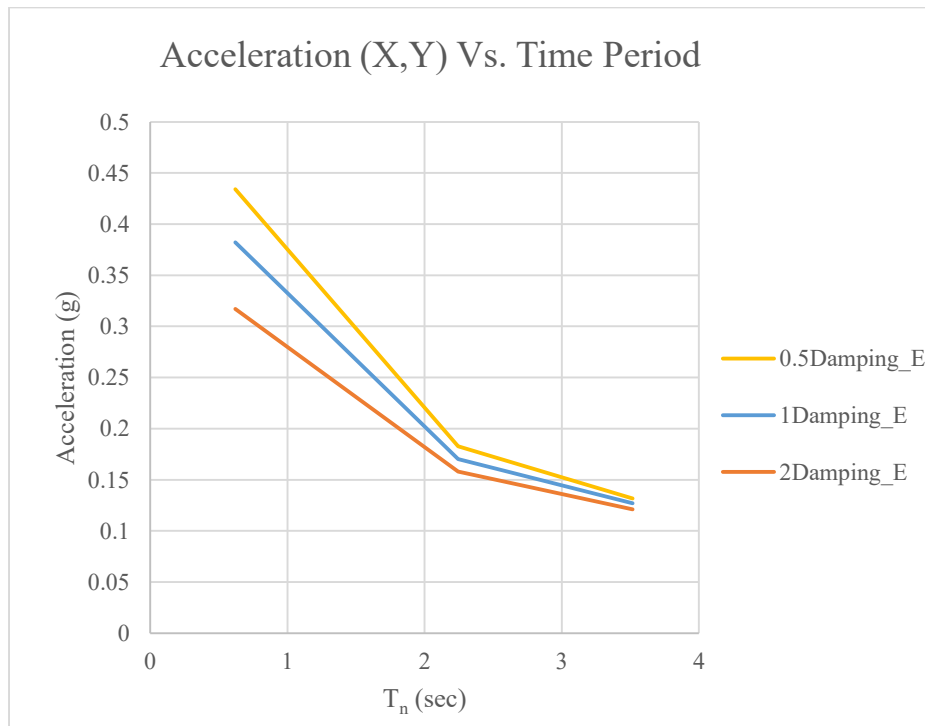


Figure 40. Horizontal Acceleration Vs. Time Period (El Centro)

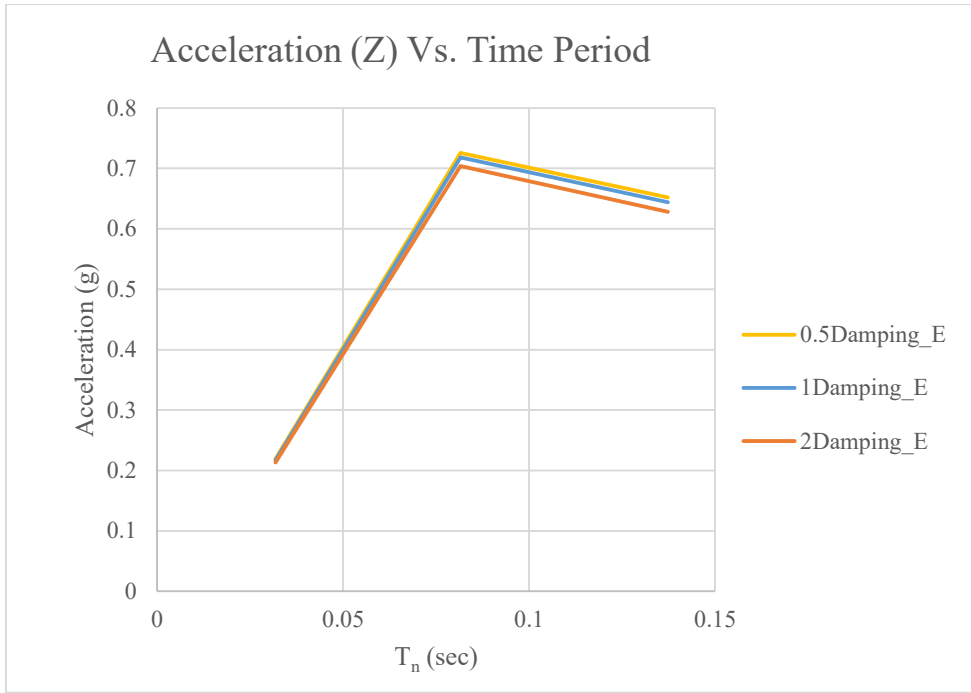


Figure 41. Vertical Acceleration Vs. Time Period (El Centro)

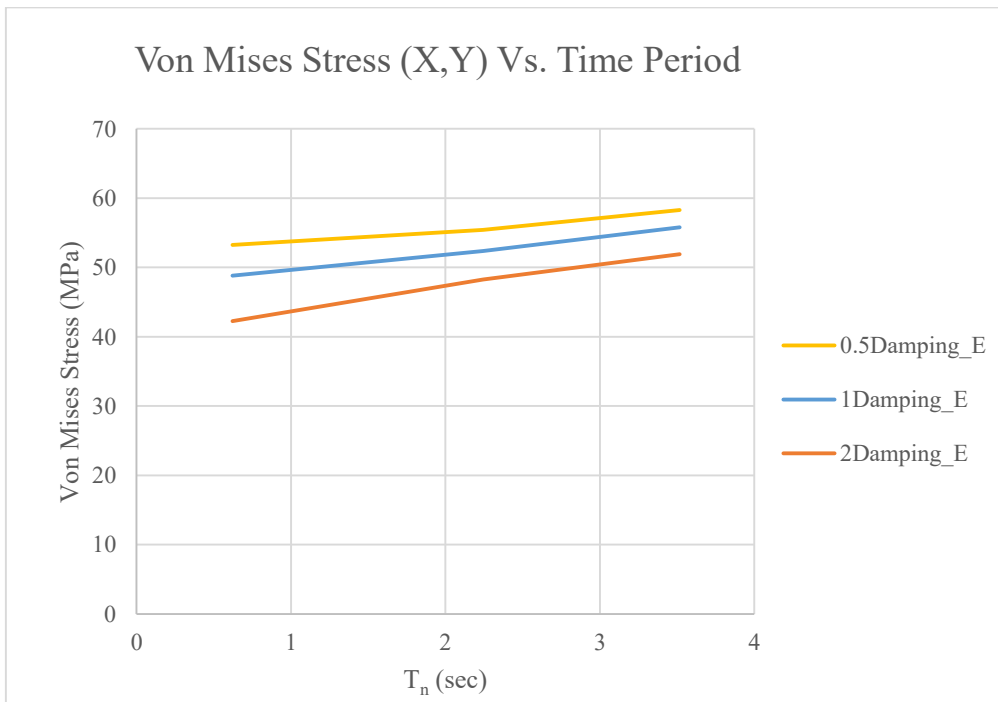


Figure 42. Horizontal Von Mises Stress Vs. Time Period (El Centro)

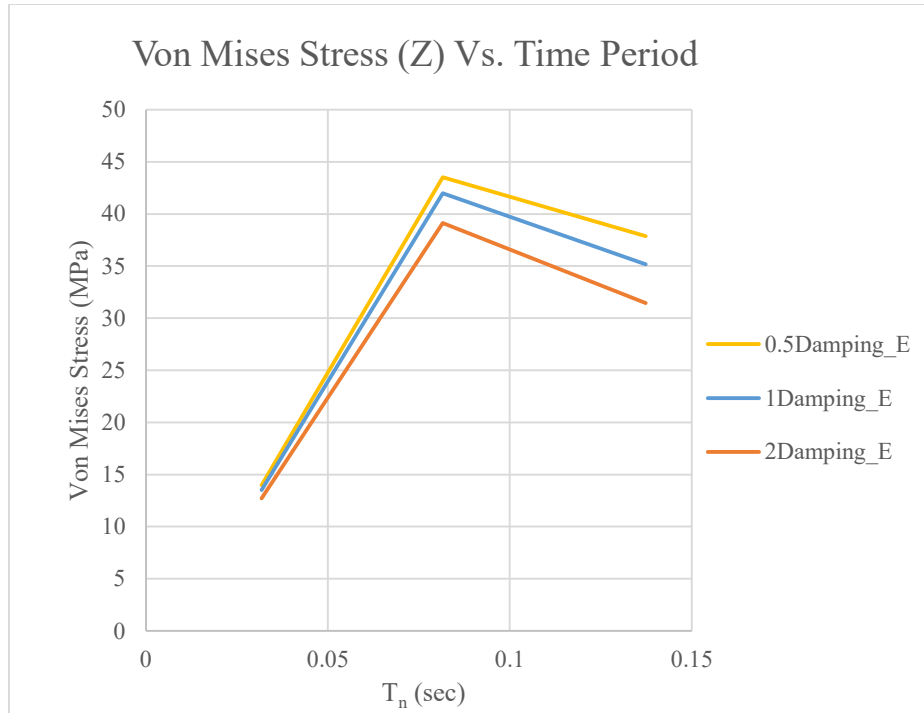


Figure 43. Vertical Von Mises Stress Vs. Time Period (El Centro)

Results from Northridge Earthquake

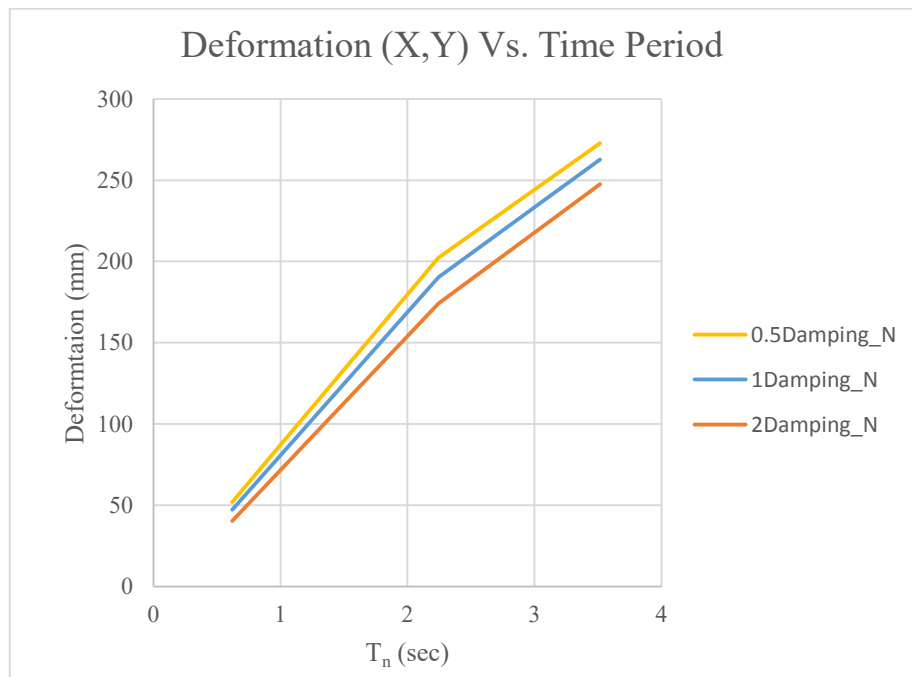


Figure 44. Horizontal Deformation Vs. Time Period (Northridge)

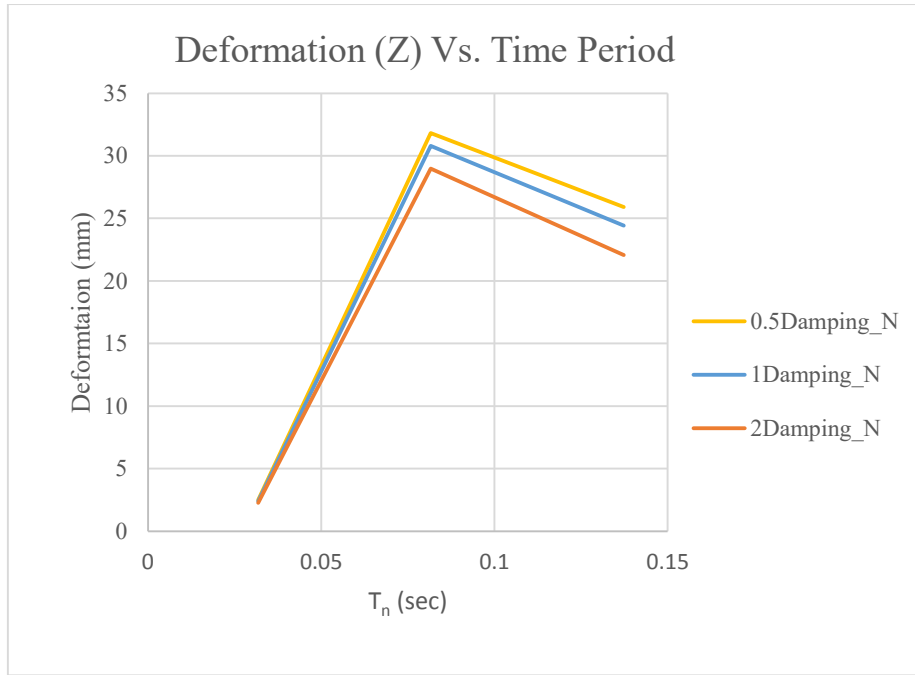


Figure 45. Vertical Deformation Vs. Time Period (Northridge)

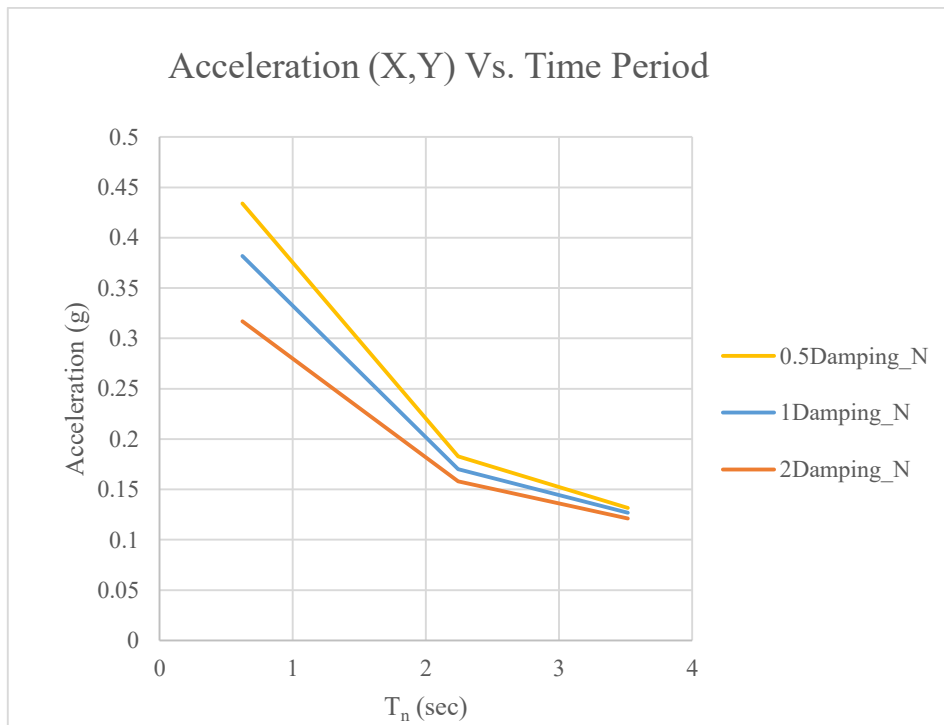


Figure 46. Horizontal Acceleration Vs. Time Period (Northridge)

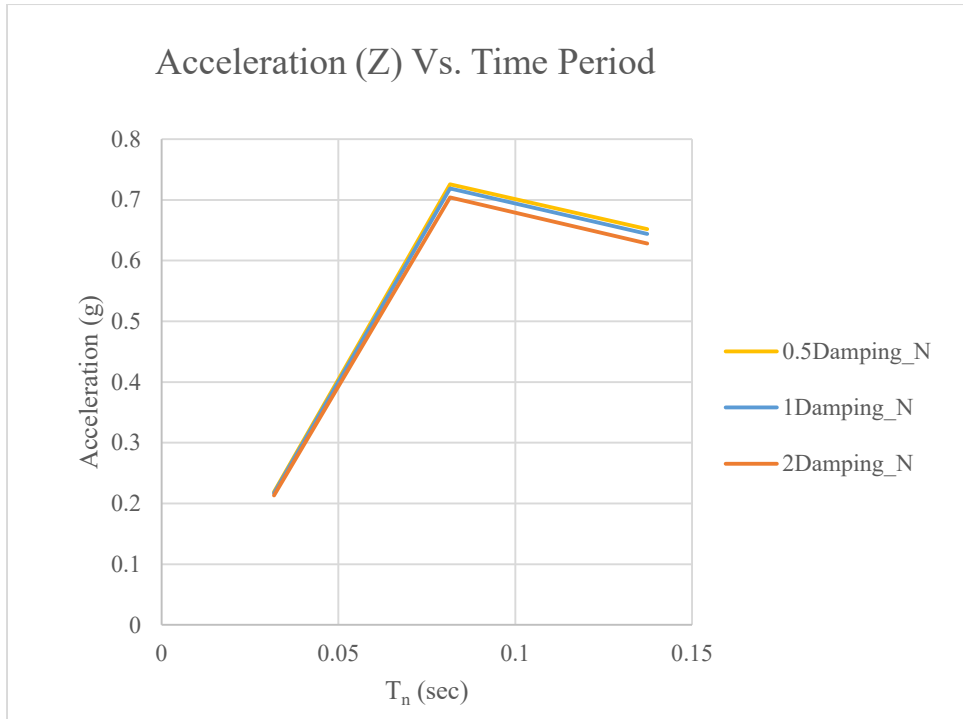


Figure 47. Vertical Acceleration Vs. Time Period (Northridge)

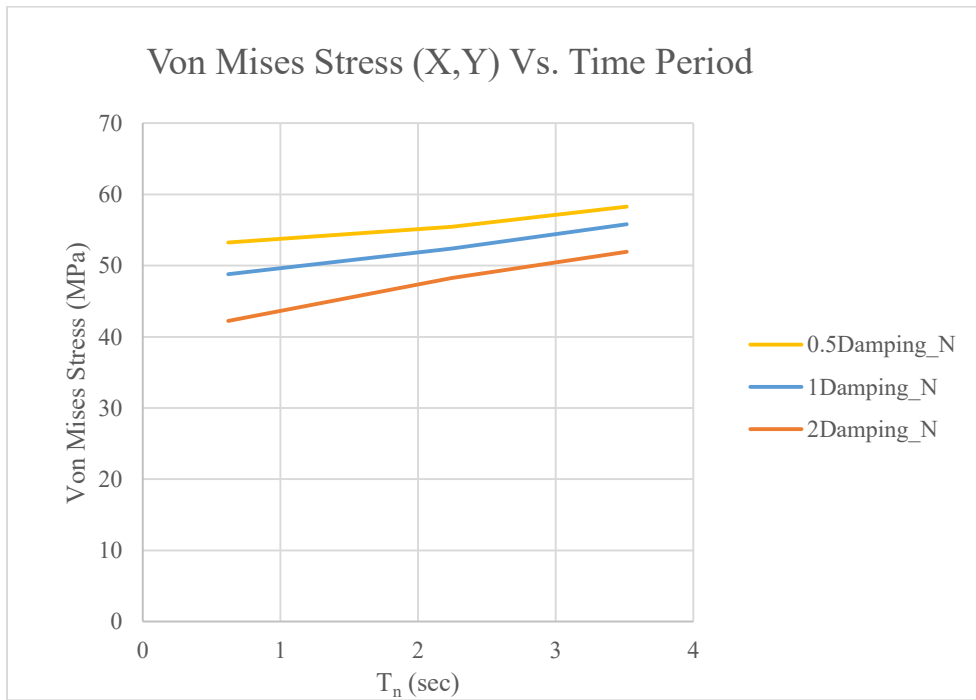


Figure 48. Horizontal Von Mises Stress Vs. Time Period (Northridge)

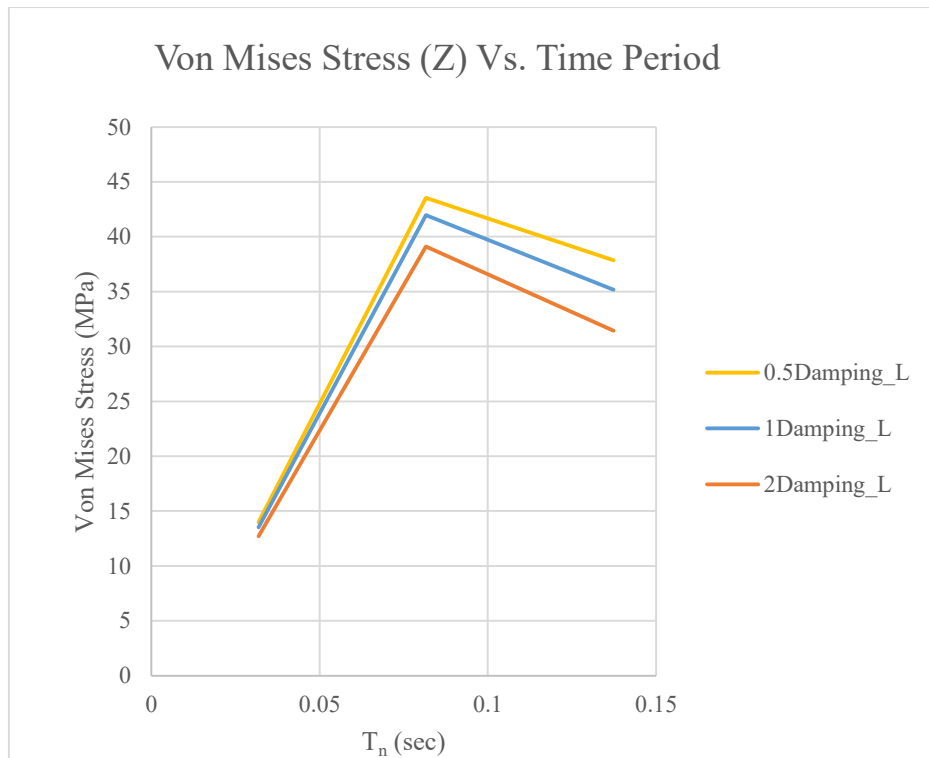


Figure 49. Vertical Von Mises Stress Vs. Time Period (Northridge)

CHAPTER VI

CONCLUSIONS

The structural analysis of three wind turbines is performed using the finite element software ANSYS Workbench.

1. The natural frequencies obtained from the finite element analysis for 65 KW wind turbine are found comparable to the natural frequencies obtained from the shake table test performed. This indicates that the transient dynamics approach is a valid tool for the analysis of wind turbine. It also shows that there is nothing wrong with the wind turbine model built in the finite software and the physical properties of the model constructed in the software resembles the one used in the experiment. The type of elements chosen for different components of wind turbines and the materials used for the modelling are in correspondence to the experimental model. So ANSYS WORKBENCH can be used for further analysis purpose.
2. Modal analysis shows that for the first mode, which is the fundamental mode, the ratio of the effective mass to the total mass is found to be maximum in each direction. This means that the maximum percentage of the effective mass of the turbine is involved during the modal analysis of the fundamental mode. It is observed that the fundamental mode of frequency decreases with the increase in the size of the wind turbines which also refers to the fact that the time period is higher for the larger wind turbines than the small wind turbines. Similarly, the modal frequency for each wind turbine in X and Y direction are comparable

but the modal frequency in Z direction for each wind turbine varies a lot from the other two directions.

3. The results from transient analysis are shown in Table 10. Maximum responses for each loading are observed in the direction of the application of the load. Similar to the case of modal frequencies the horizontal responses of each wind turbine are comparable in X and Y direction. Not much difference is observed in those two directions but significant variation is observed in the responses shown in Z direction when compared to X and Y direction.
4. It is clearly observed that the peak deformation recorded at the top of the nacelle and the maximum stress near the base of the tower increases as the size of the wind turbine increases under the same earthquake and the damping applied in X and Y direction. In case of the peak acceleration at the top of the nacelle, it decreases as the turbine size increases for X and Y direction. This might be due to the fact that larger wind turbines have higher time period. But in case of the responses seen in Z direction, response first increase with the increase in the size of the wind turbine and decrease after that. The self-weight of the wind turbine that acts towards gravity plays vital role during the application of load in Z-direction.
5. From the response graphs plotted, we can see that variation in damping ratio has caused significant changes in the peak responses observed. Increase in damping has resulted in the decrement of magnitude of deformation, acceleration and stress in each direction. For the same damping ratio, the magnitude of mass and stiffness coefficient decreases with the increase in the size of wind turbine. Similarly, the values of these coefficients in Z direction is relatively higher than in X and Y direction.

6. The central idea of this thesis is to construct a response spectrum graph which provides a convenient measure to find the peak responses to a particular component of ground motion to different earthquakes. Here we have plotted the peak response against the natural time period T_n of wind turbines. It means the peak value of deformation or other responses is readily available for a given ground motion component corresponding to T_n and damping ratio ξ of the wind turbine. This will eliminate the labor and time consumption to model and run the transient simulation in the FE software since we can easily study the graph and obtain the values.

Further additions on this thesis can be that we can consider few more wind turbines of different power capacities to obtain more data points on the response spectrum graph. At the same time we can also consider the wind loads for the FE analysis in ANSYS Workbench. Finally we can combine all the response spectrum graphs together to construct a new graph to give displacement and acceleration so that a single graph is sufficient to determine the peak responses with the consideration of all the parameters.

APPENDICES

65 KW

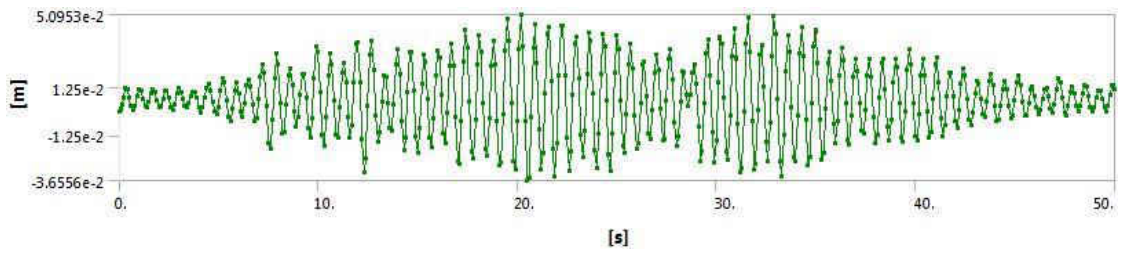


Figure 50. 0.065S0.5-LX

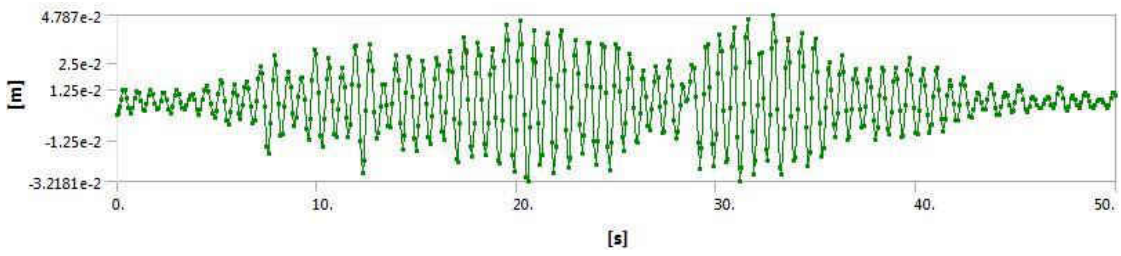


Figure 51. 0.065S1.0-LX

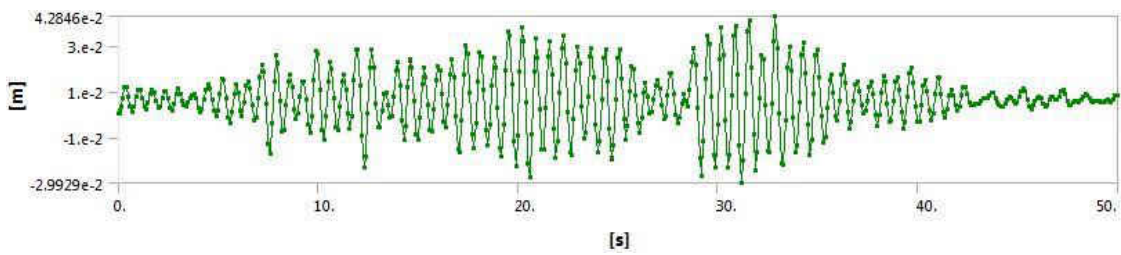


Figure 52. 0.065S2.0-LX

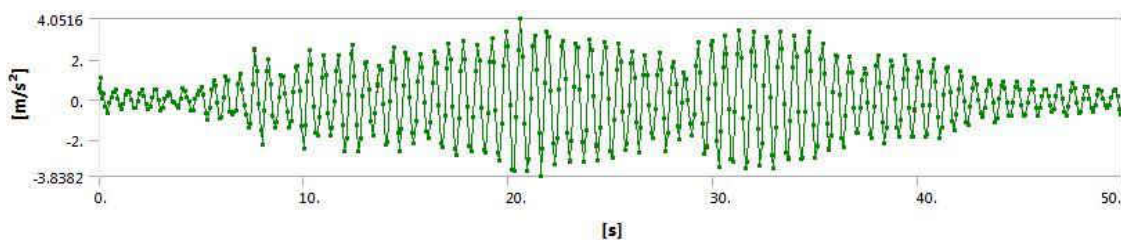


Figure 53. 0.065S0.5-LX

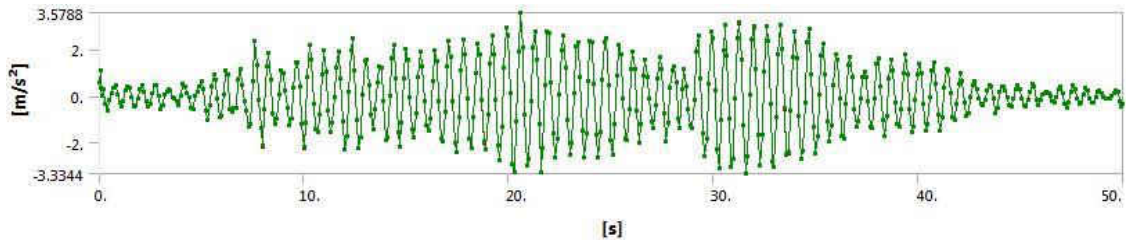


Figure 54. 0.065S1.0-LX

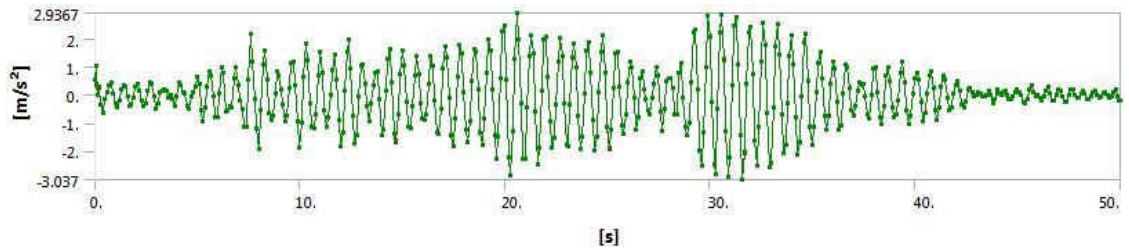


Figure 55. 0.065S2.0-LX

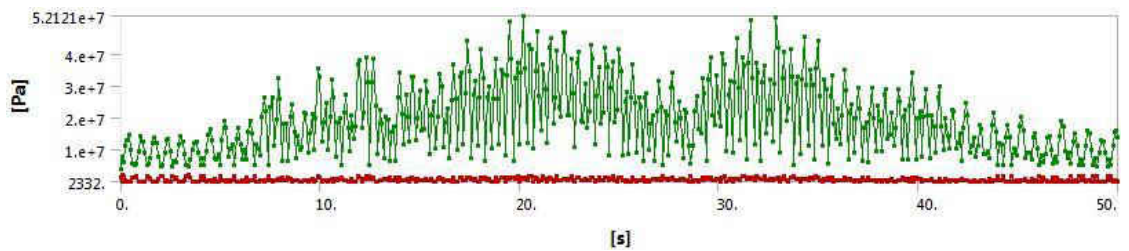


Figure 56. 0.065S0.5-LX

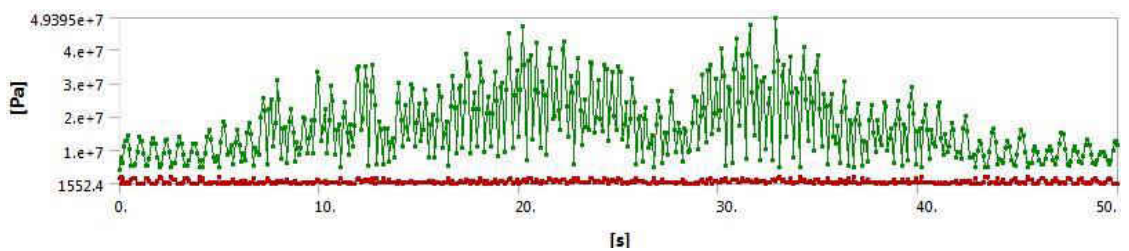


Figure 57. 0.065S1.0-LX

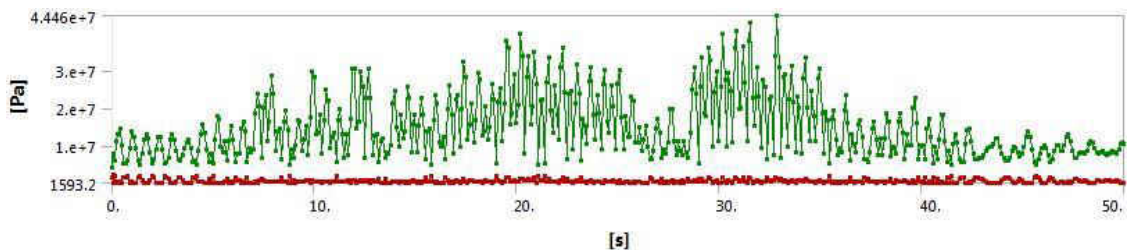


Figure 58. 0.065S2.0-LX

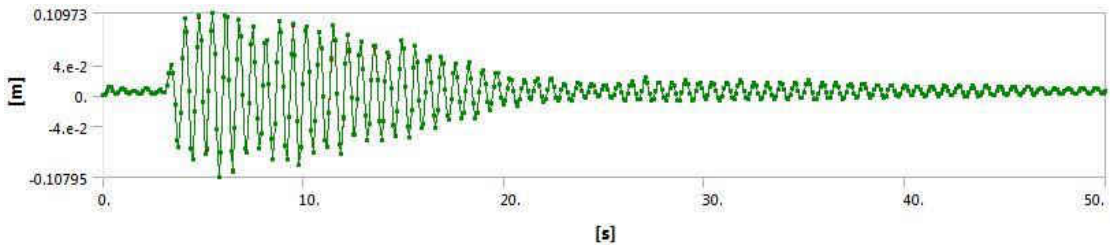


Figure 59. 0.065S0.5-NX

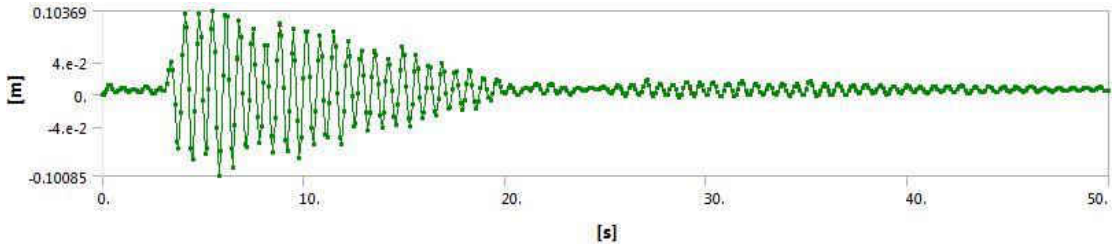


Figure 60. 0.065S1.0-NX

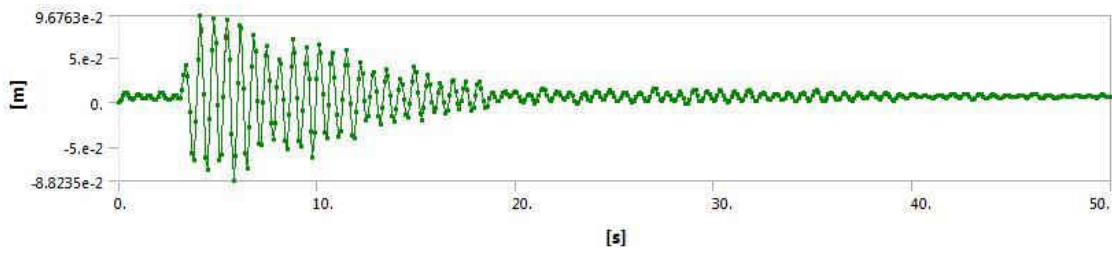


Figure 61. 0.065S2.0-NX

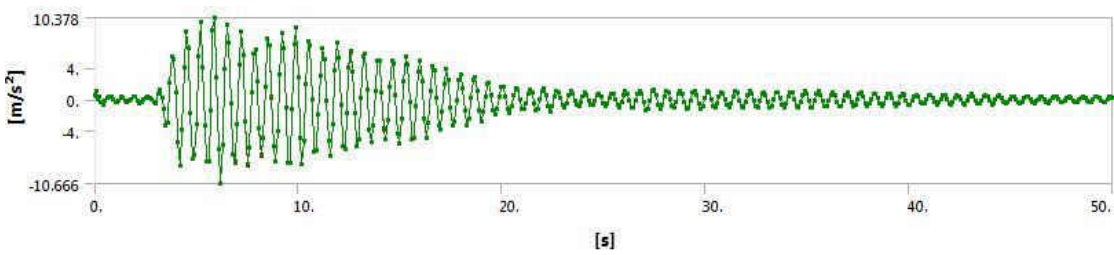


Figure 62. 0.065S0.5-NX

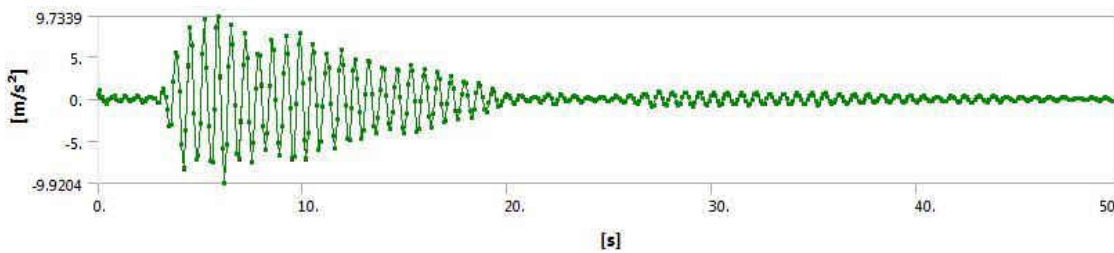


Figure 63. 0.065S1.0-NX

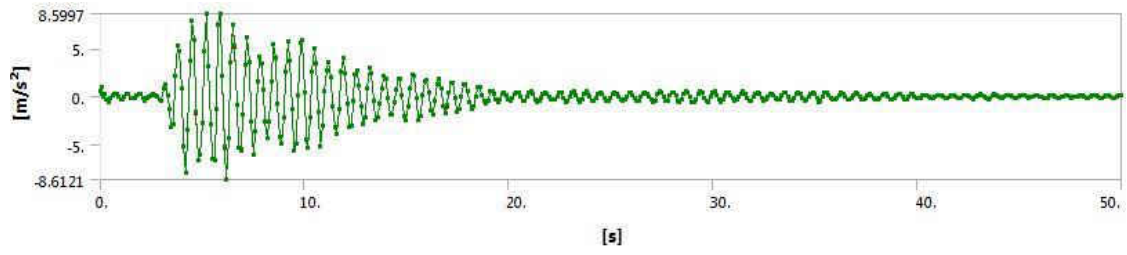


Figure 64. 0.065S2.0-NX

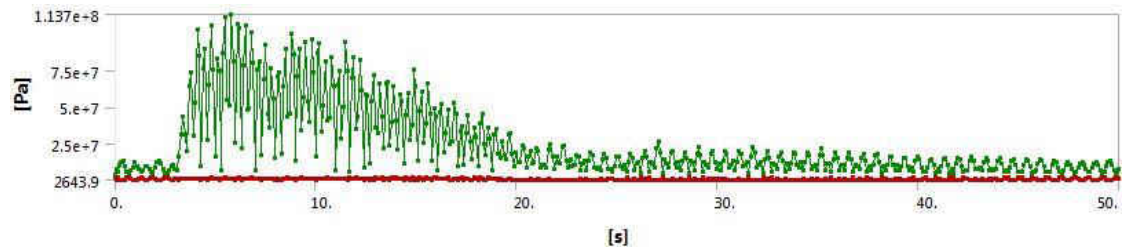


Figure 65. 0.065S0.5-NX

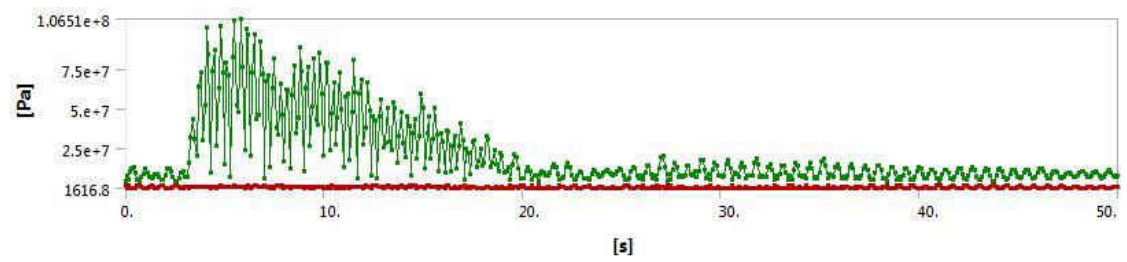


Figure 66. 0.065S1.0-NX

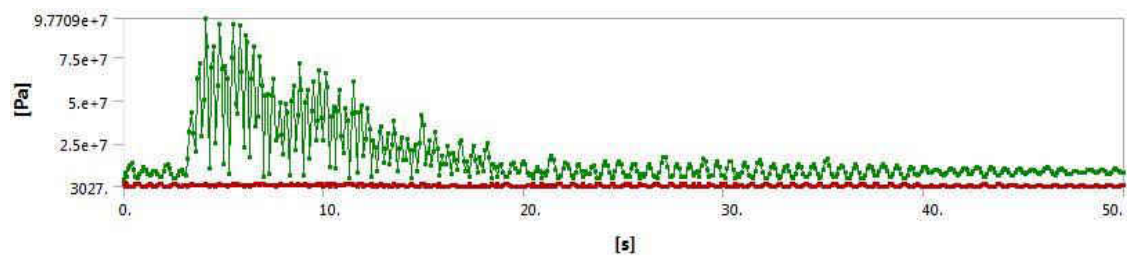


Figure 67. 0.065S2.0-NX

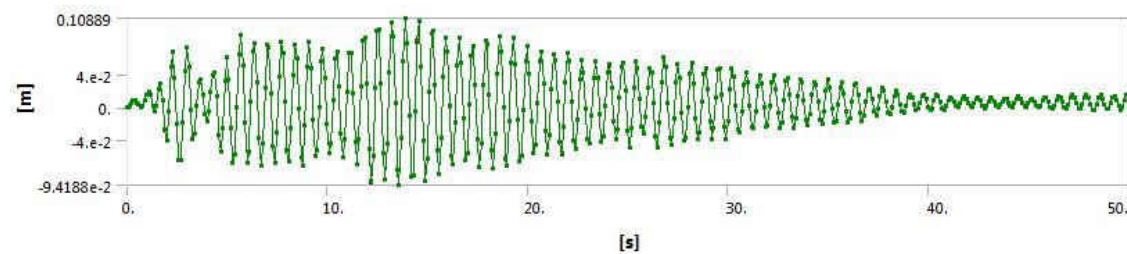


Figure 68. 0.065S0.5-EX

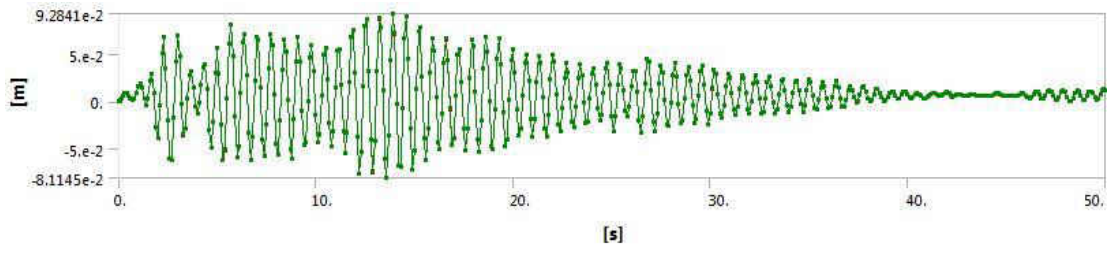


Figure 69. 0.065S1.0-EX

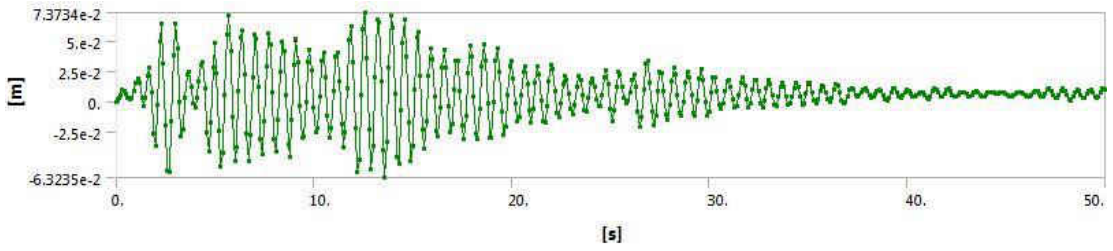


Figure 70. 0.065S2.0-EX

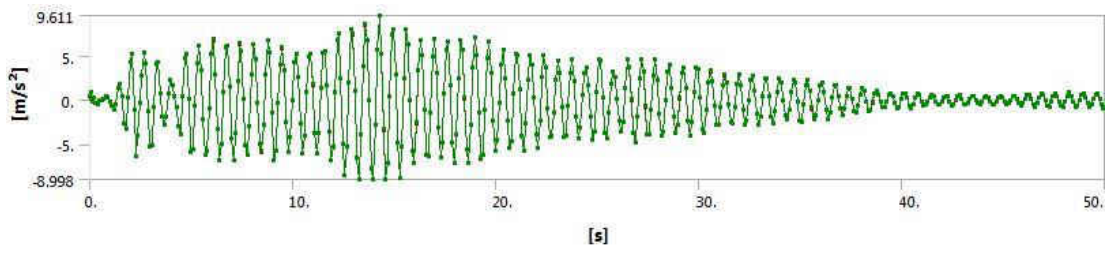


Figure 71. 0.065S0.50-EX

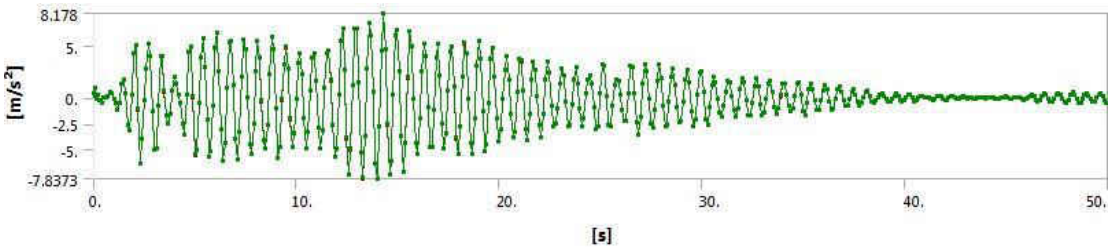


Figure 72. 0.065S1.0-EX

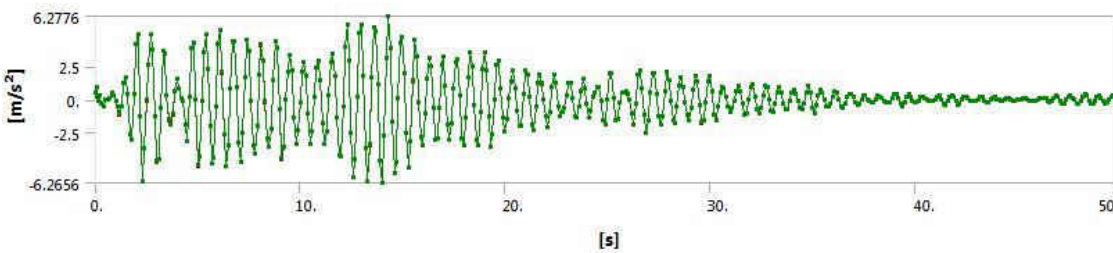


Figure 73. 0.065S2.0-EX

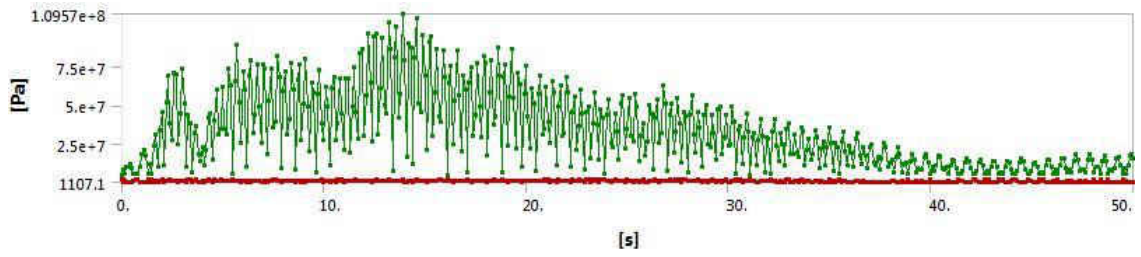


Figure 74. 0.065S0.5-EX

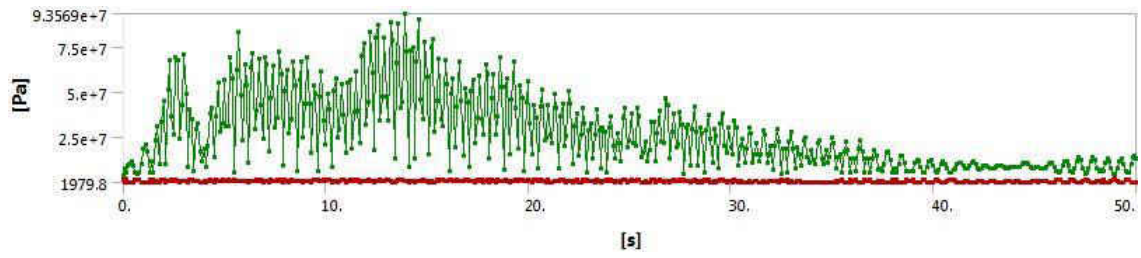


Figure 75. 0.065S1.0-EX

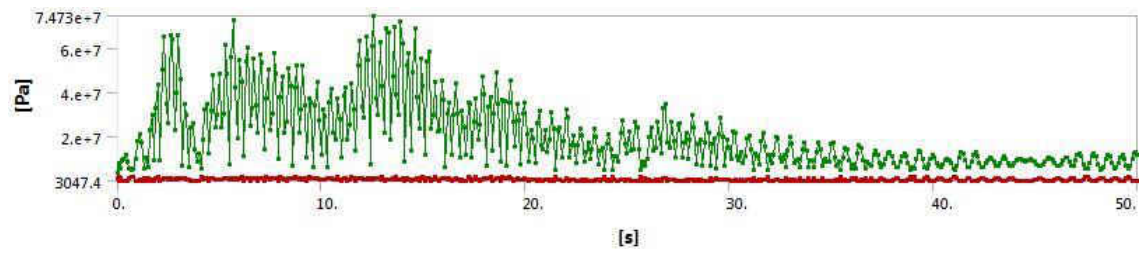


Figure 76. 0.065S2.0-EX

1 MW

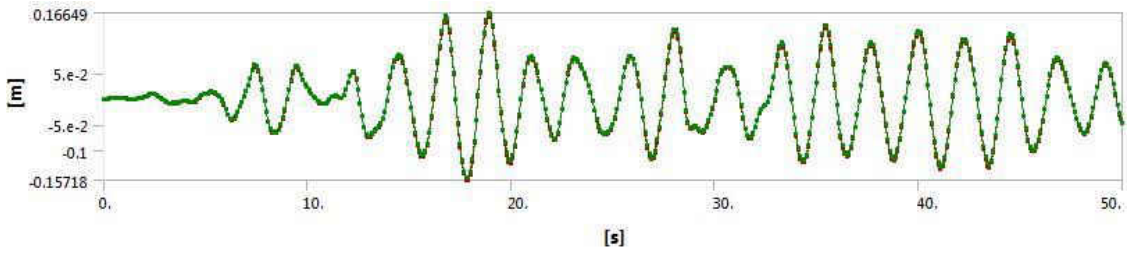


Figure 77. 1.0S0.5-LY

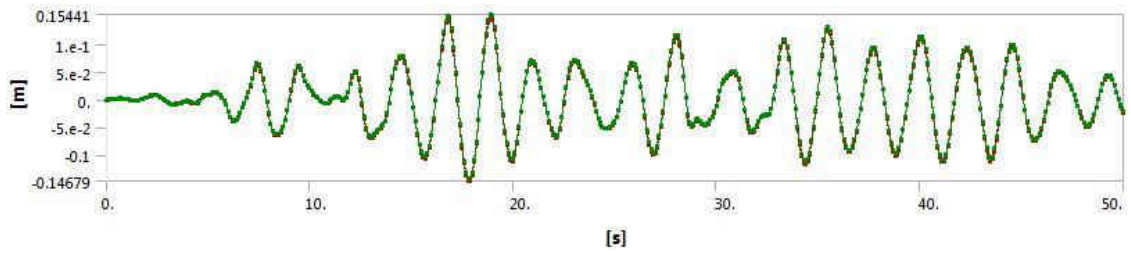


Figure 78. 1.0S1.0-LY

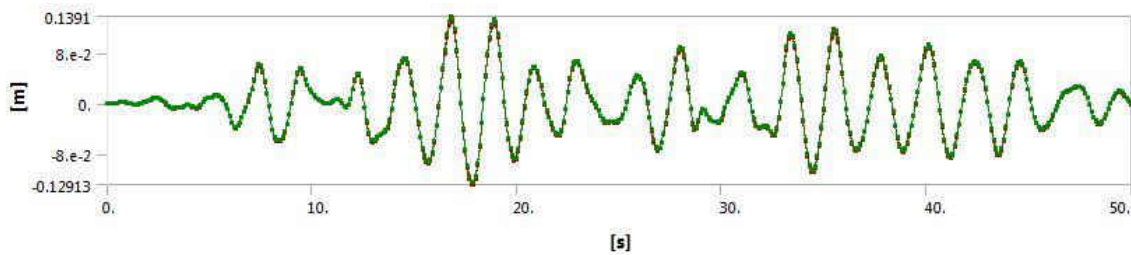


Figure 79. 1.0S2.0-LY

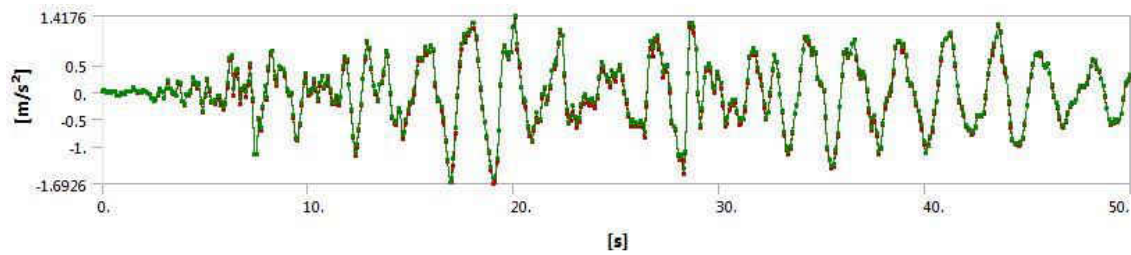


Figure 80. 1.0S0.5-LY

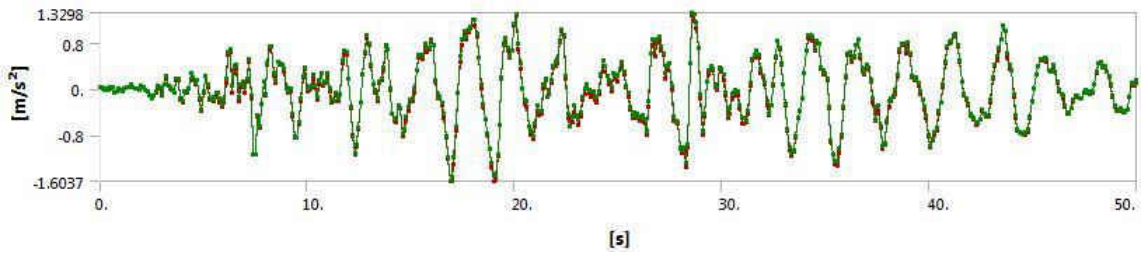


Figure 81. 1.0S1.0-LY

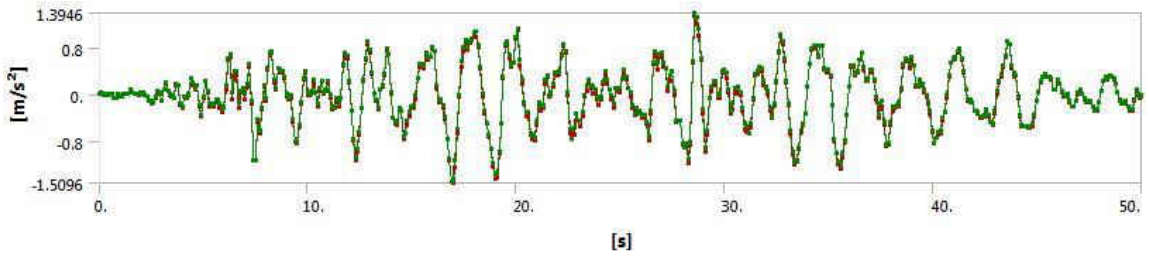


Figure 82. 1.0S2.0-LY

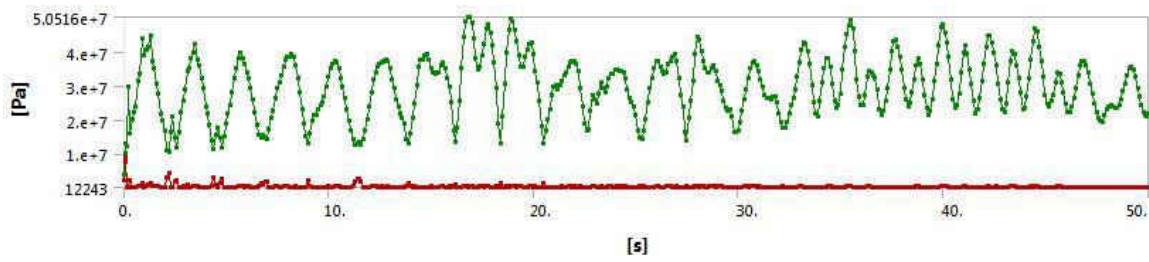


Figure 83. 1.0S0.5-LY

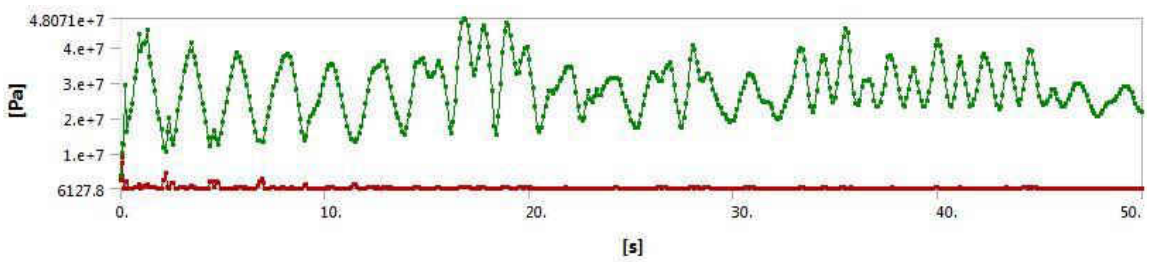


Figure 84. 1.0S1.0-LY

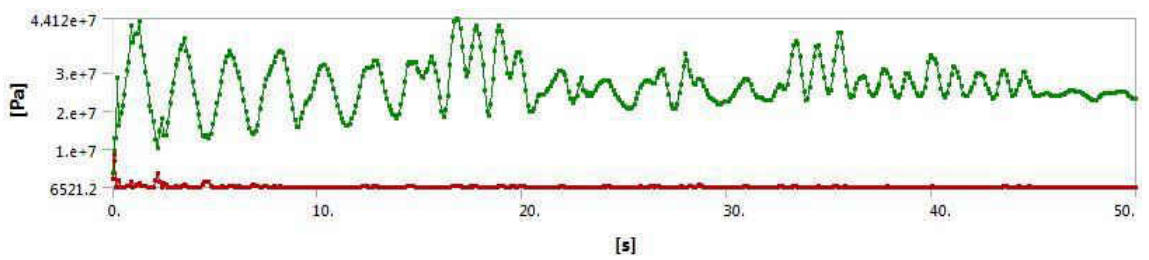


Figure 85. 1.0S2.0-LY

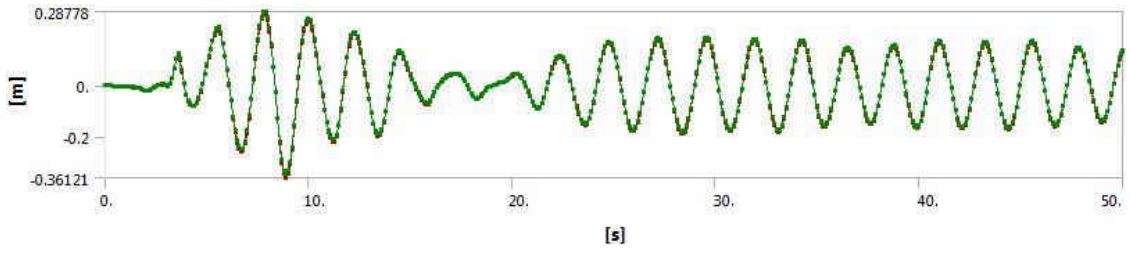


Figure 86. 1.0S0.5-NY

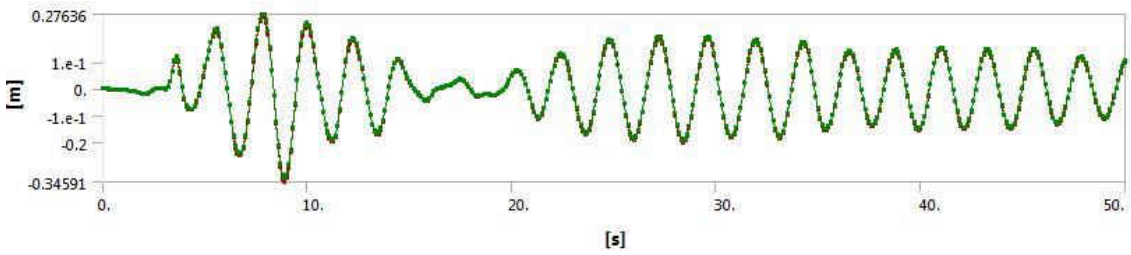


Figure 87. 1.0S1.0-NY

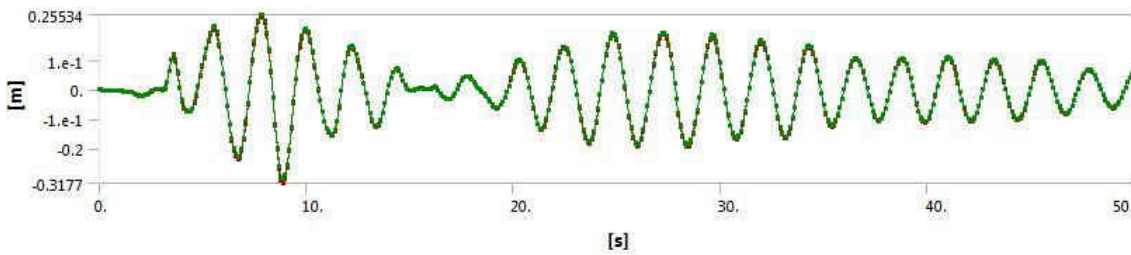


Figure 88. 1.0S2.0-NY

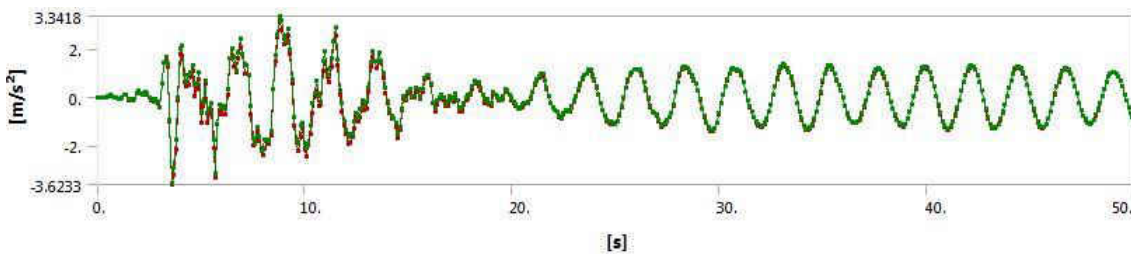


Figure 89. 1.0S0.5-NY

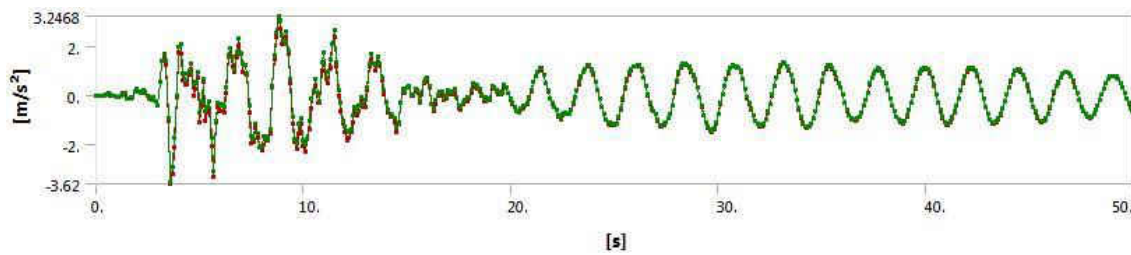


Figure 90. 1.0S1.0-NY

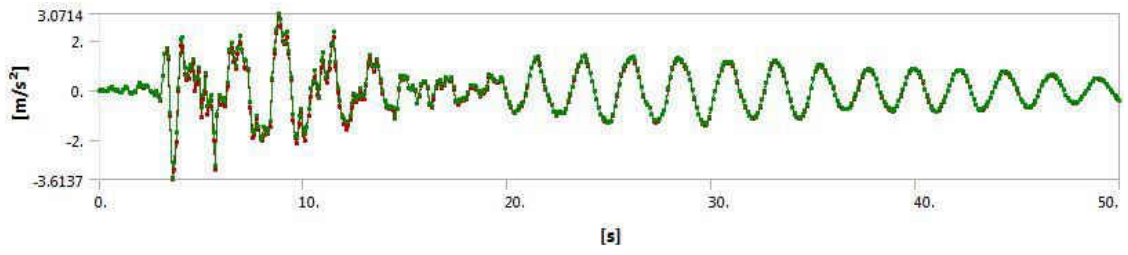


Figure 91. 1.0S2.0-NY

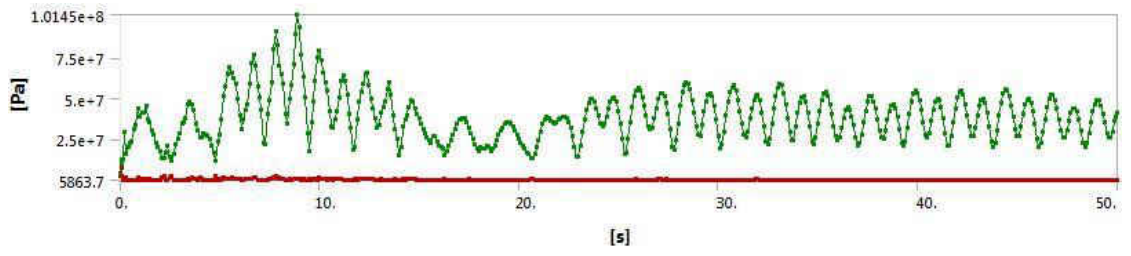


Figure 92. 1.0S2.0-NY

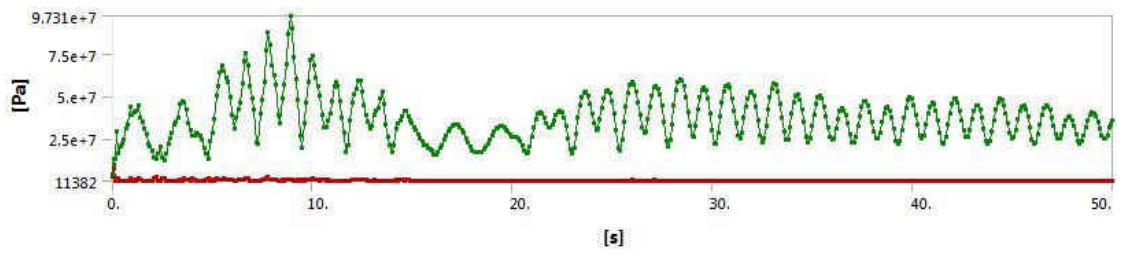


Figure 93. 1.0S2.0-NY

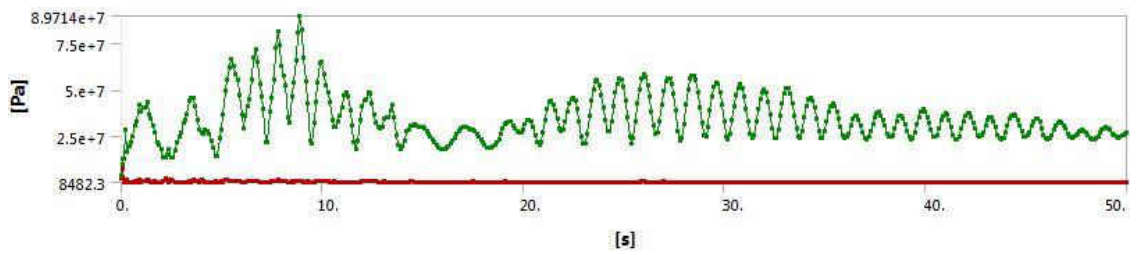


Figure 94. 1.0S2.0-NY

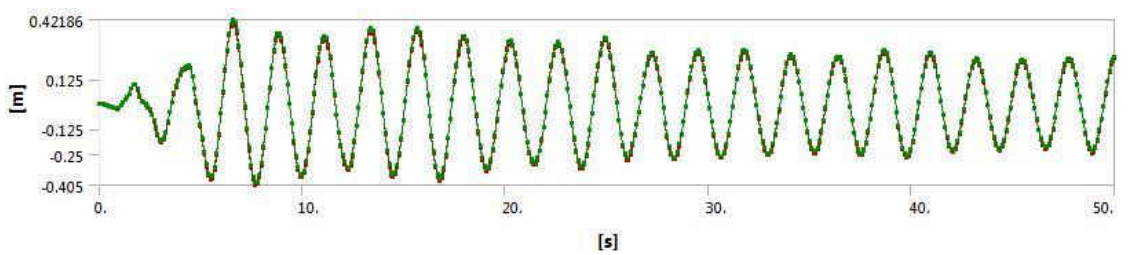


Figure 95. 1.0S0.5-EY

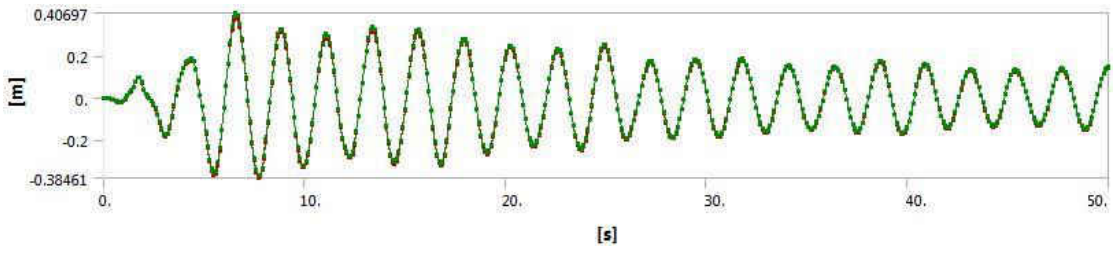


Figure 96. 1.0S1.0-EY

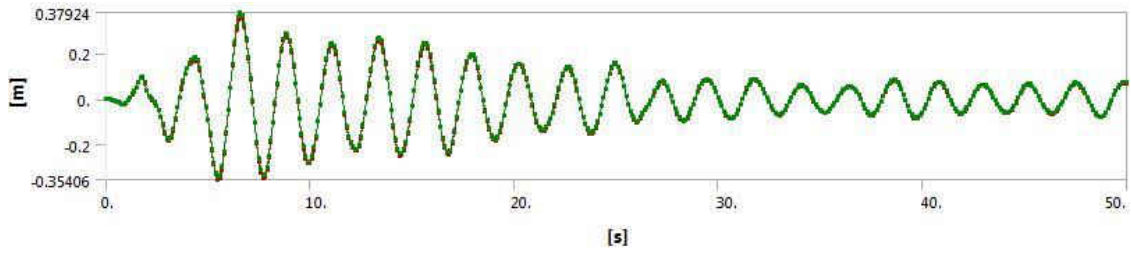


Figure 97. 1.0S2.0-EY

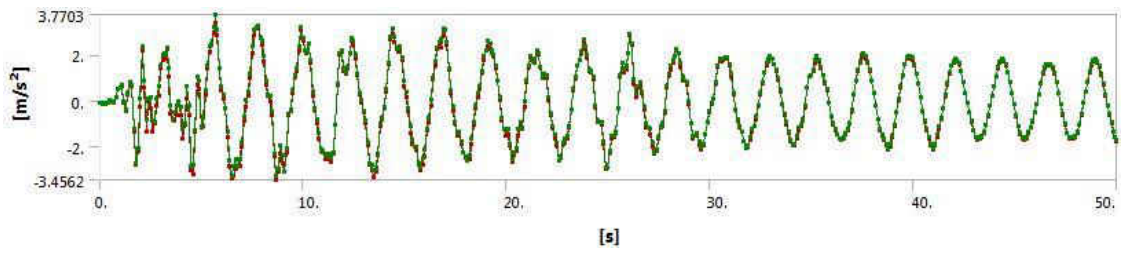


Figure 98. 1.0S0.5-EY

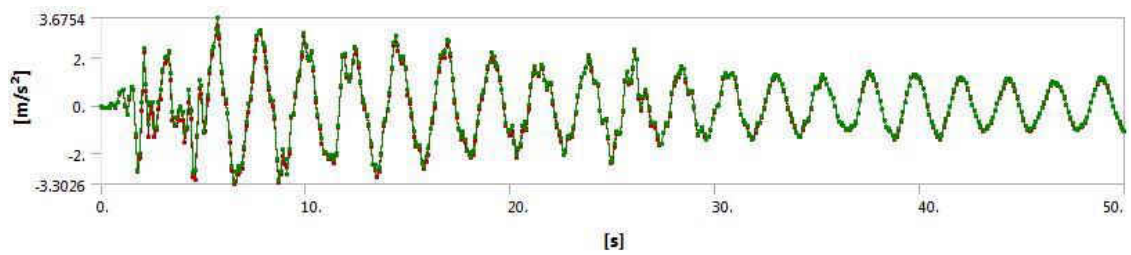


Figure 99. 1.0S1.0-EY

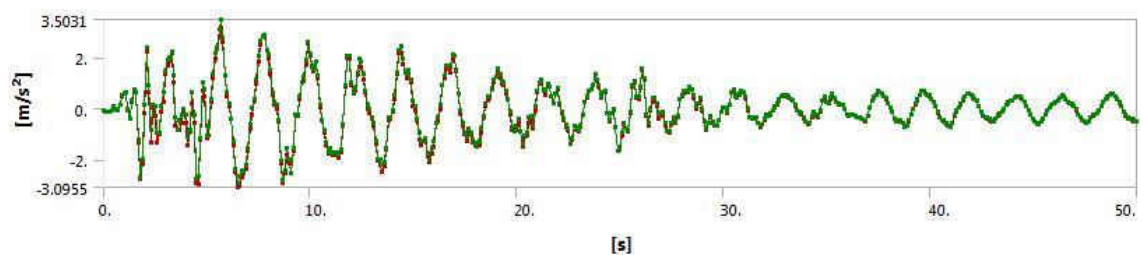


Figure 100. 1.0S2.0-EY

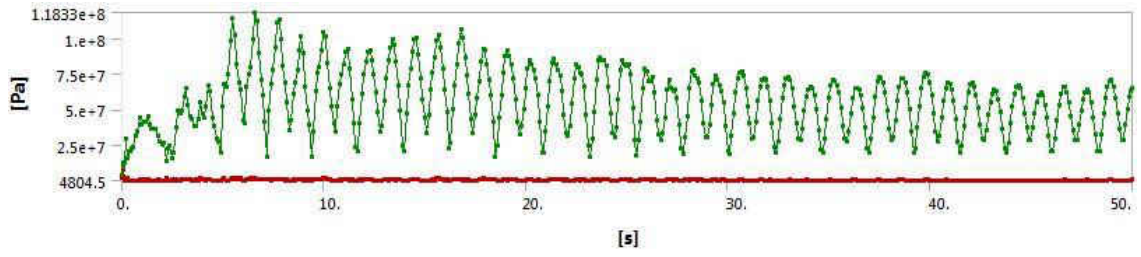


Figure 101. 1.0S0.5-EY

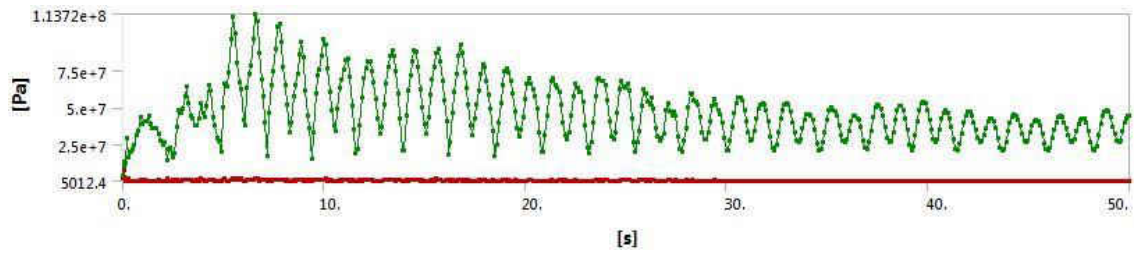


Figure 102. 1.0S1.0-EY

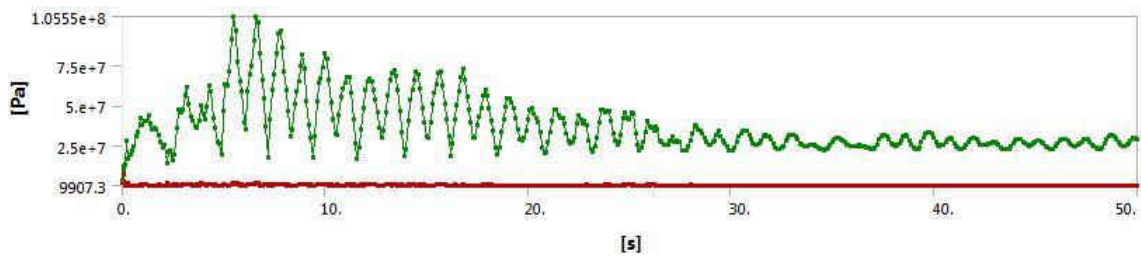


Figure 103. 1.0S2.0-EY

5 MW

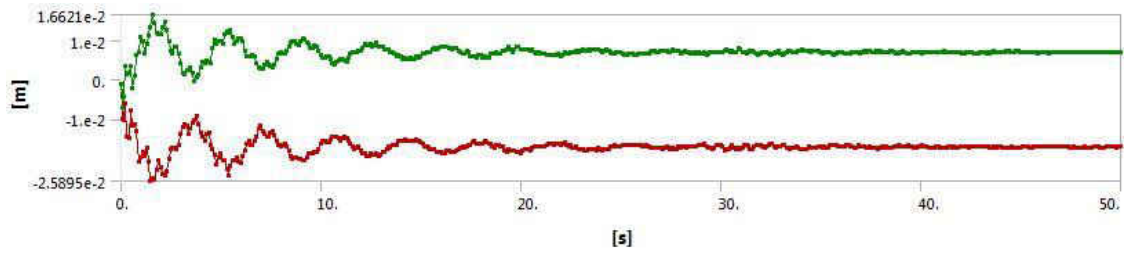


Figure 104. 5.0S0.5-LZ

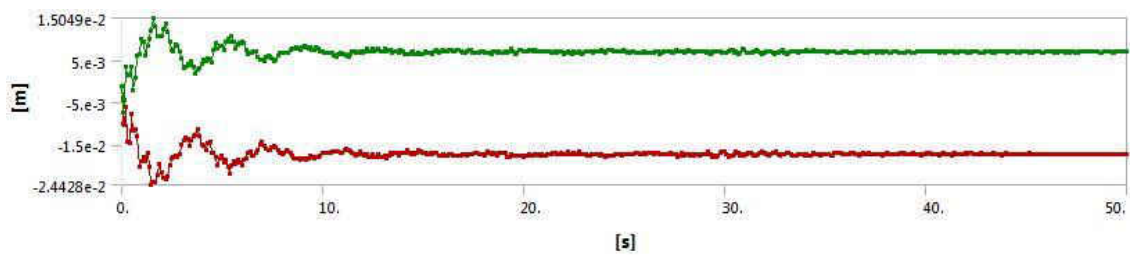


Figure 105. 5.0S1.0-LZ

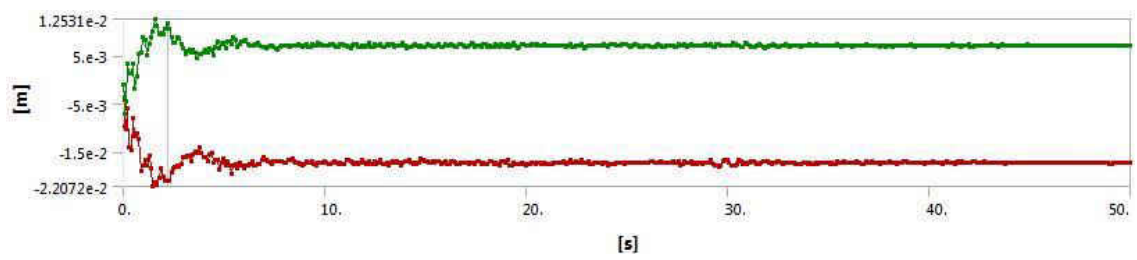


Figure 106. 5.0S2.0-LZ

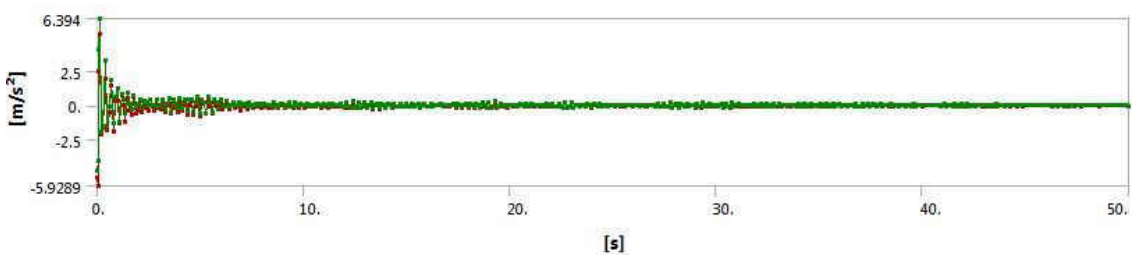


Figure 107. 5.0S0.5-LZ

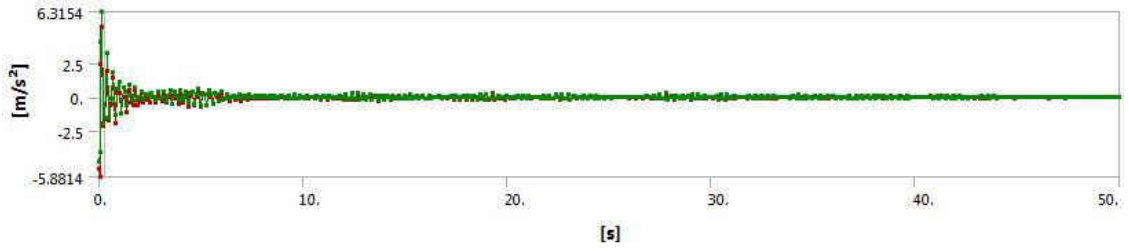


Figure 108. 5.0S1.0-LZ

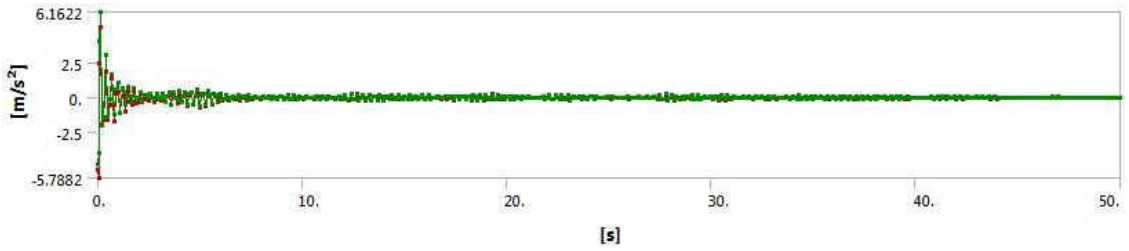


Figure 109. 5.0S2.0-LZ

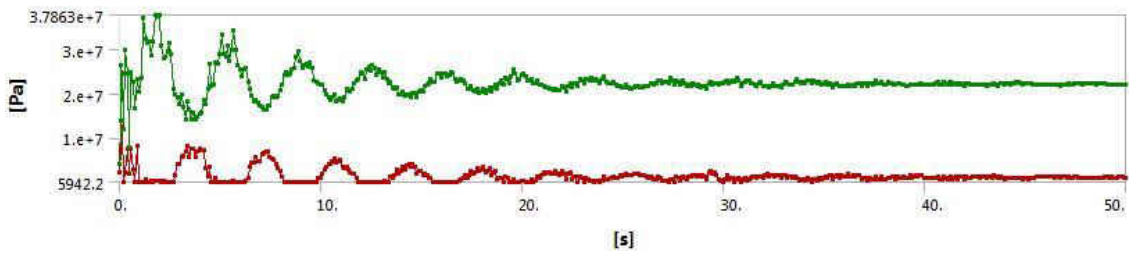


Figure 110. 5.0S0.5-LZ

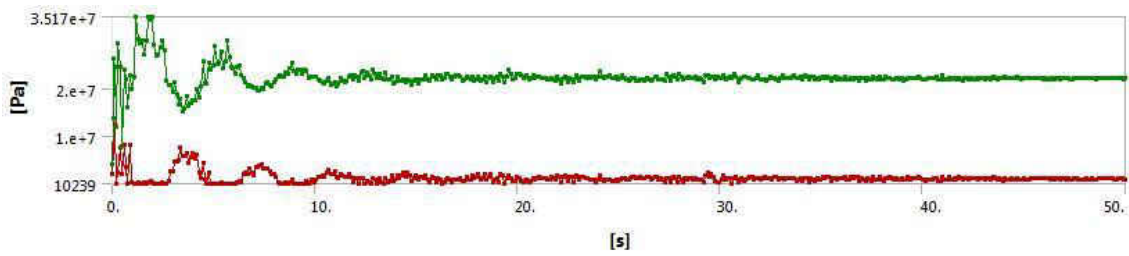


Figure 111. 5.0S1.0-LZ

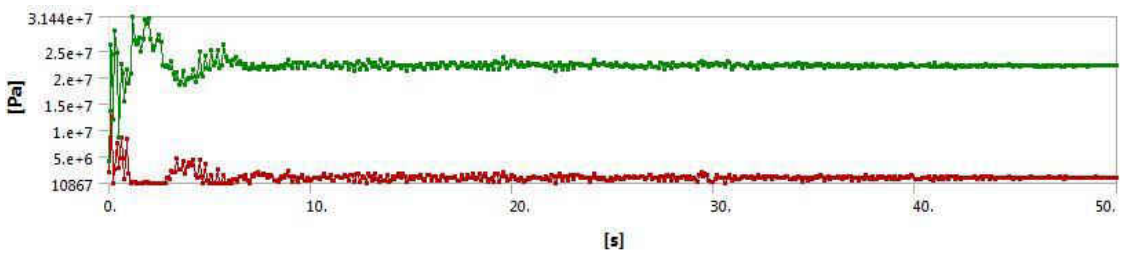


Figure 112. 5.0S2.0-LZ

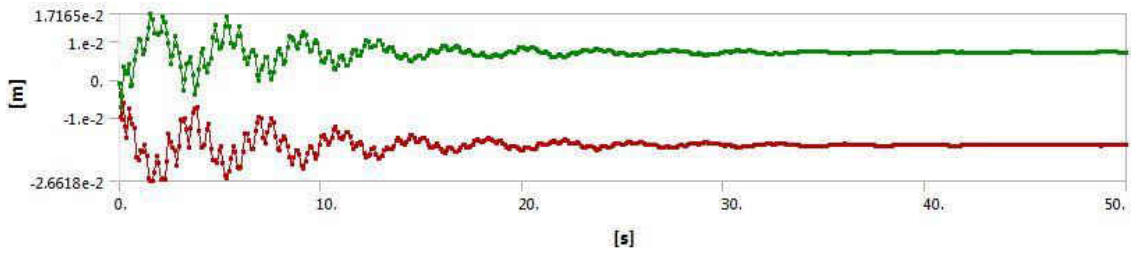


Figure 113. 5.0S0.5-NZ

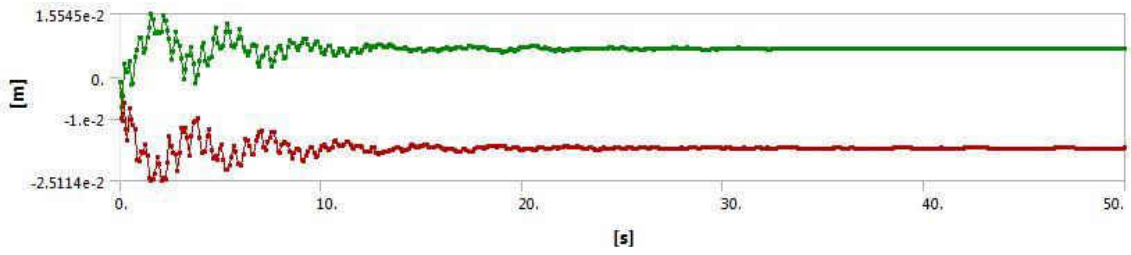


Figure 114. 5.0S1.0-NZ

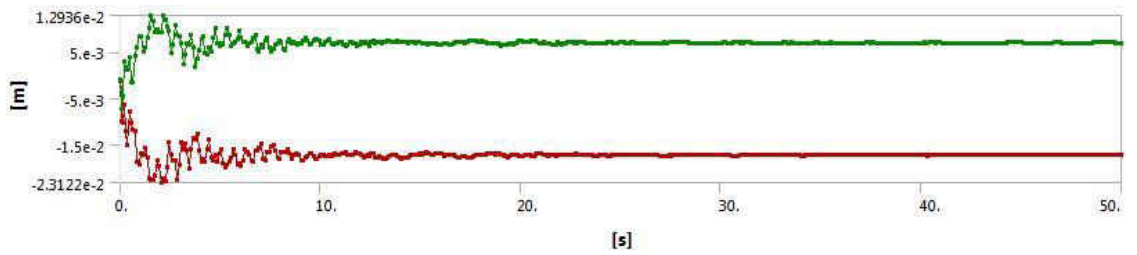


Figure 115. 5.0S2.0-NZ

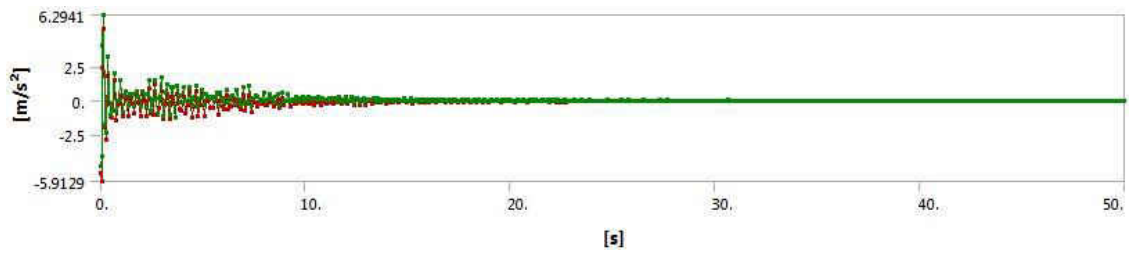


Figure 116. 5.0S2.0-NZ

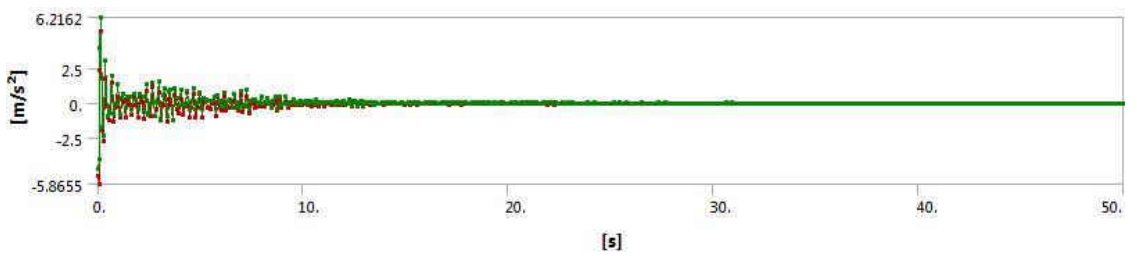


Figure 117. 5.0S2.0-NZ

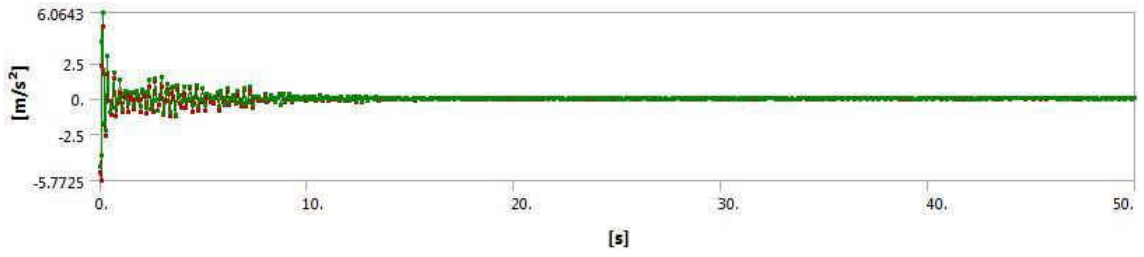


Figure 118. 5.0S2.0-NZ

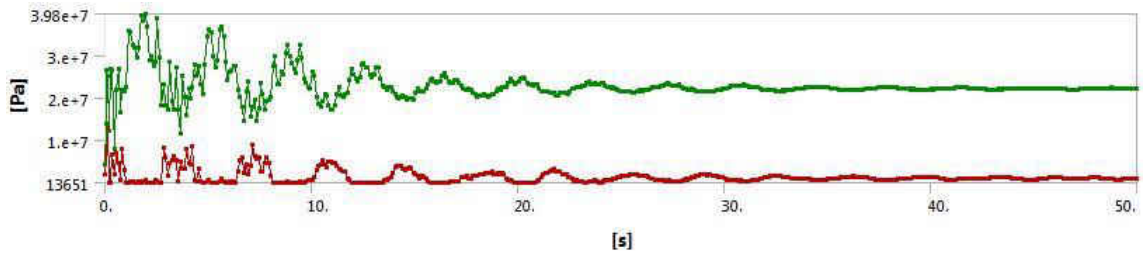


Figure 119. 5.0S0.5-NZ

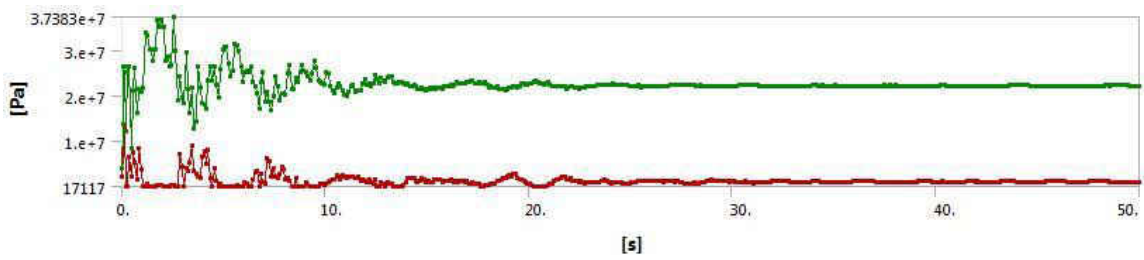


Figure 120. 5.0S1.0-NZ

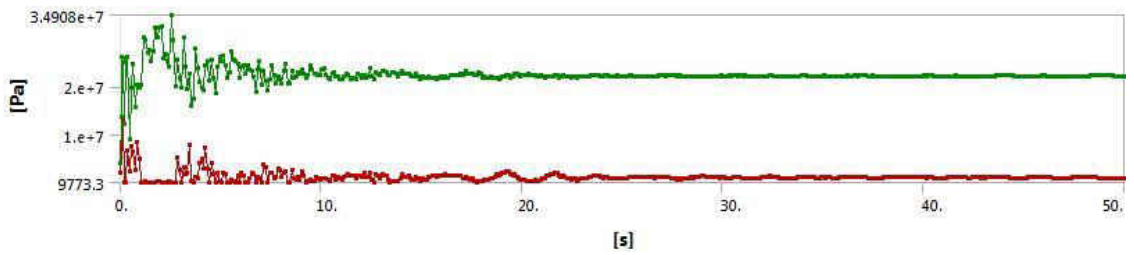


Figure 121. 5.0S2.0-NZ

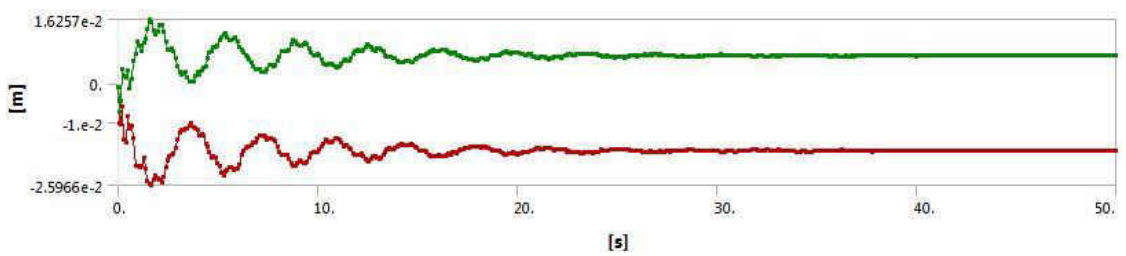


Figure 122. 5.0S0.5-EZ

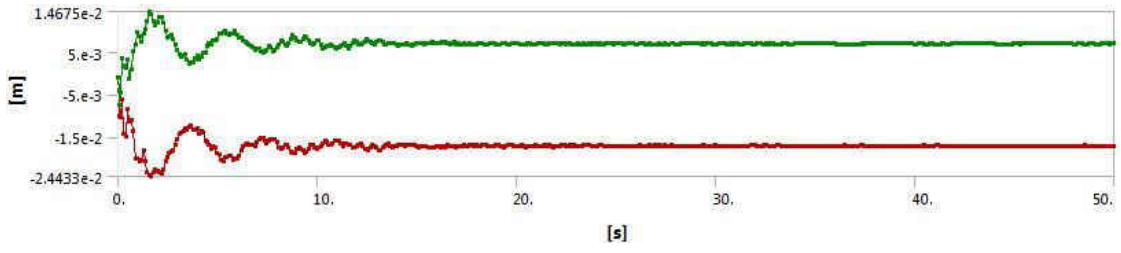


Figure 123. 5.0S1.0-EZ

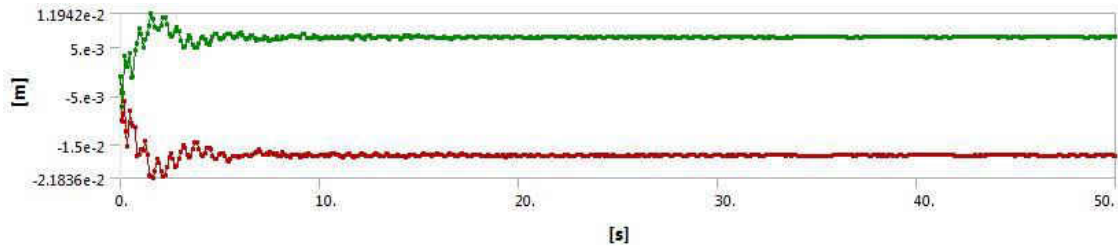


Figure 124. 5.0S2.0-EZ

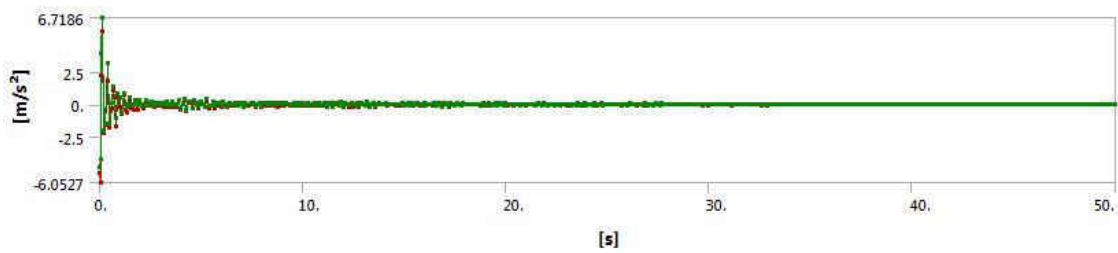


Figure 125. 5.0S0.5-EZ

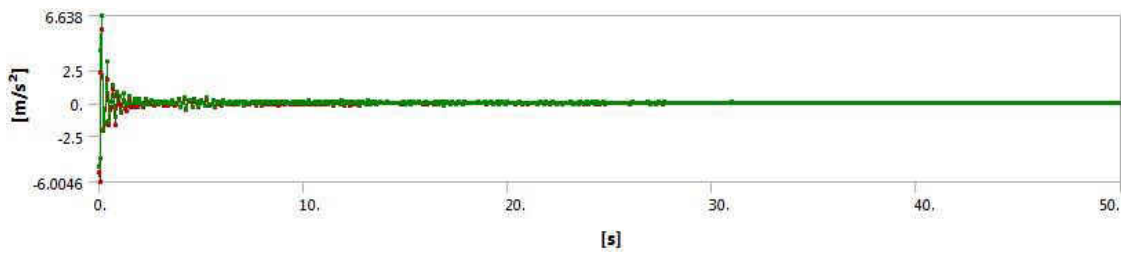


Figure 126. 5.0S1.0-EZ

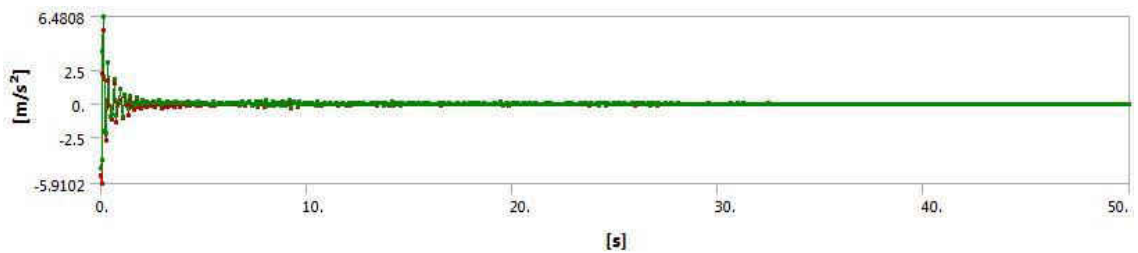


Figure 127. 5.0S2.0-EZ

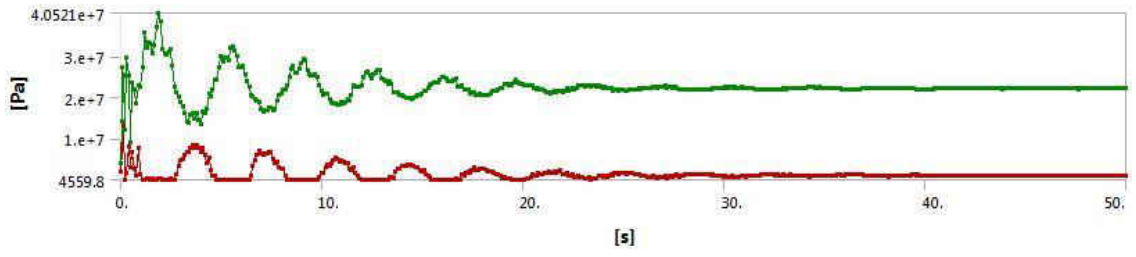


Figure 128. 5.0S0.5-EZ

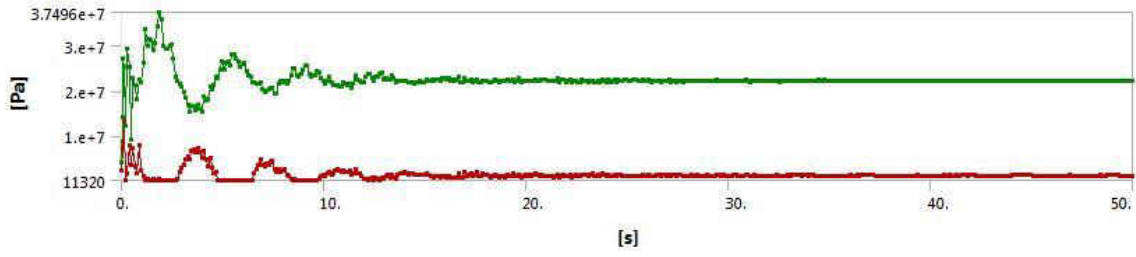


Figure 129. 5.0S1.0-EZ

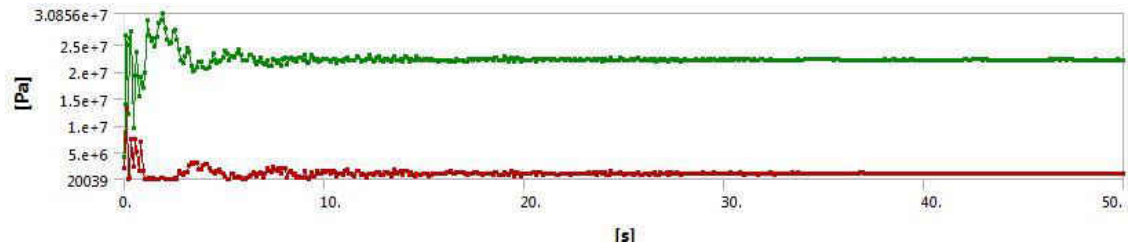


Figure 130. 5.0S2.0-EZ

References

- Agbayani, N. A. (2014). A Technical Overview of ASCE/AWEA RP2011: Recommended Practice for Compliance of Large Land-Based Wind Turbine Support Structures. *Structures Congress 2014*. Boston: AWEA and ASCE.
- American Wind Energy Association. (2016). *AWEA U.S. Wind Industry Annual Market Report Year Ending 2015*. AWEA.
- American Wind Energy Association. (2016). *U.S. Wind Industry Third Quarter 2016 Market Report*. AWEA Data Services.
- Ancona, D., & McVeigh, J. (2001). *Wind Turbine-Materials and Manufacturing Fact Sheet*. Princeton Energy Resources International, LLC.
- ANSYS. (2013, 11). *ANSYS Mechanical APDL Element Reference*. ANSYS Inc.
- Asareh, M.-A., & Prowell, I. (2012). A Simplified Approach for Implicitly Considering Aerodynamics in the Seismic Response of Utility Scale Wind Turbines. *53rd AIAA/ASME/ASCE/AHS/ASC Structures, Structural Dynamics and Materials Conference*, (p. 1829). Honolulu.
- AWEA. (2015). *The "Average" Utility-Scale Wind Turbine Installed During 2014*. AWEA.
- Bajaro, D. C. (2011, 3 8). Horizontal and Vertical Axis Wind Turbines. Retrieved from Vertical Axis Wind Turbine:
http://www.ivt.ntnu.no/offshore2/?page_id=394
- Bazeos, N., Hatzigeorgiou, G., Hondros, I., Karamaneas, H., & Karabalis, D. (2002). Static, Seismic and Stability Analyses of a Prototype Wind Turbine Steel Tower. *Engineering Structures* 24(8), 1015-1025.
- Bir, G., & Jonkman, J. (2007). Aeroelastic Instabilities of Large Offshore and Onshore Wind Turbines. *Journal of Physics: Conference Series, Volume 75*, 012069.
- Building Seismic Safety Council of the National Institute of Building Sciences. (2003). *NEHRP Recommended Provisions for Seismic Regulations for New Buildings and Other Structures (FEMA-450)*. Washington, D.C.: Building Seismic Safety Council.
- Clarke, S. (2003). *Electricity Generation Using Small Wind Turbines at Your Home or Farm*. OMAFRA.
- Claxton, O. (2014). *Analysing the effects of earthquakes on wind turbines*.

- Clough, R. W., & Penzien, J. (2003). *Dynamics of Structure*. Berkeley: Computers and Structures Inc.
- Darling, D. J. (2017, 3 16). *Wind Turbine*. Retrieved from Encyclopedia of Alternative Energy:
http://www.daviddarling.info/encyclopedia/W/AE_wind_turbine.html
- DNV, Risø. (2001). *Guidelines for Design of Wind Turbines*. Copenhagen: DSI Grafisk Service.
- Font, V. (2016, 10 18). Wind Energy Setting Records, Growing Still: The Wind Energy Outlook for 2016. Retrieved from renewableenergyworld:
<http://www.renewableenergyworld.com/articles/2016/02/wind-energy-setting-records-growing-still-the-wind-energy-outlook-for-2016.html>
- Germanischer Lloyd. (2010). *Guideline for the Certification of Wind Turbines*. Hamburg: Germanischer Lloyd.
- Global Wind Energy Council. (2017, 3 16). *Wind Power to Dominate Power Sector Growth*. Retrieved from <http://www.gwec.net/wind-power-to-dominate-power-sector-growth/>
- Gwon, T.-g. (2011). *Structural Analyses of Wind Turbine Tower for 3 KW Horizontal-Axis Wind Turbine*. San Luis Obispo: California Polytechnic State University.
- Hänler, M., U., R., & I., W. (2006). Systematic modelling of wind turbine dynamics and earthquake loads on wind turbines. *European Wind Energy Conference and Exhibition* (pp. 1-6). Athens: European Wind Energy Association.
- Hilber, H. M., Hughes, T. J., & Taylor, R. L. (1977). Improved numerical dissipation for time integration algorithms in structural dynamics. *Earthquake Engineering and Structural Dynamics*, 283-292.
- Hodges, D., & Pierce, G. (2011). *Introduction to Structural Dynamics and Aeroelasticity*. Cambridge University Press.
- Hughes, T. J. (1987). *The finite element method. Linear static and dynamic finite element analysis*. Englewood Cliffs, N.J.: Prentice-Hall, Inc.
- ICC. (2006). *International Building Code 2006*. Illinois: International Code Council.
- Intergovernmental Panel on Climate Change. (2012). *Renewable Energy Sources and Climate Change Mitigation*. Intergovernmental Panel on Climate Change.
- International Electrotechnical Commission. (2005). *Wind Turbines-Part 1: Design Requirements*. IEC.
- Kiyomiya, O., Rikiji, T., & Van Gelder, P. H. (2002). Dynamic Response Analysis of Onshore Wind Energy Power Units during Earthquakes and Wind. *International Offshore and Polar Engineering Conference*. Kitakyushu: International Society of Offshore and Polar Engineers.

- Kjørlaug, R. A. (2013). *Seismic Response of Wind Turbines: Dynamic Analysis of a Wind Turbine in Horizontal and Vertical Direction-Subject to Earthquake, Wind & SSI*.
- Laura, P. A., Pombo, J. L., & Susemihl, E. A. (1974). A note on the vibrations of a clamped-free beam with a mass at the free end. *Journal of Sound and Vibration, Vol 37(2)*, 161-168.
- Lavassas, I., Nikolaidis, G., Zervas, P., Efthimiou, E., Doudoumis, I., & Baniotopoulos, C. (2003). Analysis and design of the prototype of a steel 1-MW wind turbine tower. *Engineering Structures 25*, 1097-1106.
- McCaffrey, B. (2005). *Wind Turbine Technology*. Albany: Global Energy Concepts.
- Mehta, D., & Gandhi, N. (2008). Time Response study of tall chimneys, under the effect of soil structure Interaction and Long period earthquake Impulse. *The 14th World Conference on Earthquake Engineering*.
- Miceli, F. (2012, 5 31). Wind Farms Construction. *Wind Turbine Tower*.
- NEWEN. (2017, 3 16). *Wind Turbines*. Retrieved from <http://www.newen.com.au/Wind-Facts/Wind-Facts/Wind-turbine-.asp>
- Nuta, E., Christopoulos, C., & Packer, J. (2011). Methodology for seismic risk assessment for tubular steel wind turbine towers: application to Canadian seismic environment. *Canadian Journal of Civil Engineering 38(3)*, 293-304.
- Peschel, T. (2016, 3 31). Offshore Wind Industry. *Monitoring offshore Wind Farms in the North Sea*. Retrieved from offshorewindindustry: <http://www.offshorewindindustry.com/news/monitoring-offshore-wind-farms-north-sea>
- POWER-TALK.NET. (2017, 3 16). *Upwind Vs. Downwind*. Retrieved from <http://www.power-talk.net/upwind-turbine.html>
- Power-Technology. (2014, 1 2). The world's 10 biggest wind turbines. *SeaTitan 10 MW Wind Turbine*. Retrieved from power-technology: <http://www.power-technology.com/features/featurethe-worlds-biggest-wind-turbines-4154395/>
- Prowell, I. (2011). *An experimental and numerical study of wind turbine seismic behavior*.
- Prowell, I., & Veers, P. (2009). *Assessment of Wind Turbine Seismic Risk: Existing Literature and Simple Study of Tower Moment Demand*. Sandia National Laboratories.
- Prowell, I., Elgamal, A., Uang, C., & Jonkman, J. (2010). *Estimation of Seismic Load Demand for a Wind Turbine in the Time Domain*. NREL.
- Prowell, I., Veletzos, M., & Elgamal, A. (2008). *Full Scale Testing for Investigation of Wind Turbine Seismic Response*.

- Prowell, I., Veletzos, M., Elgamal, A., & Restrepo, J. (2009). Experimental and Numerical Seismic Response of a 65 kW Wind Turbine. *Journal of Earthquake Engineering, Vol. 13(8)*, 1172-1190.
- Ritschel, U., Warnke, I., & Kirchner, J. (2003). WIND TURBINES AND EARTHQUAKES. *2nd World Wind Energy Conference* (pp. 1-8). Cape Town: World Wind Energy Association.
- Schwartz, M., & Elliott, D. (2005). Towards a Wind Energy Climatology at Advanced Turbine Hub-Heights. Savannah: NREL.
- Shahan, Z. (2014, 11 21). History of Wind Turbine. Retrieved from Renewable Energy World:
<http://www.renewableenergyworld.com/ugc/articles/2014/11/history-of-wind-turbines.html>
- Singh, A. (2007). Concrete Construction for Wind Energy Towers. *The Indian Concrete Journal, 81(9)*, 43-49.
- Smith, R. (2007, 6 4). Vertical-Axis Wind Turbine.
- Tricklebank, A. H., Halberstadt, P. H., & Magee, B. J. (2007). *Concrete Towers for Onshore and Offshore Wind Farms*.
- Web Zone1. (2015, 2 18). Green Energy. *Wind Energy Economy: The Numbers Tendency*.
- Witcher, D. (2005). Seismic Analysis of Wind Turbines in the Time Domain. *Wind Energy 8*, 81-91.
- Wood, W., Bossak, M., & Zienkiewicz, O. (1980). An alpha modification of Newmark's method. *International Journal for Numerical Methods in Engineering, Vol 15(10)*, 1562-1566.
- Zavitz, B., & Kirkley, K. (2012, 1). *Optimal Tower and Foundation Design*.
- Zhao, X., & Maisser, P. (2006). Seismic response analysis of wind turbine towers including soil-structure interaction . *Proceedings of the Institution of Mechanical Engineers, Part K: Journal of Multi-body Dynamics*, (pp. 53-61).
- Zhao, X., MaiXer, P., & Wu, J. (2007). A new multibody modelling methodology for wind turbine structures using a cardanic joint beam element. *Renewable Energy 32 (3)*, 532-546.
- Zienkiewicz, O. C., Taylor, R. L., & Taylor, R. L. (1977). *The Finite Element Method (Vol 3)*. London: McGraw-hill.